A PSEUDOFUNCTION APPROACH TO THE DESCRIPTION OF VISCOUS CROSSFLOW IN MULTI-LAYERED PERMEABLE MEDIA

APPROVED:

Supervisor: _____
Larry W. Lake

_____
Vito J. Zapata

Dedicated, With Love, To My Parents
Roberto and Maria Gloria Thiele

A PSEUDOFUNCTION APPROACH TO THE DESCRIPTION OF VISCOUS CROSSFLOW IN MULTI-LAYERED PERMEABLE MEDIA

by

Marco Roberto Thiele, B.S.

THESIS

Presented to the Faculty of the Graduate School of

The University of Texas at Austin

in Partial Fulfillment

of the Requirements

for the Degree of

MASTER OF SCIENCE IN ENGINEERING

THE UNIVERSITY OF TEXAS AT AUSTIN

December 1988

ACKNOWLEDGMENTS

There are many people I am deeply indebted to for helping me, either directly or indirectly, in my education and in the formulation of this work.

My family, and above all my parents, Roberto and Maria Gloria Thiele, who have done so much for me and who have always given me the opportunity to pursue my interests and my curiosity.

My teachers and professors who have made it their duty to educate students like myself. Of these I owe Dr. Vito J. Zapata special thanks for having helped me start on this particular project. A very special recognition is extended to Professor Larry W. Lake for the many invaluable comments and hints and for his masterful teaching of the fundamentals of science and engineering. His patience and clarity in answering even the most trivial of questions will never be forgotten.

My fellow students for the many interesting and fruitful discussions (even if not always technically related), for the help with the many rough spots of engineering research, and who have made the office atmosphere a pleasant one to work in.

There are, of course, many whom I am indebted indirectly by helping me get through this part of my life successfully. Of these, two have been very special to me. Wayne Martin, a very good friend, who has taught me so much about the United States and who has made my Texas stay truly an unforgettable one. Nicola Erbe, my girlfriend, being always a bright star at the horizon even in darkest of times and who has made many sacrifices for me.

The financial support of the Department of Energy, contract DE-AC19-85BC-10849, and of Cray Research was greatly appreciated.

Marco Thiele

The University of Texas at Austin
December, 1988

ABSTRACT

A PSEUDOFUNCTION APPROACH TO THE DESCRIPTION OF VISCOUS CROSSFLOW IN MULTI-LAYERED PERMEABLE MEDIA

BY

MARCO ROBERTO THIELE, B.S.

SUPERVISING PROFESSOR: LARRY W. LAKE

Under the conditions of vertical equilibrium, viscous forces only, and sharp front displacement, Hearn's model for the description of a waterflood in a two-dimensional layered reservoir is not correct for end-point mobility ratios greater than one. Under these conditions, the flow does not remain segregated as the Hearn model assumes but instead the direction of crossflow creates viscous mixing zones. Compared to the Hearn model, viscous mixing aids recovery.

A central assumption in the analysis of viscous mixing is that the system be in vertical equilibrium. Formally, this requires the vertical absolute permeability to be infinitely large. It is shown that for all practical purposes this must not be the case and that vertical equilibrium is attained as long as a dimensionless parameter, called the effective length-thickness ratio, exceeds a value of two.

The functionality of viscous mixing is investigated with respect to three parameters: the end-point mobility ratio (M^o), the Craig coefficient (V_C), a measure of reservoir heterogeneity, and the type of layer ordering. The dominant factor controlling the extent of viscous mixing is found to be the layer arrangement. Four

types of ordering schemes are proposed. Of the four, the "random" ordering arrangement is found to have the strongest degree of viscous mixing and the largest increase in recovery.

If the type of layering is fixed, viscous mixing and the improved recovery because of it, can be related to the end-point mobility ratio only. The simplicity of the Hearn model allows for a pseudofunction approach to correct for viscous mixing by introducing an effective end-point mobility ratio. For a descending (ascending) type layer ordering, the effective end-point mobility ratio is linearly related to the true end-point mobility ratio of the displacement. Within certain limits of the Craig coefficient and the true end-point mobility ratio this approach works well.

An alternative approach to correct for viscous mixing effects, using effective permeability-height products, is presented. Contrary to the effective mobility ratio approach this is a N-1 parameter fit, where N is the number of layers. It also allows for calculating the pseudo relative permeability curves of the system.

In conclusion, it is pointed out that under the assumptions of the study, viscous mixing effectively makes the system look less heterogeneous than it really is and always aids in the overall recovery compared to the case in which the phenomenon is neglected.

TABLE OF CONTENTS

CHAPTER I

INTRODUCTION

As in many other engineering research fields, economic reasons are a primary driving force for petroleum research and development. The general idea being to attempt to maximize revenues with the least cost possible. So it should come as no surprise that the bulk of petroleum research in the area of waterflooding is really dedicated to the best possible solution of Eq. (I.1).

$$N_{PD} = (\overline{S}_w - S_{wi}) \qquad (I.1)$$

where

N_{PD} = Cumulative dimensionless recovery

$\overline{S}_w$ = Average water saturation

S_{wi} = Initial water saturation

The importance of Eq. (I.1) stems from the fact that it leads automatically to a time versus recovery plot, which in turn is an important link between the world of petroleum research and that of economic forecasting and evaluation. Because it represents a vital connection between these almost diametrically opposed fields, the appearance of Eq. (I.1) is simple. But its simplicity is really artificial since the average water saturation of the system, and even the initial water saturation, can be made a function of as many physical variables as one desires complexity. Suffice to say that Eq. (I.1) really spans an enormous area of research and represents an extreme condensation of work.

The research presented in this thesis is in line with the above ideas. Its ultimate goal is to offer a better approximation to cumulative production versus time for a very specific set of physical properties and geological features. The work can stand alone and be used directly or can be incorporated into other predictive tools such as numerical simulators.

The model investigated is that presented by Hearn in 1971 and generally referred to as the Hearn model. Specifically, Hearn derived a solution for a two-phase displacement process (oil-water) occurring in a two-dimensional layered permeable media under vertical equilibrium conditions. His original intent was to derive pseudo relative permeability curves that could be used in numerical simulation to better match real field data rather than use the model directly for recovery predictions.

The correct solution to the Hearn model rests on two fundamental assumptions. That the system be in vertical equilibrium and that the end-point mobility ratio be less or equal to one. Even though there exist a dimensionless group to help identify when a system is in vertical equilibrium, called the effective length to thickness ratio (Goddin et al., 1966), this group is by no means unique. The magnitude of this parameter, identifying the onset of vertical equilibrium, may change depending on the type of displacement, the vertical and horizontal permeability distributions as well as the systems length and height. It is therefore necessary before using Hearn's model to establish certainty about the systems state of vertical equilibrium. This is probably best done by simulation.

When the end-point mobility ratio is greater than one Hearn's solution is no longer correct, even for a system in vertical equilibrium (Zapata and Lake, 1981). The reason for this is the occurance of viscous mixing around the front regions during the displacement which surprisingly aids recovery. The Hearn solution, which does not take into account viscous mixing, therefore underestimates recovery for end-point mobility ratios greater than one. The severity of the error increases with increasing heterogeneity of the system. Zapata and Lake (1981) derived an

analytical solution for a two layered system that correctly solves for the effect of viscous mixing, but the solution becomes tedious and unpractical for a larger number of layers.

Because of the simplicity of Hearn's model, an attractive approach to correct for the discrepancy in the solution as explained above is to find an effective end-point mobility ratio. In essence, this is a pseudo-function approach. Pseudo-functions do not necessarily have to give a correct physical interpretation of the process taking place, but rather are to approximate the net outcome of the physical process in an average sense. This approach, while it retains simplicity and accuracy, does sacrifice correct physical interpretation and universal applicability. But the trade-off may very well be worth while, especially if it aids in reducing the dimensionality of large scale field problems that are to be solved by numerical simulation.

It is important to keep in mind the limitations of such an investigation as presented here. Being essentially a simulation study, the number of parameter combinations to be investigated can become very large if a good approximation to all possible reservoir configurations is to be found. The real benefit of a study as this one is to point out trends and limitations that allow a better understanding of the overall outcome of the physical process and guide in creating a problem-specific investigation and solution when it is called for.

CHAPTER II

LITERATURE REVIEW

Waterflooding has been the most popular method in improving the production of crude oil from petroleum reservoirs. Even today, with increasingly complex enhanced oil recovery technology finding its way to the field, waterflooding still plays a central and crucial role. Almost all EOR methods, in fact, rely at some point on a water drive for successful completion.

Waterflooding began in 1865 when, by accident, water was injected in the Pithole area of Pennsylvania (API, 1961). 1924 marked the first planned five-spot pattern flood on the Bradford field in Pennsylvania (Fettke, 1938). Since then, the general availability of water, the ease with which it can be injected, the pressure it generates, and its efficiency in the displacement process are but four of the many reasons that have made waterflooding the most popular method for increasing oil recovery (Craig, 1971).

Waterflooding has been the subject of an enormous volume of literature, all of which can not be reviewed here. The most comprehensive work is probably Craig's waterflooding monograph (Craig, 1971) and the reader is referred to this work for a good and general introduction.

The first breakthrough in the description of two-phase flow in permeable media was presented by Buckley and Leverett in 1942. The Buckley and Leverett problem, as it is known today, is a two-phase, immiscible displacement in a one-dimensional, homogeneous, isotropic porous media, under incompressible and

isothermal conditions, with no capillary pressure. Even being the simplest possible two-phase model, it has been used extensively and the insight gained from the solution has been invaluable to petroleum engineering and research. So much so that the Buckley and Leverett problem has served as a model for the solution of much more complicated systems such as cation exchange (Pope et al., 1978) , precipitation/dissolution (Walsh et al., 1984), and multicomponent polymer flooding (Johansen et al, 1988). In 1952, Welge introduced a graphical approach to the solution of the Buckley and Leverett problem generally known as the Welge construction.

The next major step was introduced orally in 1948 and published in 1950 by Dykstra and Parsons with an investigation of recovery from a stratified system. The Dykstra and Parsons study was an experimental one, though it is seldom thought of this way, and attempted to identify the most important parameters affecting oil recovery from waterfloods. They investigated 52 core floods and concluded that recovery was a function of mobility ratio, the permeability variation, and the initial oil and water saturations.

The analytical model proposed for matching their laboratory results made simplifying assumptions: a two-dimensional, layered system with no communication between the layers except at the production and injection well. Each layer was essentially treated as a separate Buckley and Leverett problem but with the additional assumption that the displacement be piston-like everywhere. In their conclusions, Dykstra and Parsons made the comment that their proposed analytical method did not seem to match field data particularly well in that they are were unable to find a universal method to predict oil recovery with equal precision for different fields. One of the lasting parameters introduced by Dykstra and Parsons is what today is generally known as the Dykstra-Parsons coefficient, a measure of reservoir heterogeneity.

The Dykstra and Parsons method is analytically correct for any end-point mobility ratio as long as the assumption of a piston-like displacement is not violated. For the special case of an end-point mobility ratio of one, a simpler solution was presented by Stiles in 1949. Though Stiles derived the recovery

equations by making the assumption of a unit mobility ratio, he later used them to predict recovery for non-unit mobility ratio displacement introducing an error in the prediction. The Stiles method is really to be considered as a special case of the more general Dykstra and Parsons method. For a unit mobility ratio the Stiles, Dykstra and Parsons, and Hearn model all return the exact same solution.

The other limiting case for stratified systems is that in which the layers are in perfect vertical communication leading to a state of vertical equilibrium. Investigations on this type of systems include those of Craig et al. (1957), Warren et al. (1964), Root et al.(1965), Goddin et al.(1966), Coats et al.(1971), Hearn (1971), and Zapata and Lake (1981). The introduction of a non-zero vertical permeability complicates the problem considerably since it essentially adds one more dimension.

The concept of vertical equilibrium has probably been best illustrated by Coats et al.(1971) with an analogy to heat conduction. If one were to describe heat conduction in a metal plate with several square feet of area but a thickness of only an eight of an inch, no allowance would be made for the heat distribution in the vertical direction. Rather, the assumption of thermal equilibrium would be invoked letting the temperature gradient in the vertical direction be equal to zero. In petroleum reservoirs, which often have the same dimensional proportionality to the metal plate described, the vertical equilibrium condition would correspond to a zero potential gradient in the vertical direction. In the literature, the condition of a zero potential gradient is often thought as equivalent to an infinite vertical permeability or an infinitely fast vertical redistribution of fluids (Coats et al., 1971). This interpretation though has been the subject of controversy and the idea of a zero potential gradient, or the sum of all driving forces in the vertical direction being equal to zero, remains the more transparent explanation. Because of the multitude of factors involved in the description of vertical equilibrium, such as the interaction between capillary, gravity, and viscous forces, the magnitude and variability of permeability, it becomes difficult to exactly quantify the contribution of any one parameter to the overall phenomenon during the displacement process.

The best known analytical model for the description of displacements in stratified reservoirs under the condition of vertical equilibrium is probably that of Hearn (1971). Hearn neglected crossflow caused by capillary and gravity forces and derived a simple model considering only viscous forces. As Zapata and Lake (1981) have shown, Hearn's model is only correct for end-point mobility ratios equal or less than one but underestimates recovery for end-point mobility ratios greater than one.

In 1981, Zapata and Lake published a theoretical analysis of viscous crossflow. They showed that viscous crossflow in layered media, resulting from an end-point mobility ratio greater than one, will create viscous mixing zones around the front regions and improve the vertical sweep efficiency compared to the no-crossflow case. They also concluded that viscous mixing will only aid recovery as long as the water fronts are sharpening waves and that different layer ordering schemes in systems with more than two layers will strongly affect the vertical sweep efficiency.

In between the assumption of no vertical communication in the Dykstra and Parsons model and infinite vertical communication in the Hearn model there are a range of cases which do not fall under either of the two limiting models. For these, there is no analytical solution, again, underlining the difficulty of trying to accurately describe the displacement process under the condition of vertical equilibrium, quantify it, and determine its functionality on various reservoir parameters.

CHAPTER III

RESERVOIR PARAMETERS AND ANALYTICAL MODELS

This chapter introduces various reservoir parameters and concepts used to describe, analyze, and uniquely fix the system under study. Furthermore, it gives a brief derivation of the two limiting cases for immiscible displacements in layered permeable media assuming viscous forces only: the Dykstra and Parsons model and the Hearn model.

3.1 RESERVOIR HETEROGENEITY

The term "reservoir heterogeneity" has occupied the petroleum and water resources literature for many years. Attempts to quantify reservoir heterogeneities in order to include them in numerical models commonly used for the description of fluid flow in real permeable media has met only with limited success.

One of the problems with attempting to quantify reservoir heterogeneities is the number of parameters involved as well as the scale at which they may occur. Heterogeneities can range from spatial variations of flow parameters such as permeability and porosity, to irregular reservoir geometries, to changes in the chemical composition of the fluids and the reservoir. In general, any parameter that changes explicitly or implicitly as a function of space may fall under the heading of reservoir heterogeneity. Needless to say, the importance of parameters across various scale lengths complicates matters even further.

The model of reservoir heterogeneity used here is that of a layered system. While the model is undisputedly simple, it does mirror many real geological settings and is conceptually easy to understand.

3.1.1 LAYERED SYSTEMS

The concept of a layered system as a model for reservoir heterogeneity was introduced by Dykstra and Parsons in 1950. A schematic of a layered reservoir model is shown in Fig. III.1.

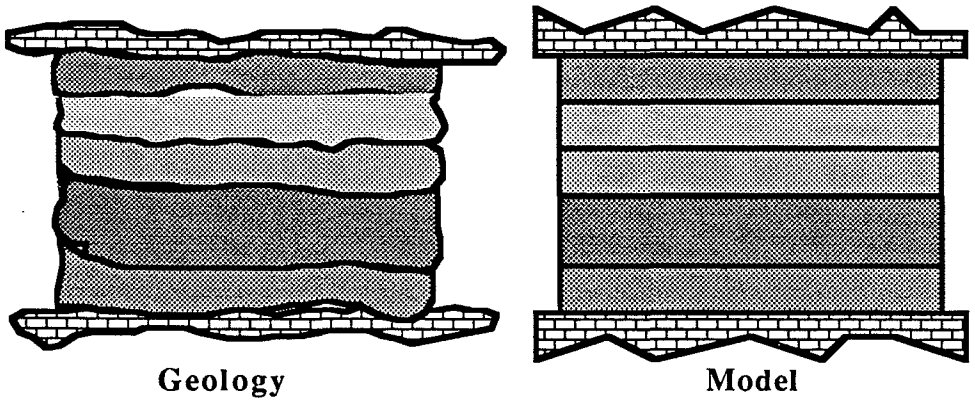

Fig. III.1: Stratified Reservoir

The model is one in which discrete layers make up the reservoir. While the layers may differ from each other in one or more flow properties such as permeability, porosity, residual water and oil saturations, relative permeability curves, height, and in certain cases even phase viscosities, each layer is treated as being homogeneous in itself (Caudle, 1968).

Depending on the type of model considered, the vertical communication between the layers may be zero or non-zero. The Dykstra and Parsons model

assumes a zero vertical permeability while the Hearn model assumes "infinite" vertical permeability.

3.1.2 THE DYKSTRA-PARSONS AND THE CRAIG COEFFICIENTS

As mentioned in Chap.II, one of the lasting parameters introduced by Dykstra and Parsons (1950) is what today is generally referred to as the Dykstra-Parsons coefficient.

In order to characterize the cores used in their floods, Dykstra and Parsons investigated the absolute permeability to air on the face of each core. They quantified the permeability variation by the following procedure:

1. Permeabilities in a distribution are tabulated in descending order.
2. The per cent of the permeabilities exceeding each tabulated entry is computed for a second column entitled "cumulated per cent greater than."
3. Column 1 is plotted on a log scale, and column 2 is plotted on the probability scale of log-probability graph paper.
4. The best straight line is drawn through the points. If the points do not lie approximately on a straight line, the terminal points are weighted less heavily than the central points.
5. The permeability at 84.1 cumulative per cent is read from the straight line and subtracted from the median permeability. This difference is divided by the median permeability. The ratio is the "permeability variation," (V).

Step 5 in the above procedure translates into the following equation

$$V_{DP} = \frac{k|_{.5} - k|_{.841}}{k|_{.5}} \qquad \text{(III.1)}$$

where

$k|_{.5}$ = permeability at 50%.

$k|_{.841}$ = permeability at 84.1%.

Equation (III.1) is not a coefficient of variation in the standard statistical sense, since $k|_{.5}$ is the median of the distribution and not the mean. Assuming a log-normal permeability distribution, the correct formulation of Eq.(III.1) should really be (Craig, 1971)

$$V_{DP} = \frac{\ln(k)|_{.5} - \ln(k)|_{.841}}{\ln(k)|_{.5}} \qquad \text{(III.2)}$$

Specifying only V_{DP} as in Eq.(III.2) is not sufficient to fix a systems permeability distribution. The average permeability, $\ln(k)|_{.5}$, must also be specified. This is because V_{DP} alone does not fix the standard deviation of the system. In light of this, a better measure is the Craig coefficient , which follows naturally from Eq. (III.2) is given by

$$V_C = V_{DP} \ln(k)|_{.5} \qquad \text{(III.3.a)}$$

or

$$V_C = \ln(k)|_{.5} - \ln(k)|_{.84} \qquad \text{(III.3.b)}$$

Stratified systems having the same Craig coefficient will also have the same permeability distribution and consequently the same flow characteristics. This is demonstrated in Fig.III.2. The Craig coefficient is used in this study as a measure of reservoir heterogeneity rather than the Dykstra-Parsons coefficient. The relation between the two is shown in Fig.III.3.

Dykstra and Parsons did mention some difficulty in trying to match real field data with their analytical method. This may in part have been because of the problem associated with attempting to force a log-normal distribution on real permeability data. Lambert (1981) presented an extensive statistical study of permeability data from 25 fields in which she shows that permeability rarely fits one of the three more commonly used distributions, normal, lognormal, and exponential. Nevertheless, she does make the point that between the three, the

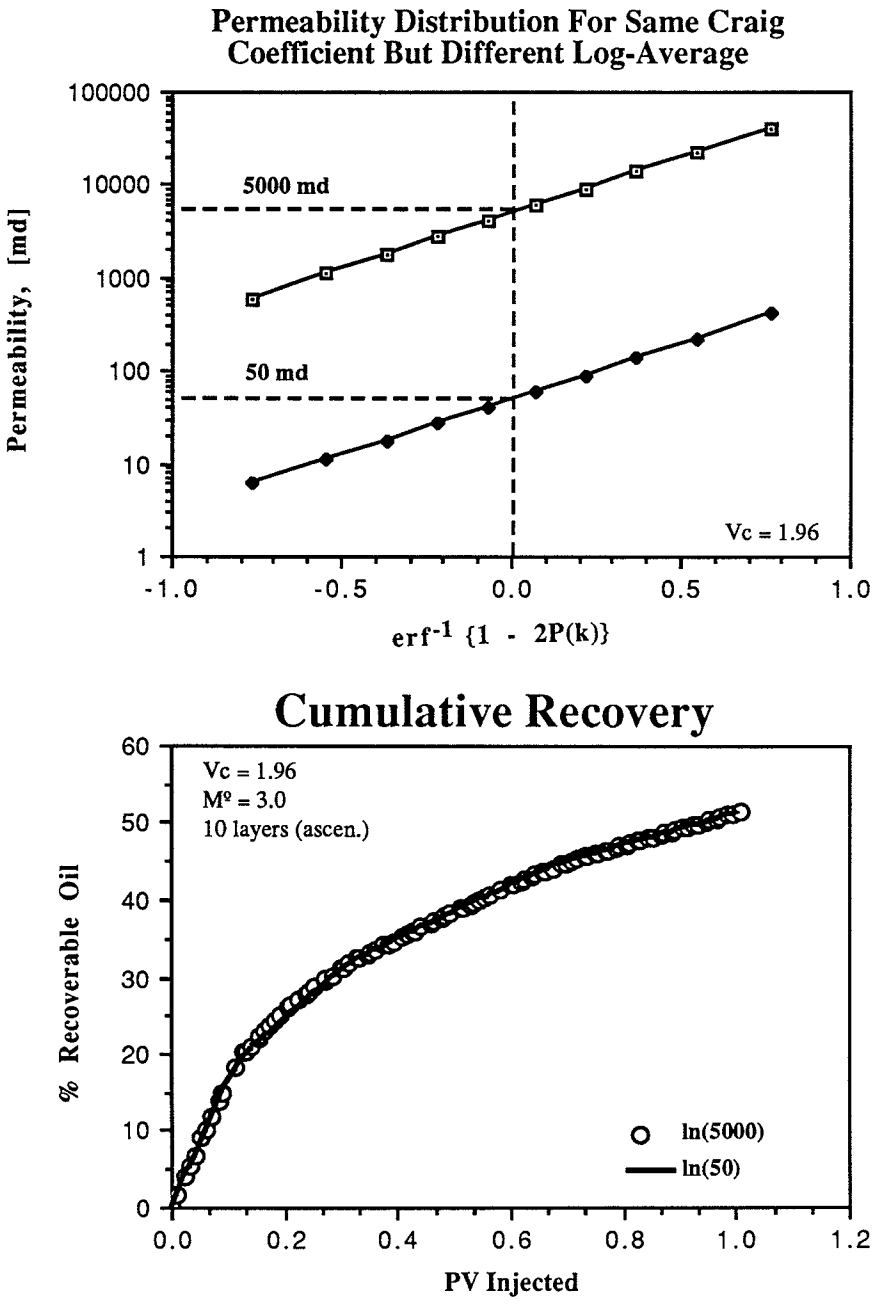

Fig. III.2: Cumulative Recovery for Layered System With Same Vc but Different Log-Average Permeability

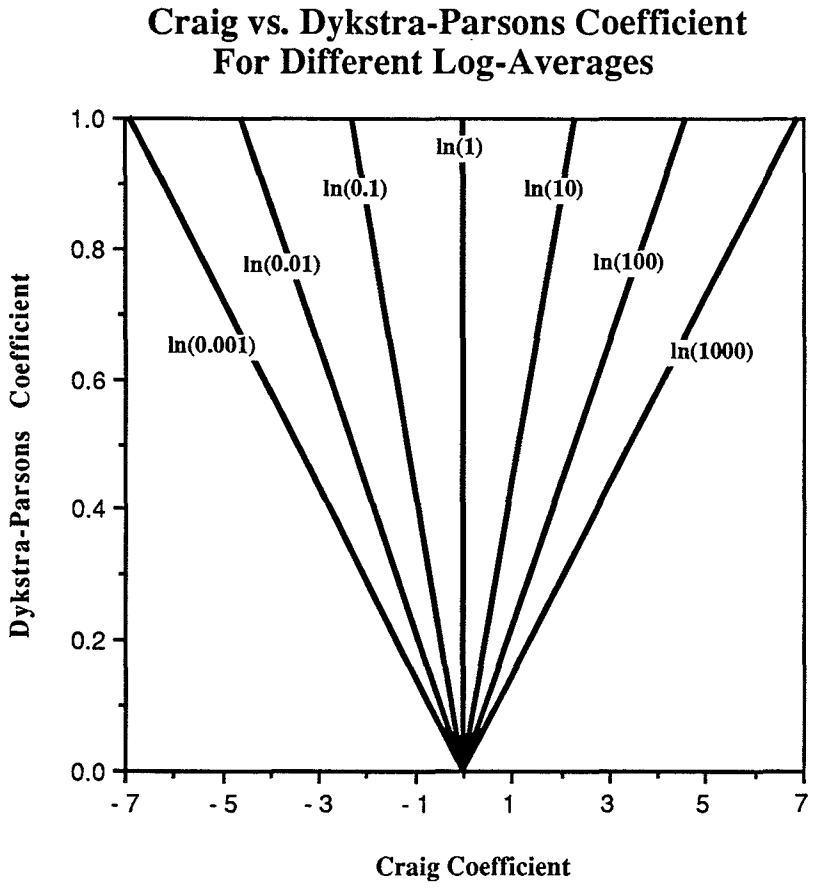

Fig. III.3: Craig vs Dykstra-Parsons Coefficient For Different $\ln(k)|_{.5}$

log-normal appears to fit most of the data best. This is the distribution used in this study as well.

Jensen and Lake (1986) showed that real permeability data which does not exhibit a log-normal distribution can, for certain cases, be made to fit a log-normal distribution by using a power transformation. The magnitude of the power would then be an additional parameter to the Dykstra-Parsons or the Craig Coefficient for characterizing a given set of permeabilities.

3.1.3 GENERATING A LAYERED RESERVOIR WITH GIVEN V_C

The idea is to generate a layered system with a given Craig coefficient. The central assumption is a log-normal distribution for permeability. Let K be the transformation

$$K_i = \ln(k_i) \qquad i=1,...,N \qquad \text{(III.4)}$$

where

K_i = Transformed permeability value of layer i

k_i = Original permeability value of layer i in [md]

N = Number of layers

The normal probability density function for K is given by

$$p(K_i) = \frac{1}{\sqrt{2\pi}\sigma} e^{\frac{-(K_i-\bar{K})^2}{2\sigma^2}} \qquad i=1,...,N \qquad \text{(III.5)}$$

where

$\bar{K}$ = Log average of permeability

σ = Standard deviation

Integrating Eq. (III.5) leads to the cumulative distribution function of K given by

$$P(K_i) = \frac{1}{2}\left[\ 1\text{-erf}\{\frac{(K_i-\bar{K})}{\sqrt{2}\sigma}\}\right] \qquad i=1,...,N \qquad \text{(III.6.a)}$$

where erf is the tabulated error function. By definition, the standard deviation is given by

$$\sigma = K|_{.841} - K|_{.5} = V_C \qquad \text{(III.3)}$$

Solving Eq. (III.6.a) for K_i gives

$$K_i = \bar{K} + \sqrt{2}V_C\ \text{erf}^{-1}\{1-2P(K_i)\} \qquad \text{(III.6.b)}$$

where

$$\bar{K} = \frac{\sum_{i=1}^{N} \ln(k_i)}{N} \qquad \text{(III.7)}$$

$$V_C = \ln(k)|_{.5} - \ln(k)|_{.841} \qquad \text{(III.3.b)}$$

$P(K_i)$ = Cumulative probability

The final value of permeability is then given by transforming back according to Eq. (III.4)

$$k_i = e^{Ki} \qquad i=1,...,N \qquad \text{(III.4)}$$

$P(K_i)$ is the percent of permeability values less or equal to K_i, point #2 in the procedure given by Dykstra and Parsons. $P(K_i)$ can be related to the individual thicknesses of the layers since each layer is homogeneous in itself. It follows

$$P(K_i) = \left\{\sum_{n=1}^{i-1} \frac{h_n}{H}\right\} + \frac{h_i}{2H} \qquad i=1,...,N \qquad \text{(III.8.a)}$$

where i is the layer for which K is to be determined. Equation (III.8.a) is for a discrete (layered) system with the cumulative probability (percentage) being determined at the center of each layer.

Using Eq. (III.6.b) and Eq. (III.8.a) is equivalent to saying that all the data (100%) will fall on a line given by a specific V_C. Yet as Lambert (1981) has shown, permeability values at the low and high end tend to deviate from the log-normal assumption. The permeability data for this study was thus generated by discarding 10% on either end of the distribution, i.e. $0.1 < P(K_i) < 0.9$. Warren and Cosgrove (1964) make a similar argument and come to the conclusion that using the limits above is the proper way to truncate the permeability distribution. Equation (III.8.a) then becomes

$$P(K_i) = 0.1 + 0.8\left[\left\{ \sum_{n=1}^{i-1} \frac{h_n}{H} \right\} + \frac{h_i}{2H} \right] \quad i=1,...,N \qquad \text{(III.8.b)}$$

3.2 VISCOUS CROSSFLOW AND VERTICAL EQUILIBRIUM

While the concept of crossflow may appear simple and straight forward at first, at a closer look it takes on considerable complexity and can become misleading. Crossflow in general may occur as a result of various driving forces such as viscous, capillary, gravity, and dispersive forces. In the discussion that follows and the presentation of the results in Chap.V, only viscous forces are considered in the analysis, a major assumption that should not be forgotten. This does not imply that viscous forces are usually dominant in the mechanism of viscous mixing during a waterflood, rather, it reflects a lack of theoretical development regarding the other forces.

Viscous crossflow effects are divided into two major categories. Those which take place in displacements with an end-point mobility ratio less than one ($M^o < 1$) and those in displacements with an end-point mobility ratio greater than

one ($M^o > 1$). This division occurs naturally since for a mobility ratio equal to one ($M^o = 1$) the solution will be the same for both cases. Contrary to general belief, these displacements are not symmetric about the unit mobility ratio case and show considerable differences in flow behavior (Waggoner et al., 1988).

3.2.1 DISPLACEMENTS WITH $M^o < 1$

For a single homogeneous layer with a piston-like displacement the velocities of each phase are given by

$$v_w = \frac{k}{\phi\Delta S}\lambda^o_{rw}\left(\frac{P_0 - P_x}{x}\right) \qquad \text{(III.9.a)}$$

$$v_o = \frac{k}{\phi\Delta S}\lambda^o_{ro}\left(\frac{P_x - P_L}{L - x}\right) \qquad \text{(III.9.b)}$$

where

k = Absolute permeability

$\phi\Delta S$ = Active porosity, fraction of bulk volume open to flow

$\lambda^o_{rw} = \frac{k^o_{rw}}{\mu_w}$ = End-point water mobility

$\lambda^o_{ro} = \frac{k^o_{ro}}{\mu_o}$ = End-point oil mobility

k^o_{rw}, k^o_{ro} = End-point relative permeabilities of water and oil

μ_w, μ_o = Water and oil viscosities

P = Pressure.

Because material balance must be satisfied and the assumption of incompressible fluids has been made, the velocities of the two phases must be equal at the interface and thus

$$v_w = v_o \tag{III.10}$$

Solving Eq. (III.10) for the unknown pressure P_x gives

$$P_x = \frac{M^o \frac{P_0}{x} + \frac{P_L}{L - x}}{M^o \frac{1}{x} + \frac{1}{L - x}} \tag{III.11}$$

where

$$M^o = \frac{\lambda^o_{rw}}{\lambda^o_{ro}} = \text{End-point mobility ratio.}$$

The pressure profile is shown in Fig.III.4. Applying the same equations to a two-layered non-communicating system with different absolute permeabilities in each layer will lead to pressure profiles shown in Fig.III.5.

Figure III.5 also shows the direction in which crossflow would occur for an end-point mobility ratio less than one if one were to allow, instantaneously, a finite vertical permeability. The largest transverse pressure gradients occur at the front positions. Because of the direction of these gradients water will crossflow from the top (fast) layer to the bottom (slow) layer at the trailing front and oil will crossflow from the bottom layer to the top layer at the leading front. In both cases only one phase , either water or oil, is crossflowing into the other layer. The net effect is that the distance between the two fronts is decreased compared to the no-crossflow case. The flow remains segregated since water, crossflowing from the top layer to the bottom layer at the trailing front, has a mobility less than the oil and therefore will remain behind the oil-water interface. Similarly, the oil crossflowing at the leading front from the bottom layer to the top layer will remain ahead of the interface because of the higher mobility. In the limiting case of vertical equilibrium, the vertical permeability can be thought as being infinite and the pressure drop approaching zero since the amount of fluid crossflowing must remain finite (Zapata and Lake, 1979).

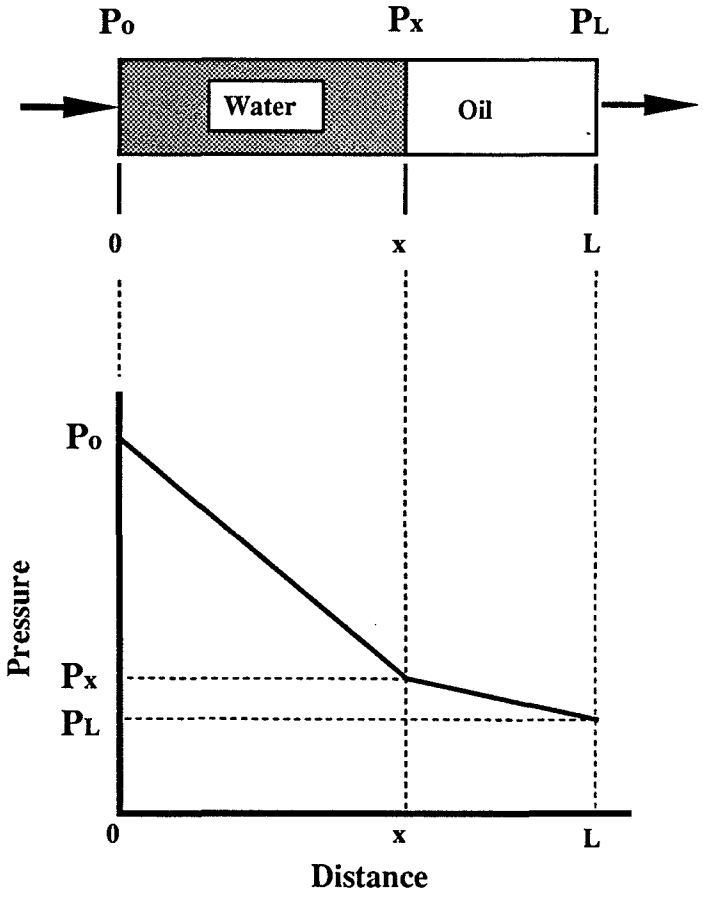

Fig. III.4: Schematic Pressure Profile For Piston-Like Displacement in a Single Layer ($M^o < 1$)

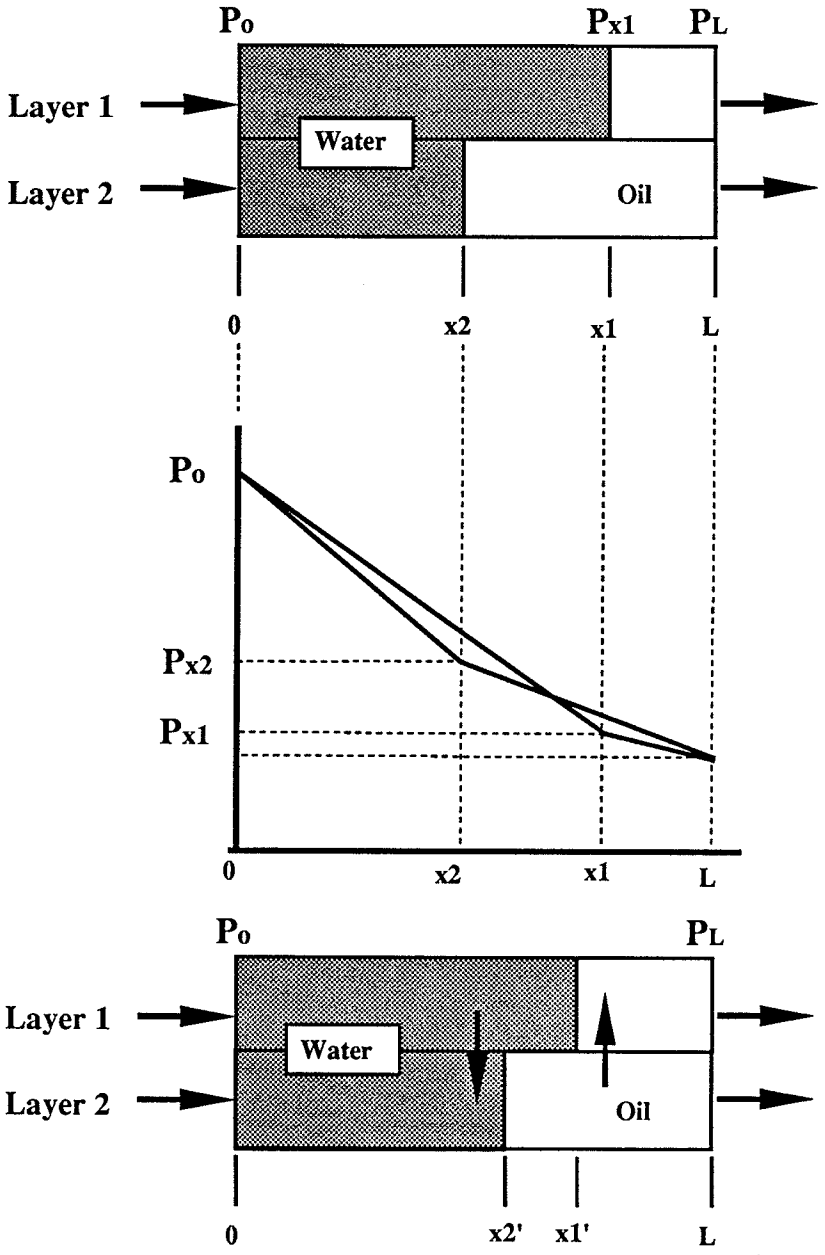

Fig. III.5: Schematic Pressure Profiles And Crossflow Direction For Piston-Like Displacement in Two Layers ($M^o < 1$)

One of the problems with representing viscous crossflow as in Fig. III.5 is the incorrect belief that some of the water from the fast layer may crossflow into the oil ahead of the trailing front and some of the oil in the slow layer may crossflow into the water behind the leading front. This does not happen. Because vertical equilibrium is present from the start of the flood, any viscous crossflow will occur instantaneously at the fronts and keep the flow segregated. That is, the transverse pressure drop will be zero everywhere except for a delta-like change at the fronts (Zapata, 1979) which will redistribute fluids infinitely fast in order to maintain vertical equilibrium.

An interesting exercise associated with the distance between the fronts decreasing due to viscous crossflow for a favorable end-point mobility displacement, compared to the no crossflow case, is to show that an end-point mobility ratio can be picked such that all reservoir heterogeneity will be suppressed and the fronts will travel together. The velocities in each layer are given by Darcy's Law

$$v_1 = \left(\frac{k}{\phi \Delta S}\right)_1 \lambda^o_{r1} \left(\frac{dP}{dx}\right)_1 \qquad \text{(III.9.c)}$$

$$v_2 = \left(\frac{k}{\phi \Delta S}\right)_2 \lambda^o_{r2} \left(\frac{dP}{dx}\right)_2 \qquad \text{(III.9.d)}$$

If the system is in vertical equilibrium the sum of all driving forces in the vertical direction will be equal to zero. Allowing viscous forces only, the vertical equilibrium condition reduces to

$$\left(\frac{dP}{dx}\right)_1 = \left(\frac{dP}{dx}\right)_2 \qquad \text{(III.12)}$$

Assuming equal porosity and mobile phase saturation for both layers

$$\frac{v_1}{v_2} = \frac{k_1}{k_2} M^o = \frac{dx_1}{dx_2} \qquad \text{(III 13.a)}$$

Integrating Eq. (III.13.a) with $x_1|_0 = 0$ and $x_2|_0 = 0$ yields

$$x_1 = x_2 \frac{k_1}{k_2} M^o \qquad \text{(III.13.b)}$$

and shows that for

$$M^o = \frac{k_2}{k_1} \qquad \text{(III.13.c)}$$

the fronts will travel together.

3.2.2 DISPLACEMENTS WITH $M^o > 1$

For displacements with $M^o > 1$ much of the same qualitative arguments can be used as in the previous case ($M^o < 1$). For a piston-like displacement in a single homogeneous medium, the equations remain the same. For a two-layered system, with sharp-front displacement, the pressure profiles and the corresponding directions of crossflow are shown in Fig. III.6. In comparison to the $M^0 < 1$ case, crossflow is now reversed at each of the front positions. One immediate result, paralleling the previous case, is that the leading front will speed up while the trailing front is retarded. In addition, there is a second phenomenon taking place called viscous mixing (Zapata and Lake, 1981). Because of the reversal of the vertical pressure gradient, there are now two phases crossflowing at each front instead of one. Water and oil at the trailing front crossflowing into the water of the top layer and water and oil at the leading front crossflowing in to the oil of the bottom layer. The net effect is the development of a mixing zone between the two fronts. Mixing zone means that water saturations other than the residual phase saturations exist. Contrary to the $M^o<1$ case, the flow no longer remains segregated. This is because oil crossflowing from the bottom layer into the top layer at the trailing front has a lower end-point mobility than the water, and the

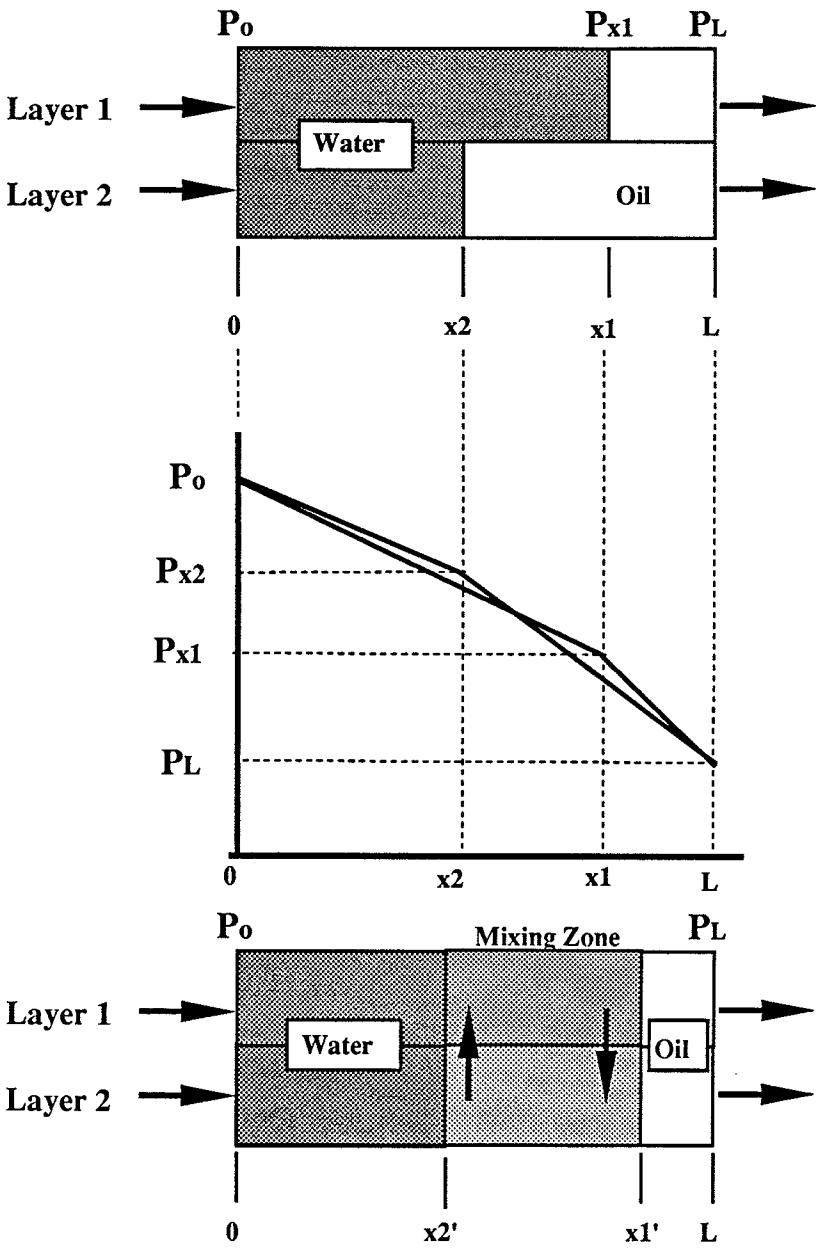

Fig. III.6: **Schematic Pressure Profiles And Crossflow Direction For Piston-Like Displacement in Two Layers ($M^o > 1$)**

water crossflowing from the top layer into the bottom layer at the leading edge has a higher mobility than the oil. With the change in the end-point mobilities and the direction of crossflow the systems preferred state is that of a mixing zone and does not tend to the restoration of segregated flow as in the $M^o<1$ case.

Zapata and Lake (1981) have shown that viscous mixing and viscous crossflow improve recovery compared to the solution assuming segregated flow (Hearn, 1971) and are therefore beneficial to the displacement. This because the oil in the slow layer is produced in part by the fast layer as a result of crossflow and consequently will show up earlier at the production well compared to the no-crossflow case. Furthermore, because the fronts do not tend to move apart to extent they do without viscous mixing, the overall sweep efficiency will be improved.

3.2.3 A Scaling Parameter for Vertical Equilibrium

The assumption of an infinite vertical permeability is, of course, unrealistic. But as the analogy to the heat conduction problem mentioned in Chap.II indicates (Coats et al., 1971), vertical equilibrium may be attained for reservoirs where the vertical permeability is finite but where other dimensions of the reservoir make the assumption a reasonable one.

A scaling parameter, called the reservoir effective length-thickness ratio has been proposed in the literature as the appropriate dimensionless group to use for identifying vertical equilibrium (Rapoport, 1955; Goddin et. al., 1966). From Darcy's Law, the vertical and horizontal flowrates of a layered system with finite permeabilities in each direction is given by

$$Q_V = k_{eV}\, WL\, \lambda^o_{eV} \left(\frac{\Delta P_H}{H}\right) \qquad \text{(III.14.a)}$$

$$Q_H = k_{eH}\, WH\, \lambda^o_{eH} \left(\frac{\Delta P_L}{L}\right) \qquad \text{(III.14.b)}$$

$$\frac{1}{k_{eV}} = \frac{1}{H}\sum_{i=1}^{N}\frac{1}{k_i} \qquad \text{(III.15)}$$

$$k_{eH} = \frac{1}{H}\sum_{i=1}^{N} k_i \qquad \text{(III.16)}$$

where

k_{eV} ,k_{eH} = Effective vertical and horizontal permeabilities

W, L, H = Width, length, and height of the system

λ^o_{eV} ,λ^o_{eH} = Effective vertical and horizontal end-point mobilities

$\frac{\Delta P_H}{H}$,$\frac{\Delta P_L}{L}$ = Vertical and horizontal pressure gradients

The ratio of the flowrates is then given by

$$\frac{Q_V}{Q_H} = \frac{k_{eV}}{k_{eH}}\frac{L^2}{H^2}\frac{\lambda^o_{eV}}{\lambda^o_{eH}}\frac{\Delta P_H}{\Delta P_L} \qquad \text{(III.17)}$$

with the dimensionless group

$$R_L = \frac{L}{H}\sqrt{\frac{k_{eV}}{k_{eH}}} \qquad \text{(III.18)}$$

naturally following from Eq. (III.17). R_L is called the effective length-thickness ratio.

For the limiting case where the vertical permeability is zero, i.e no communication between the layers, R_L is zero. For the limiting case of infinite vertical permeability R_L tends to infinity. It is important to note that the ratio of the flowrates given by Eq. (III.17) must always remain finite. Therefore, as R_L tends

to infinity the vertical pressure gradient must tend to zero. The two limiting cases are thus given by

$$R_L = 0 \qquad k_{eV} = 0 \text{ (no communication)}$$

$$R_L \rightarrow \infty \qquad k_{eV} \rightarrow \infty \text{ (vertical equilibrium)}$$

Using R_L as the sole scaling parameter for vertical equilibrium is only correct in the absence of any other driving forces. Zapata gives $R_L > 10$ as a realistic limit for the onset of vertical equilibrium. Waggoner (1985), presenting a sensitivity of R_L on the fractional flow curve for a two-dimensional displacement, concludes that $R_L > 10$ is probably a conservative limit and suggests that for an $R_L > 5$ all the displacements can confidently be represented using the same pseudofractional flow curve. Figures III.7, III.8, and III.9 showing the sensitivity of a typical layered system used in this study on R_L, are in line with these conclusions.

For this investigation an R_L of approximately sixteen ($R_L \approx 16$) was used throughout all simulation runs.

3.3 THE DYKSTRA AND PARSONS MODEL ($R_L = 0$)

As mentioned in Chap.II, the Dykstra and Parsons model is easily the most widely used method to describe immiscible displacements in non-communicating layered systems. The assumptions central to the Dykstra and Parsons model are

1. Horizontal, two-phase, incompressible, and immiscible flow
2. No gravity, capillary pressure, or dispersion
3. Piston-like displacement
4. No communication between layers
5. Layers are homogeneous within themselves

The velocity in each layer can be related to the total pressure drop of the system (which is the same for both layers) by substituting Eq. (III.11) into either Eq. (III.9.a) or Eq. (III.9.b). Substituting into Eq. (III.9.a) gives

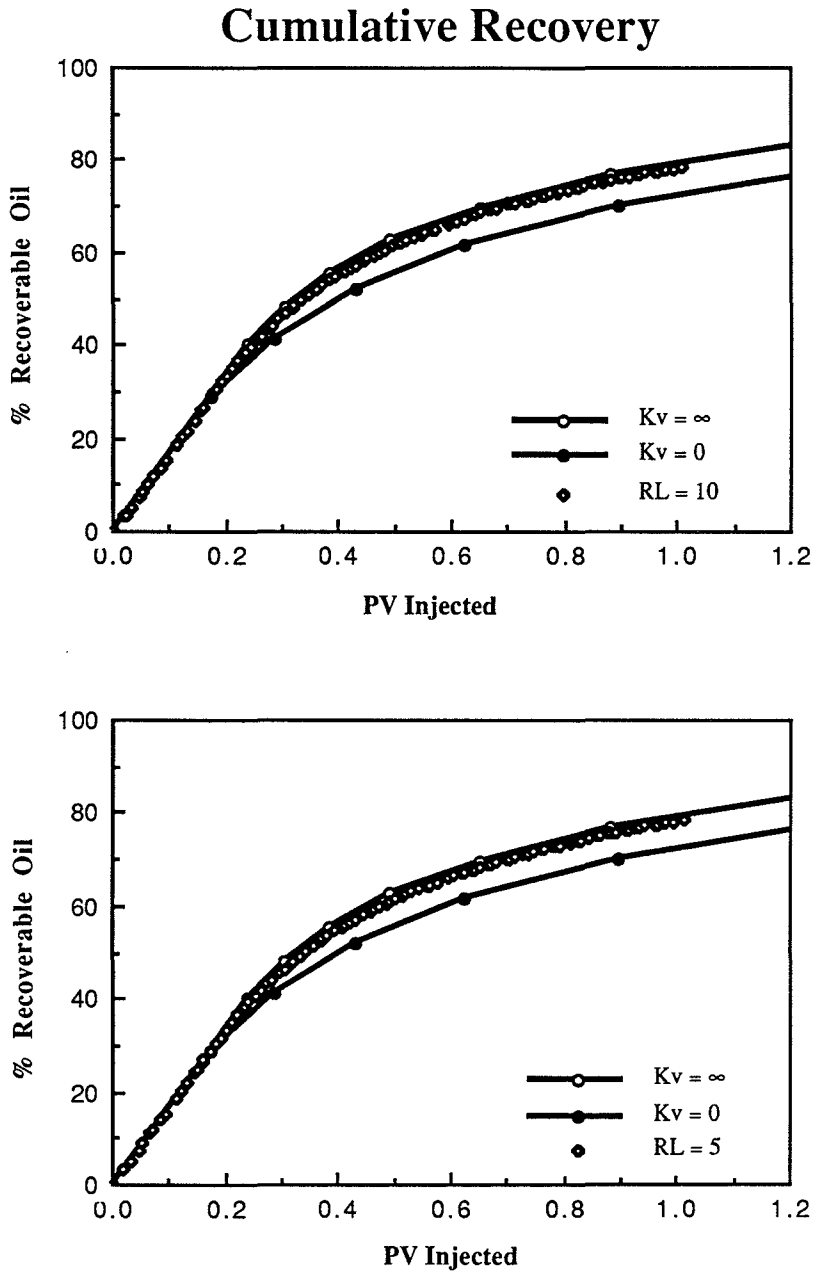

Fig. III.7: Dimensionless Time vs. Recovery For Different R_L (M^o=0.5)

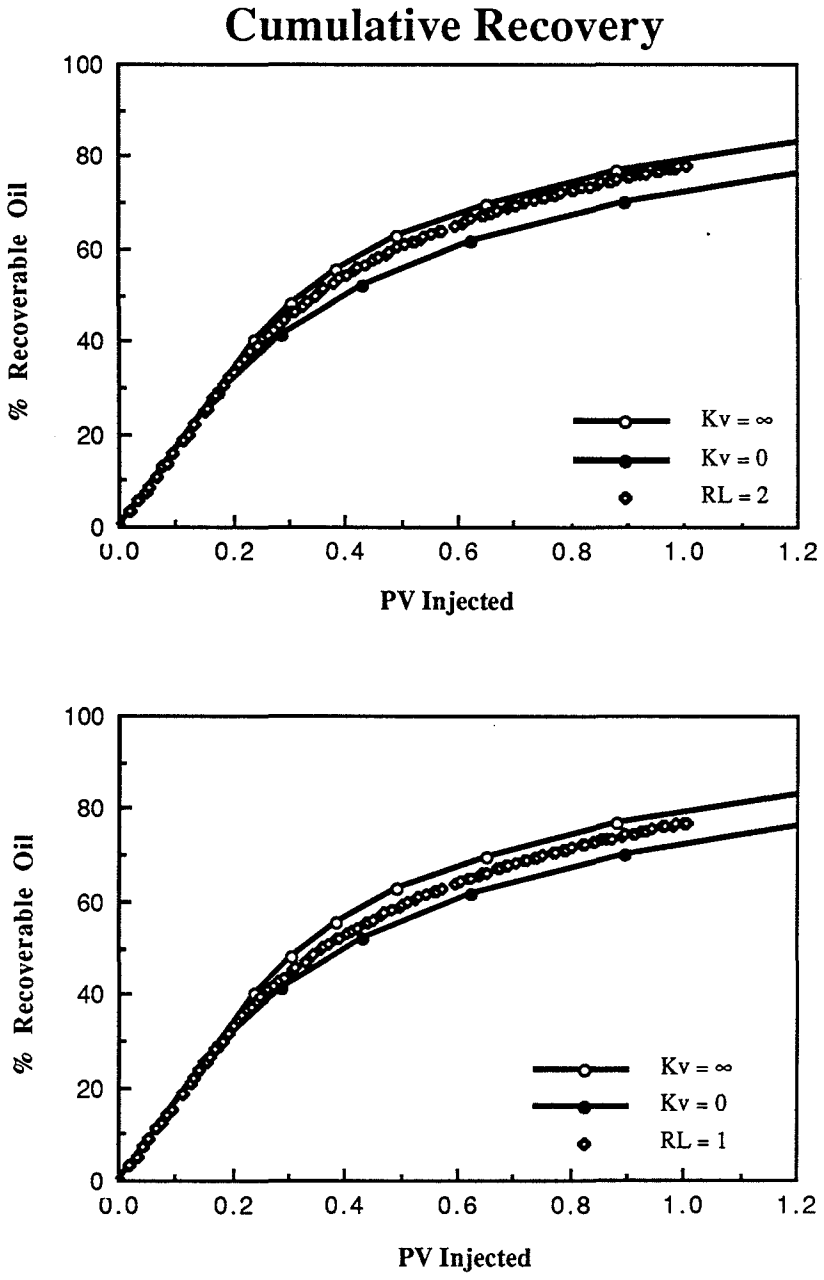

Fig. III.8: **Dimensionless Time vs. Recovery For Different R_L (M^o=0.5)**

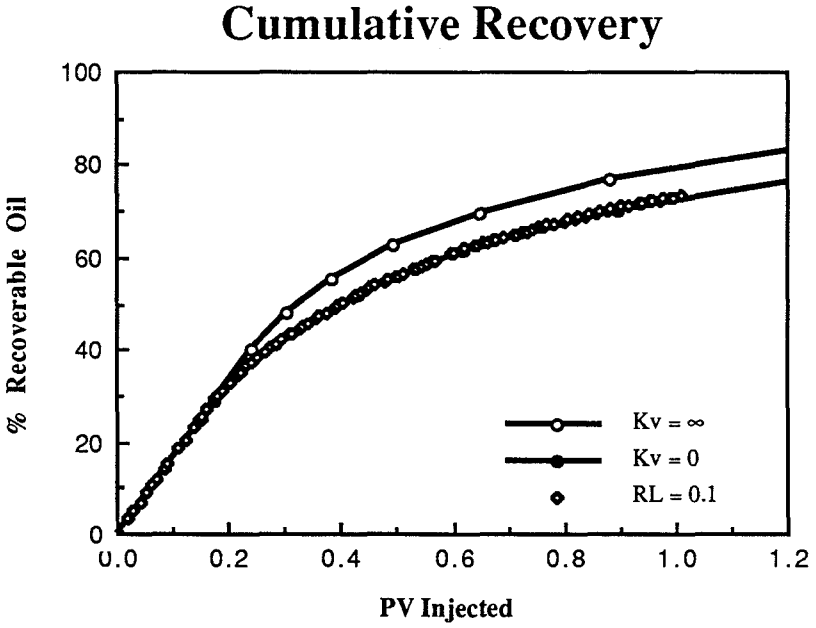

Fig. III.9: **Dimensionless Time vs. Recovery For Different R_L (M^o=0.5)**

$$v_1 = \frac{dx_1}{dt} = \left(\frac{k}{\phi \Delta S}\right)_1 \left(\frac{\lambda^o_{r1}}{x_1 + M^o(1-x_1)}\right) \Delta P \qquad \text{(III.19.a)}$$

$$v_2 = \frac{dx_2}{dt} = \left(\frac{k}{\phi \Delta S}\right)_2 \left(\frac{\lambda^o_{r1}}{x_2 + M^o(1-x_2)}\right) \Delta P \qquad \text{(III.19.b)}$$

Taking the ratio of the velocities eliminates the time dependance

$$\frac{v_1}{v_2} = \frac{dx_1}{dx_2} = \frac{\left(\frac{k}{\phi \Delta S}\right)_1}{\left(\frac{k}{\phi \Delta S}\right)_2} \frac{x_2 + M^o(1-x_2)}{x_1 + M^o(1-x_1)} \qquad \text{(III.20.a)}$$

where

x_1 = Dimensionless front position in layer 1

x_2 = Dimensionless front position in layer 2

and

$$\frac{\left(\frac{k}{\phi \Delta S}\right)_1}{\left(\frac{k}{\phi \Delta S}\right)_2} = r_{12} = \text{Heterogeneity factor.} \qquad \text{(III.21)}$$

Eq. (III.20.a) can be rewritten as

$$\left(x_1 + M^o(1-x_1)\right) dx_1 = r_{12} \left(x_2 + M^o(1-x_2)\right) dx_2 \qquad \text{(III.20.b)}$$

Integrating Eq. (III.20.b) with boundary conditions $x_1 = 0$ to $x_1 = 1$ (breakthrough) and $x_2 = 0$ to $x_2 = x_2^0$ gives

$$x_2^0 = \sqrt{\frac{1}{(\frac{1}{M^o} - 1)^2} + \frac{1 + M^o}{r_{12}(1 - M^o)}} + \frac{1}{1 - \frac{1}{M^o}} \qquad \text{(III.20.c)}$$

for $M^o \neq 1$ and $r_{12} > 1$

x_2^0 is the front position in layer 2 when layer 1 breaks through. For the unit mobility case, Eq. (III.20.b) becomes

$$dx_1 = r_{12}\, dx_2 \qquad \text{(III.20.c)}$$

Integrating Eq. (III.20.b) with boundary conditions $x_1 = 1$ to $x_1 = x_1'$ and $x_2 = x_2^0$ to $x_2 = 1$ (sweepout) gives

$$x_1' = \frac{M^o r_{12}}{2}\left\{(\frac{1}{M^o} - 1)\,(1 - (x_2^0)^2) + 2(1 - x_2^0)\right\} + x_2^0 \qquad \text{(III.20.d)}$$

where x_1' is now greater than one and represents a fictitious front position outside the system when layer 2 breaks through. The above procedure for two layers can easily be generalized to N.

For layer n breaking through, the front positions in layers with permeabilities less than k_n, i.e. layers not broken through yet, are given by

$$x_i^0 = \sqrt{\frac{1}{(\frac{1}{M^o} - 1)^2} + \frac{1 + M^o}{r_{in}(1 - M^o)}} + \frac{1}{1 - \frac{1}{M^o}} \qquad \text{(III.20.c)}$$

The front positions for layers already broken through are given by

$$x_i = \frac{M^o r_{in}}{2}\left\{(\frac{1}{M^o} - 1)\,(1 - (x_n^0)^2) + 2(1 - x_n^0)\right\} + x_n^0 \qquad \text{(III.20.d)}$$

x_n, of course, is equal to one. The total recovery versus time is then simply given by

$$t_D = \frac{\sum_{i=1}^{N} (\phi\Delta S)_i \, h_i \, x_i}{(\overline{\phi\Delta S}) \, H} \qquad \text{(III.21)}$$

$$N_{PD} = \frac{\sum_{i=1}^{n} (\phi\Delta S)_i + \sum_{i=n+1}^{N} (\phi\Delta S)_i \, h_i \, x_i}{(\overline{\phi\Delta S}) \, H} \qquad \text{(III.22)}$$

where

t_D = $\frac{\text{volume injected}}{\text{total pore volume}}$ = dimensionless time.

N_{PD} = $\frac{\text{total oil produced}}{\text{total movable oil}}$ = dimensionless recovery.

3.4 THE HEARN MODEL ($R_L \rightarrow \infty$)

The assumptions in the Hearn model are the same except for vertical communication difference. Thus, the assumptions here are

1. Horizontal, two-phase, incompressible, and immiscible flow
2. No gravity, capillary pressure, or dispersion
3. Piston-like displacement
4. Perfect vertical communication between layers
5. Layers are homogeneous within themselves

The derivation that follows parallels that given by Hearn (1971). For an end-point mobility ratio less than or equal to unity ($M^o \leq 1$) the flow remains segregated and the average water fractional flow at cross-section A in Fig. III.10 is given by

$$\tilde{f}_w|_A = \frac{Q_{w1} + Q_{w2}}{Q_T} = \frac{Q_{w1} + Q_{w2}}{Q_{w1} + Q_{w2} + Q_{o3} + Q_{o4}} \qquad \text{(III.23.a)}$$

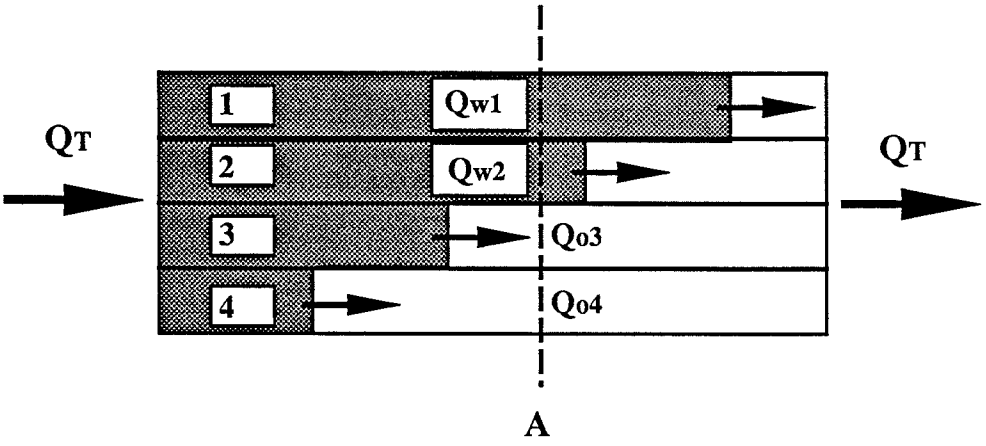

Fig. III.10: Hearn Layered Reservoir Model

From Darcy's Law, the flowrates are given by

$$Q_{w1} = - k_1 h_1 \lambda^o_{w1} \left(\frac{dP}{dx}\right)_1 \qquad \text{(III.24.a)}$$

$$Q_{w2} = - k_2 h_2 \lambda^o_{w2} \left(\frac{dP}{dx}\right)_2 \qquad \text{(III.24.b)}$$

$$Q_{o3} = - k_3 h_3 \lambda^o_{o3} \left(\frac{dP}{dx}\right)_3 \qquad \text{(III.24.c)}$$

$$Q_{o4} = - k_4 h_4 \lambda^o_{o4} \left(\frac{dP}{dx}\right)_4 \qquad \text{(III.24.d)}$$

For vertical equilibrium the vertical pressure gradient is zero everywhere, thus

$$\left(\frac{dP}{dx}\right)_1 = \left(\frac{dP}{dx}\right)_2 = \left(\frac{dP}{dx}\right)_3 = \left(\frac{dP}{dx}\right)_4 \qquad \text{(III.25)}$$

Substituting Eq. (III.24.a) through Eq. (III.24.d) into Eq. (III.23.a)

$$\tilde{f}_w = \frac{k_1 h_1 \lambda^o_{w1} + k_2 h_2 \lambda^o_{w2}}{k_1 h_1 \lambda_{w1} + k_2 h_2 \lambda^o_{w2} + k_3 h_3 \lambda^o_{o3} + k_4 h_4 \lambda^o_{o4}} \qquad \text{(III.23.b)}$$

Rearranging

$$\tilde{f}_w = \left[1 + \frac{1}{M^o} \frac{\sum_{i=3}^{4} k_i h_i}{\sum_{i=1}^{2} k_i h_i} \right]^{-1} \qquad \text{(III.23.c)}$$

Notice that $\tilde{f}_w$ is simply the thickness averaged fractional flow and is valid for any cross-section since it is not position dependant. The corresponding thickness averaged water saturation is

$$\tilde{S}_w = \frac{\sum_{i=1}^{2} \{\phi \Delta S h (1 - S_{or})\}_i + \sum_{i=3}^{4} \{\phi \Delta S h S_w\}_i}{(\phi \overline{\Delta S}) H} \qquad \text{(III.24)}$$

because the displacement is assumed piston-like. Equations (III.23.c) and (III.24) are trivially expanded to N layers by changing the limits on the summation signs.

Effectively, Eq.(III.23.c) and Eq.(III.24) make the problem one-dimensional allowing the total recovery versus time curve to be determined using a standard Welge construction (Welge, 1952). If only water is injected, the average water saturation of the system is given by

$$\overline{S}_w = \tilde{S}_{we} - \frac{1}{\left.\frac{d\tilde{f}_w}{d\tilde{S}_w}\right|_{\tilde{S}_{we}}}\left[\tilde{f}_{we} - 1\right] \qquad \text{(III.25)}$$

where

$\tilde{S}_{we}$ = Effluent water saturation - (III.24).

$\tilde{f}_{we}$ = Effluent water fractional flow - (III.23.c)

$\left.\frac{d\tilde{f}_w}{d\tilde{S}_w}\right|_{\tilde{S}_{we}}$ = Derivative of fractional flow curve at $\tilde{S}_{we}$

From the Welge construction

$$t_D = \frac{1}{\left.\frac{d\tilde{f}_w}{d\tilde{S}_w}\right|_{\tilde{S}_{we}}} \qquad \text{(III.26)}$$

$$N_{PD} = \frac{\overline{S}_w - \tilde{S}_{wi}}{1 - \tilde{S}_{or} - \tilde{S}_{wr}} \qquad \text{(III.27)}$$

where

$$\tilde{S}_{wi} = \frac{\sum_{i=1}^{N} \{\phi h S_{wi}\}_i}{\overline{\phi} H} \qquad \text{(III.28)}$$

$$\tilde{S}_{or} = \frac{\sum_{i=1}^{N} \{\phi h S_{or}\}_i}{\overline{\phi} H} \qquad \text{(III.29)}$$

$$\tilde{S}_{wr} = \frac{\sum_{i=1}^{N} \{\phi h S_{wr}\}_i}{\overline{\phi} H} \qquad \text{(III.30)}$$

and t_D and N_{PD} are, respectively, the dimensionless time (PV Injected) and the dimensionless recovery as in the Dykstra and Parsons model.

CHAPTER IV

FINITE DIFFERENCE SIMULATION

The numerical code used for this study was an incompressible, two-phase, two-dimensional finite difference simulator. The code was originally written by McDonald (1969) and later modified by Zapata (1979). Modifications by this author were minimal.

A brief description of the simulator and how it was used is presented in this chapter. For a more in depth mathematical presentation the reader is referred to Zapata's thesis and McDonald's report as well as to an extensive body of literature on the subject.

4.1 EQUATIONS AND FINITE DIFFERENCE FORMULATION

For a simple two-dimensional, two-phase (oil-water), incompressible system with no gravity, capillary pressure, adsorption, or dispersion and a single component in each phase, the material balance equations for a representative element volume (REV) with constant porosity are given by

$$\phi \frac{\partial S_o}{\partial t} + \nabla \cdot \vec{u}_o = 0 \qquad \text{(IV.1)}$$

$$\phi \frac{\partial S_w}{\partial t} + \nabla \cdot \vec{u}_w = 0 \qquad \text{(IV.2)}$$

with the constraining equation

$$S_w + S_o = 1 \qquad \text{(IV.3)}$$

where

$$\vec{u}_j = -\left\{\frac{k_{rj}}{\mu_j}\right\} \vec{\vec{k}} \cdot \nabla P \qquad j=o,w \qquad \text{(IV.4)}$$

ϕ = Porosity of the medium

S_w, S_o = Water and oil saturation

$\vec{u}_j$ = Darcy velocity for phase j

k_{rj} = Relative permeability of medium to phase j

μ_j = Viscosity of phase j

$\vec{\vec{k}}$ = Permeability tensor

P = Pressure

∇ = Gradient operator

By substituting Eq. (IV.3) into (IV.2) and adding (IV.2) with (IV.1) the time derivative is eliminated leaving the following partial differential equation to be solved

$$f(S_w, P) = \nabla \cdot \left(\vec{\vec{\lambda}} \cdot \nabla P\right) = 0 \qquad \text{(IV.5.a)}$$

where the total mobility $\vec{\vec{\lambda}}$ tensor is defined as

$$\vec{\vec{\lambda}} = -\left\{\frac{k_{ro}}{\mu_o} + \frac{k_{rw}}{\mu_w}\right\}\vec{\vec{k}} \qquad \text{(IV.6)}$$

At the wells Eq. (IV.5.a) becomes

$$f(S_w, P) = \nabla\cdot\left(\vec{\vec{\lambda}}\cdot\nabla P\right) - q = 0 \qquad \text{(IV.5.b)}$$

The differential form of Eq. (IV.5.b) was discretized using a five-point finite differencing scheme in two dimensions yielding

$$\begin{aligned} &T_{y_{i+0.5,j}}P_{i+1,j} + T_{x_{i,j+0.5}}P_{i+1,j+1} \\ &- \left(T_{y_{i+0.5,j}} + T_{x_{i,j+0.5}} + T_{y_{i-0.5,j}} + T_{x_{i,j-0.5}}\right) P_{i,j} \\ &+ T_{y_{i-0.5,j}}P_{i-1,j} + T_{x_{i,j-0.5}}P_{i-1,j+1} - q_{i,j} = 0 \end{aligned} \qquad \text{(IV.7)}$$

where

T_x ,T_y = Transmissibility in the x-direction and y-direction

Equation (IV.7) is, in general, a first -order correct approximation of Eq. (IV.5.b). For the special case of uniform Δx and Δy Eq.(IV.7) becomes second-order correct.

4.2 SOLUTION TECHNIQUE

Equation (IV.7) is solved for the entire system implicitly in pressure and semi-implicitly in saturation. Contrary to the more common IMPES solution method (IMplicit in Pressure and Explicit in Saturation), the semi-implicit formulation approximates the new relative permeability value in the transmissibility using a Taylor Series expansion of the form

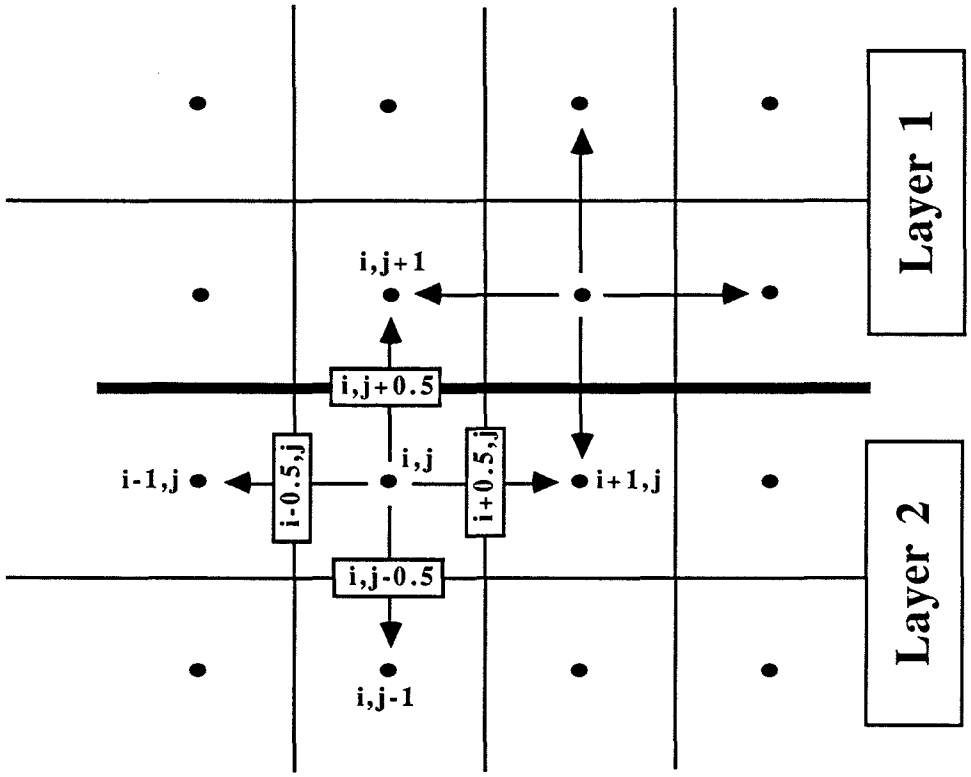

Fig. IV.1: Numbering Scheme in Finite Difference Formulation

$$k_{rw}^{n+1} = k_{rw}^{n} + \left(\frac{dk_{rw}}{dS_w}\right)^{n} \left\{ S_w^{n+1} - S_w^{n} \right\} \qquad \text{(IV.8)}$$

where

n = Old time level

$n+1$ = New time level

$\frac{dk_{rw}}{dS_w}$ = Derivative of relative permeability curve at S_w^n

Equation (IV.8) is combined with either Eq.(IV.1) or Eq.(IV.2) to form the saturation equation. The saturation is computed by using the pressure calculated from Eq.(IV.7) which in turn was calculated using the relative permeabilities at the old time level. This method is referred to as a sequential approach with semi-implicit transmissibilities.

4.3 RELATIVE PERMEABILITY CURVES

One of the central assumption of the Hearn model is segregated flow occurring in a piston-like fashion. Numerically, this is achieved by using specific permeability curves. Furthermore, the fact that sharp-front displacement in this study is to be achieved for end-point mobility ratios greater than one, imposes a further restriction on the possible choices of the relative permeability curves. The relative permeability curves used here and the associated fractional flow curves for different end-point mobility ratios are shown in Fig. IV.2. These are the same as those used by Zapata (1979) in his investigation of viscous mixing in two-layered permeable media. The resulting sharp front displacements in the simulator for end-point mobility ratios of one and five are shown in Fig. IV.3. The relative permeability curves were never changed in the course of this investigation. Only the viscosities were used to control the end-point mobility ratio.

One of the problems associated with using relative permeability curves as in Fig. IV.2 is the numerical instability they introduce. This is because the semi-

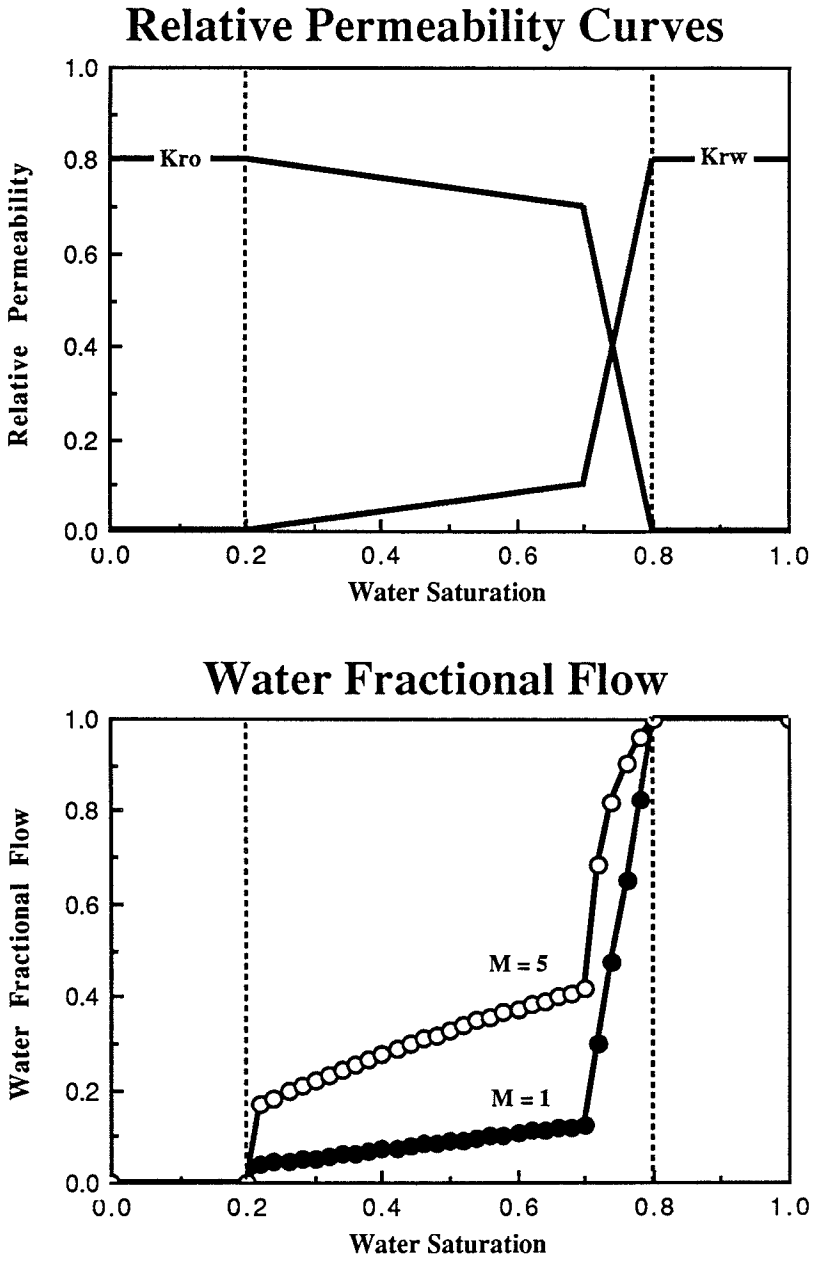

Fig. IV.2: **Relative Permeabilities and Associated Fractional Flow Curves for End-Point Mobility Ratios of One and Five (1-D)**

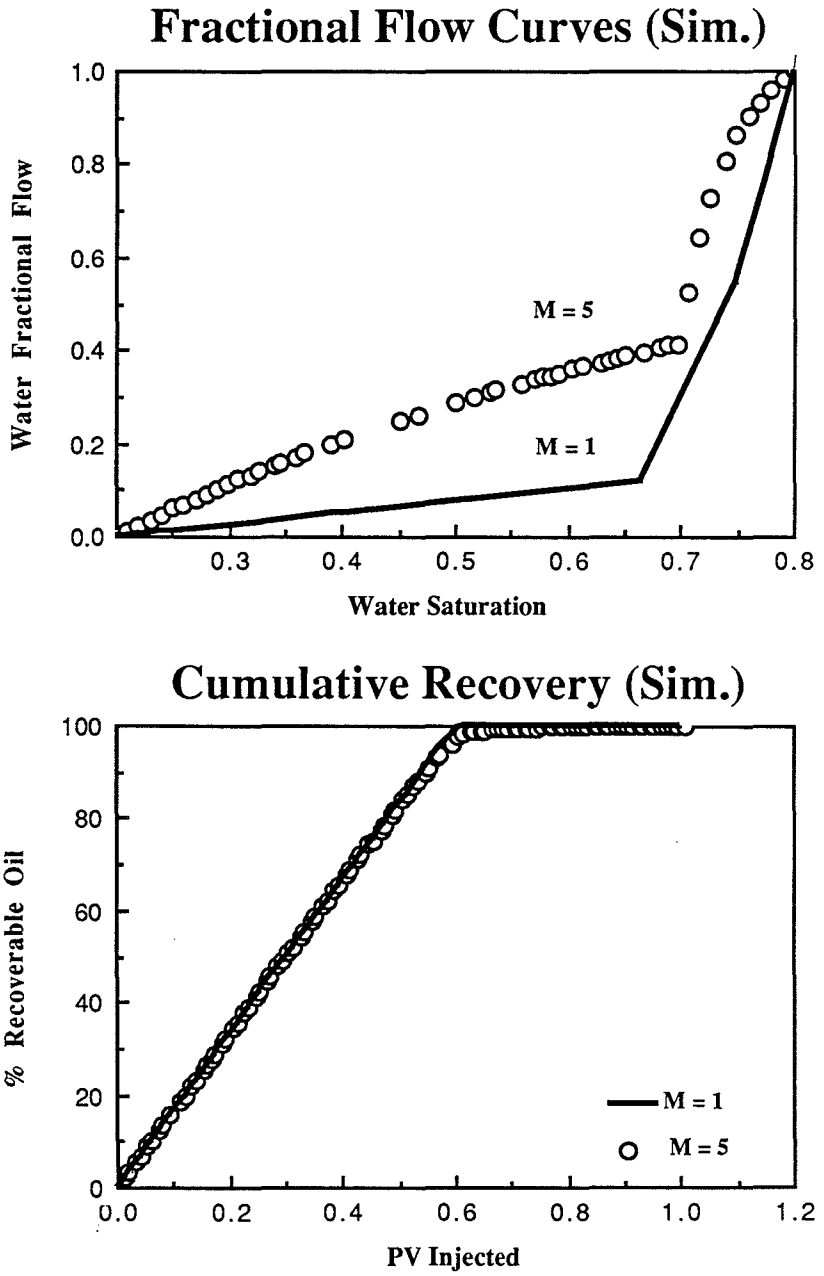

Fig. IV.3: Simulated Piston-Like Displacement for End-Point Mobility Ratios of One and Five (1-D)

implicit method uses the slope of the relative permeability curve at the old time level. If the derivative of the relative permeability curve at the new saturation is the same as the old one, then Eq. (IV.8) is exact and the solution will be correct. If, on the other hand, the new slope is not the same there will be an overshooting of the saturation caused by the drastic difference in the slopes of the relative permeability curves. An automatic time-step selector in the program guards against using the wrong slope to estimate the new saturation. As a result, the material balance error introduced is practically zero.

CHAPTER V

RESULTS AND DISCUSSION

The form and simplicity of the Hearn model make a pseudofunction approach to correct for viscous mixing and viscous crossflow, occurring in displacements with end-point mobility ratios greater than one, an attractive solution. Pseudofunction, in this case, means retaining the original form of the Hearn model but introducing effective parameters in the formulation, such as an effective end-point mobility ratio or effective permeability-height products that will result in a good approximation of the physical displacement. As discussed in Chap.III, the Hearn model is not physically correct for displacements with a true end-point mobility ratio greater than one since it assumes segregated flow and can not account for increased recovery resulting from viscous mixing. The general idea in modifying the Hearn model is that the displacement, while it is physically taking place with a given set of physical properties, may be overall modeled as if it were conducted with a different, effective set of physical properties. A similar approach that has led to successful modeling of miscible displacement in heterogeneous permeable media is that of Koval (1963).

5.1 EFFECTIVE MOBILITY RATIO AS A FUNCTION OF TRUE END-POINT MOBILITY RATIO (M^o) AND CRAIG COEFFICIENT (V_C)

5.1.1 THE MODEL

From the discussion in Chap.III, the two dominant factors expected to control viscous crossflow are the degree of heterogeneity and the original end-point

mobility ratio. The dependance of viscous mixing on these two parameters is investigated according to in Table V.1.

		MOBILITY RATIO						
		0.5	1.0	1.5	2.0	3.0	4.0	5.0
CRAIG C.	1.96	X		X	X	X	X	X
	2.35		X	X	X	X	X	X
	2.74		X	X	X	X	X	X

Table. V.1: Investigation Scheme

The permeability distributions given by the Craig coefficients in Table V.1 were determined using a $\ln(k)|_{.5} = \ln(50)|_{.5}$ and ten equally spaced layers for each reservoir. The resulting distributions are

$V_C = 1.96$: k={413.7, 226.4, 139.5, 90.88, 60.85, 41.08, 27.51, 17.93, 11.04, 6.043}

$V_C = 2.35$: k={631.3, 306.3, 171.2, 102.4, 63.29, 39.5, 24.41, 14.6, 8.162, 3.96}

$V_C = 2.74$: k={963.3, 414.3, 210.2, 115.4, 65.83, 37.98, 21.66, 11.89, 6.034, 2.595}

The idea is to find a functional relationship of the form

$$M^o_{eff} = M^o_{eff}(M^o, V_C) \qquad (V.1)$$

such that if the original end-point mobility ratio and the Craig coefficient of the system are known, an effective end-point mobility ratio may be determined. Introducing the effective mobility ratio concept into the Hearn model gives

$$\tilde{f}_{wn} = \left[1 + \frac{1}{M^{o}_{eff}} \frac{\sum_{i=n+1}^{N} k_i h_i}{\sum_{i=1}^{n} k_i h_i} \right]^{-1} \qquad (V.2)$$

where

M^{o}_{eff} = Effective end-point mobility ratio

while the water saturation equation remains unaltered since it does not depend on the mobility ratio and given by

$$\tilde{S}_{wn} = \frac{\sum_{i=1}^{n} \{\phi \Delta Sh(1-S_{or})\}_i + \sum_{i=n+1}^{N} \{\phi \Delta Sh S_w\}_i}{(\phi \overline{\Delta S})H} \qquad (III.24)$$

In all the simulations done according to Table V.I and presented in this section, the layered system was assumed to have 10 layers with a overlying simulation grid of 20 vertical blocks (5 ft/block) and 15 horizontal blocks (50 ft/block), i.e. two rows per layer. The reason for using 10 layers is demonstrated in Fig.V.1. Figure V.1 shows Hearn's analytical solution for a system with a Craig coefficient of 2.35 and a true end point mobility ratio of 0.5. The solution becomes reasonably smooth for 10 layers compared to the 2 and 5 layer cases. The 16 layer case, of course, is even smoother but in order to contain excessive computational expenses while still retaining a reasonably accurate solution the 10 layer system was used. All simulations were done with no capillary pressure, no gravity, and no physical dispersion.

5.1.2 Determining An Effective End-Point Mobility Ratio

The effective end-point mobility ratio was found by progressively lowering the initial inputted value by one tenth until the best fit of the Hearn model to the simulated results was found.

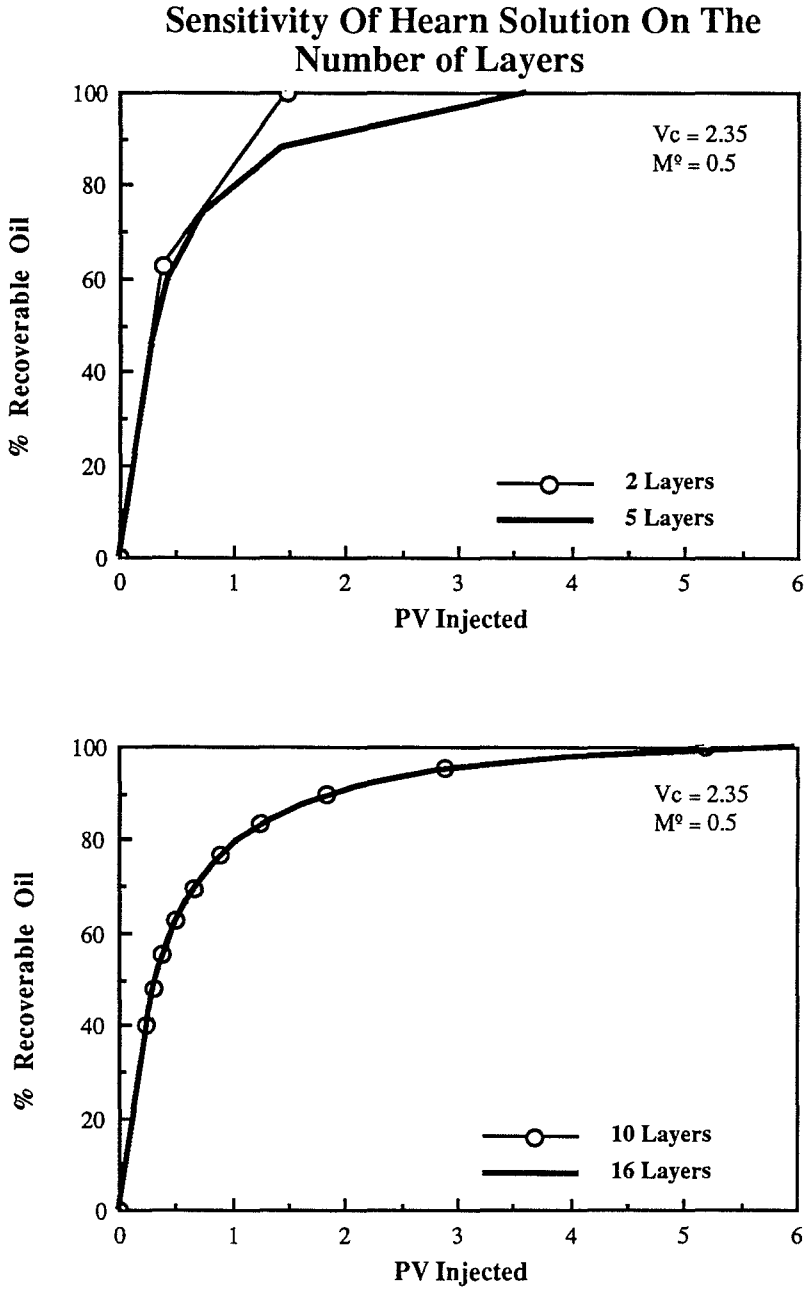

Fig. V.1: Hearn Solution For 2,5,10, and 16 Layers (M^o=0.5, V_C=2.35)

The numerical simulator generates two curves, the thickness-averaged water fractional flow curve and the cumulative recovery curve from which the effective mobility ratio can be regressed.

The average fractional flow curve, as Waggoner (1985) has demonstrated, is invariant with time and position if the system is in vertical equilibrium. This introduces the advantage of having to inject only a fraction of the pore volume to determine the entire curve since each column of grid blocks returns one point at every time step. One severe problem associated with the fractional flow curve is numerical dispersion and, in addition, as the medium becomes more heterogeneous, i.e. increasing V_C, the fractional flow curve approaches one rapidly. Since the Welge construction uses the inverse of the slope to determine the cumulative recovery from the fractional flow curve there is room for a considerable error in the prediction. Furthermore, since every column of grid blocks returns one point there will 15 points per time step (for this particular simulation grid) leading to a clustered, difficult-to-interpret, fractional flow curve as shown in Fig.V.2. In the runs presented further on, the fractional flow data was filtered by using only the largest value of the fractional flow at any one given saturation.

The cumulative recovery curve, on the other hand, does not suffer from numerical dispersion to the degree that the fractional flow curve does but has the considerable disadvantage of requiring a substantial amount of computer time to get enough data for a reasonable regression.

Figure V.3 shows an attempt to determine the sensitivity of the regressed effective mobility ratio from the fractional flow and cumulative recovery curve on the pore volumes injected. Note that Fig. V.3 refers to the specific case of V_C = 2.35 and M^o = 5.0. Nevertheless, some important observations can be made. The effective mobility ratio obtained from the cumulative recovery curve increases with increasing pore volumes injected until it plateaus off at approximately 1.5 PV. The term pore volume in this thesis is defined as the total pore volume, not pore volume open to flow. If residuals for oil and water of 0.2 are used, for example, then injecting 1.5 PV as defined in this thesis is equivalent to saying that the 2.5 times

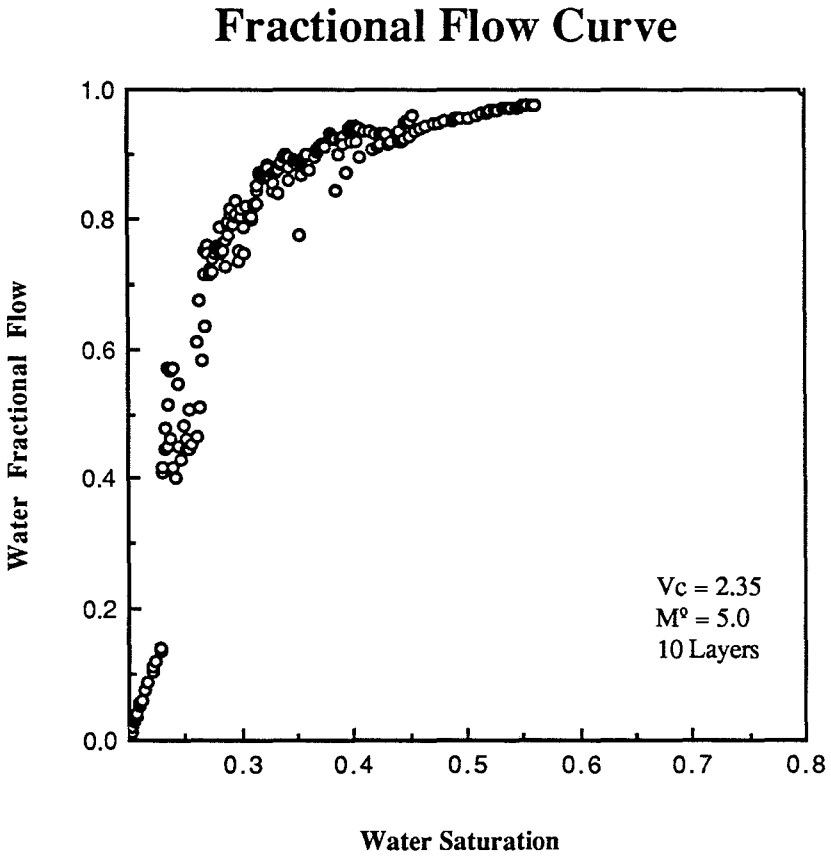

Fig. V.2: **Numerical Dispersion in Fractional Flow Curve**

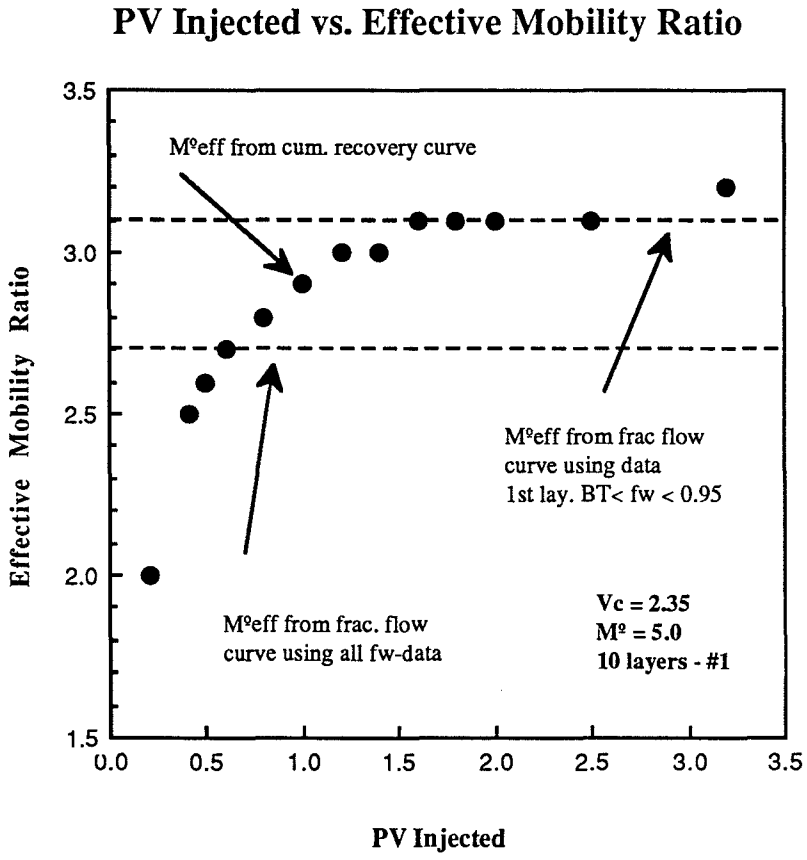

Fig. V.3: **Sensitivity Of The Effective Mobility Ratio On Pore Volume Injected**

the volume open to flow has been injected.

The fractional flow curve (filtered as described previously) displays an interesting behavior. If all the filtered data is used, the regressed end-point mobility ratio is smaller than the plateau value obtained from the cumulative recovery curve. On the other hand, if only data between breakthrough and $\tilde{f}_w = 0.95$ is used, the regressed value for the end-point mobility ratio is exactly that of the plateau value. Considering the effect of numerical dispersion at low water saturations and the the error introduced by the Welge construction at higher saturations this is an expected behavior.

In general therefore, the value of the effective end-point mobility ratio returned by either curve tends to be too optimistic. In order to contain computer costs, most cases where run out to 1.0 PV and the highest effective end-point mobility ratio value returned between the two curves was assumed to be the correct one. The data from the fractional flow curve was regressed using values only between breakthrough and a fractional flow value of $\tilde{f}_w = 0.95$.

In the plots that follow, showing the results of the simulation runs as marked in Table V.1, both the fractional flow and the cumulative recovery curve for each case are given. Every plot has three data sets: the simulation results, the Hearn model using the original end-point mobility ratio, and the Hearn model using the effective mobility ratio.

The effective mobility ratios regressed from Fig.'s V.4-V.21 are summarized in Table V.2. There are two values per run indicated in the table. The top value is obtained from the fractional flow curve and the bottom one from the cumulative recovery curve. The results in Table V.2 are also plotted in Fig.V.22. The lines enclosing the data are given by

$$0.48\, M^o + 0.52 \leq M^o_{eff} \leq 0.60\, M^o + 0.40 \qquad 1.0 < M^o < 5.0 \qquad (V.3)$$

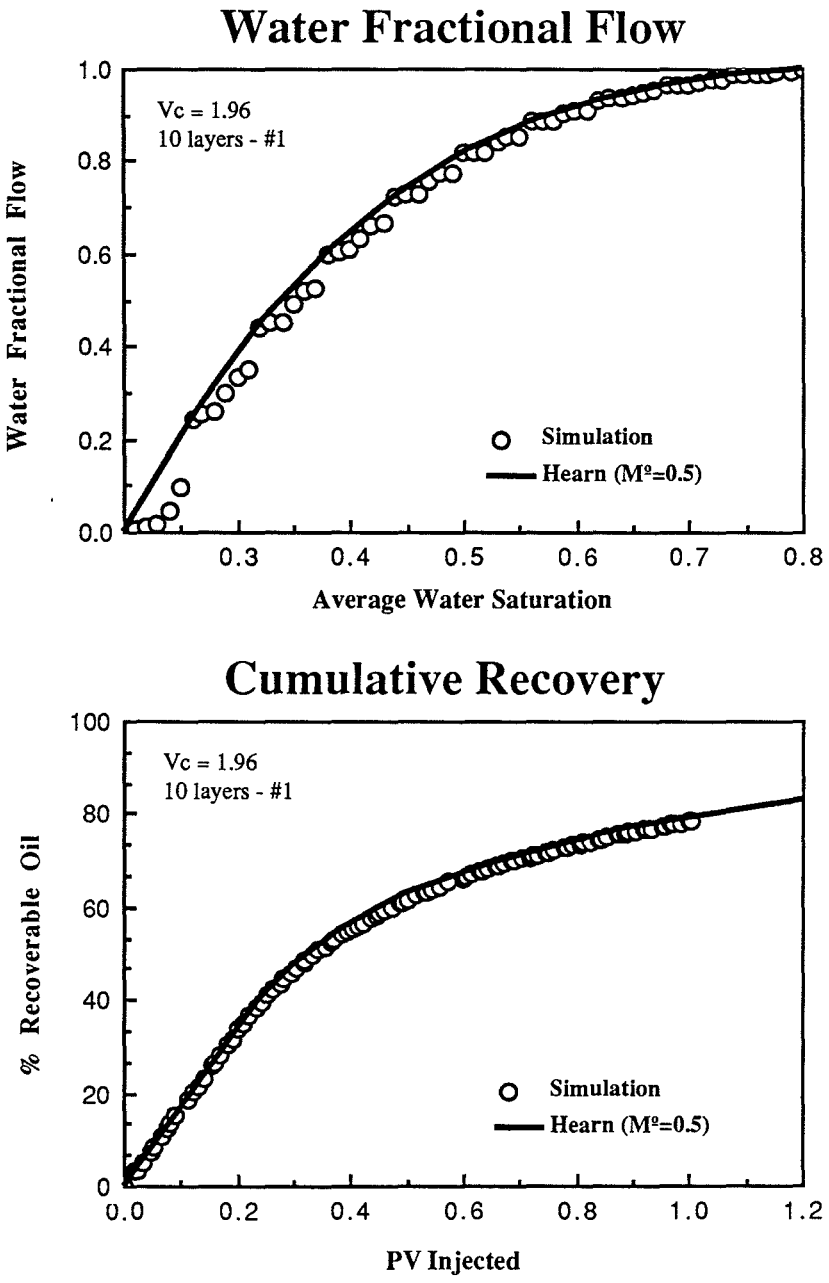

Fig. V.4: Water Fractional Flow and Cumulative Recovery (M^o=0.5; V_C=1.96)

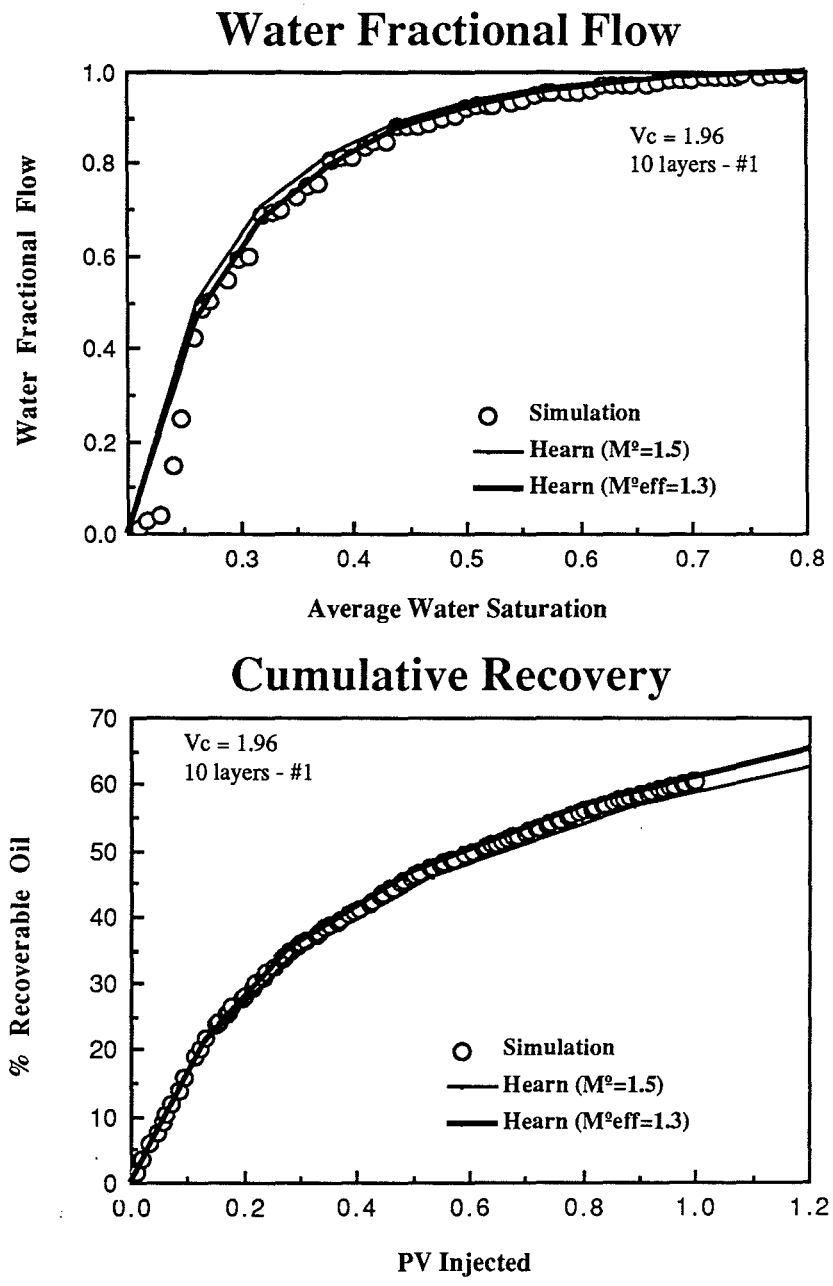

Fig. V.5: Water Fractional Flow and Cumulative Recovery (M^o=1.5; V_C = 1.96)

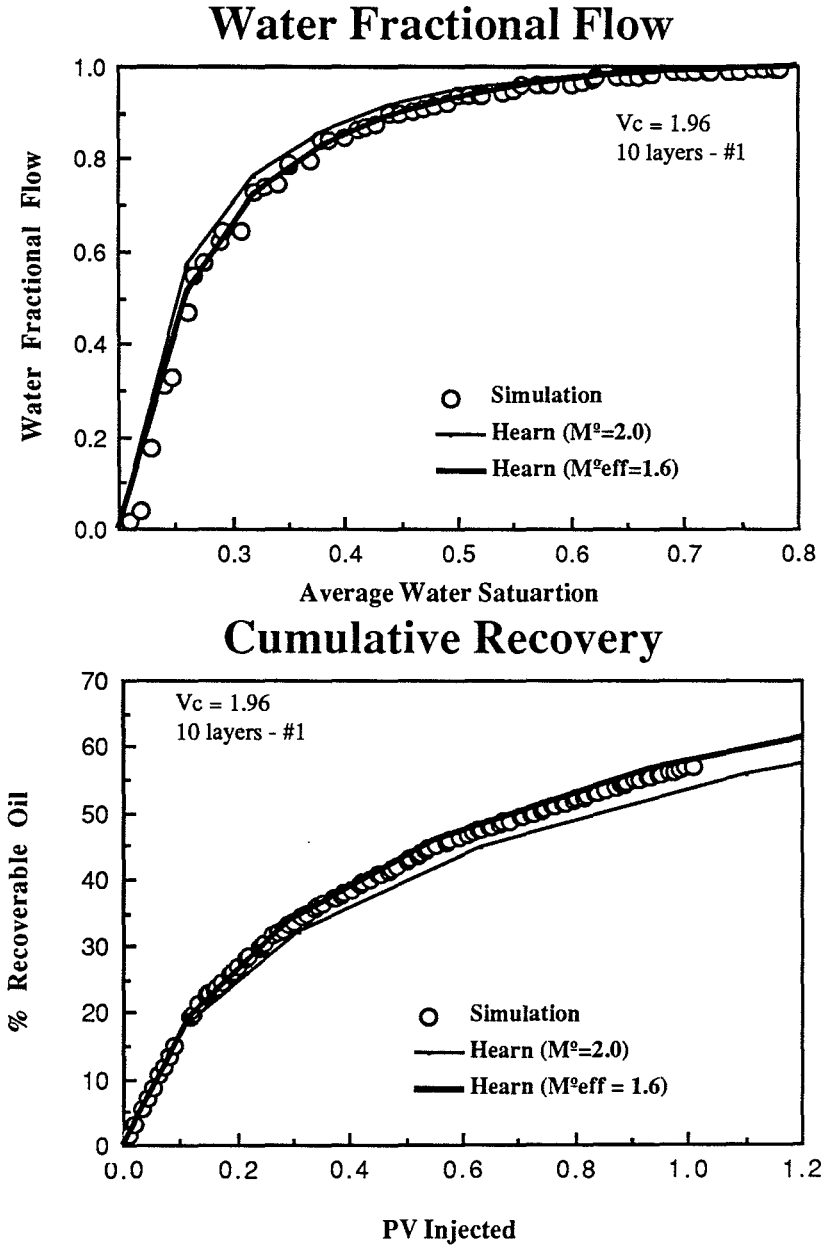

Fig. V.6: Water Fractional Flow and Cumulative Recovery (M^o=2.0; V_C=1.96)

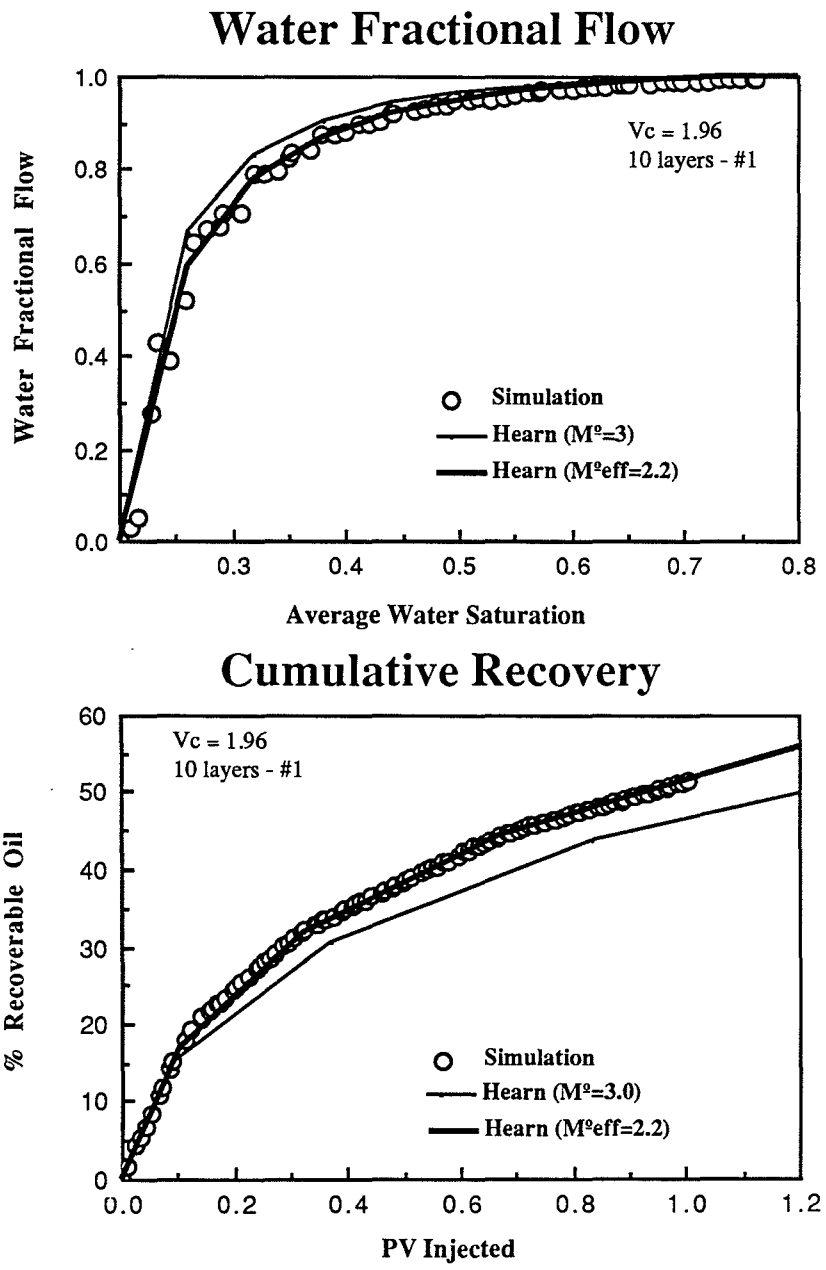

Fig. V.7: Water Fractional Flow and Cumulative Recovery (M^o=3.0; V_C=1.96)

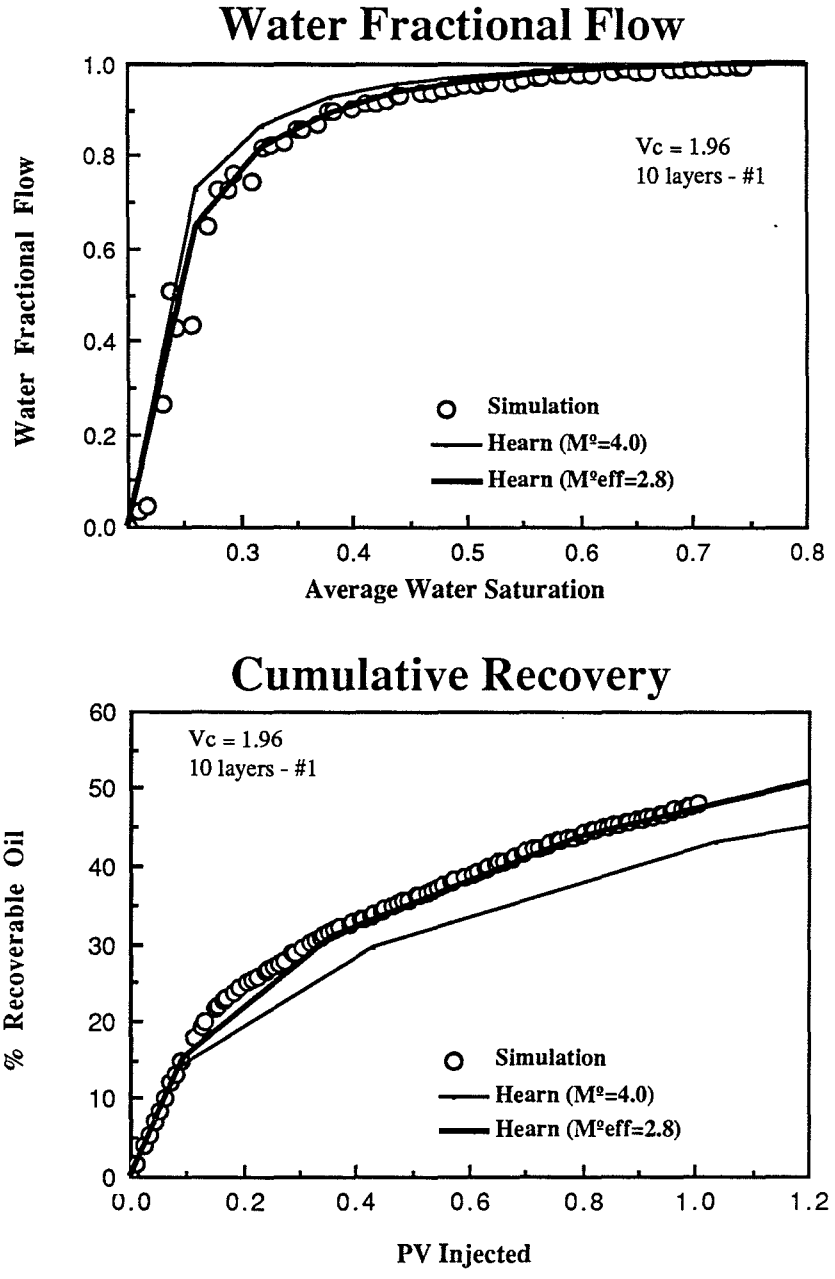

Fig. V.8: Water Fractional Flow and Cumulative Recovery (M^o=4.0; V_C=1.96)

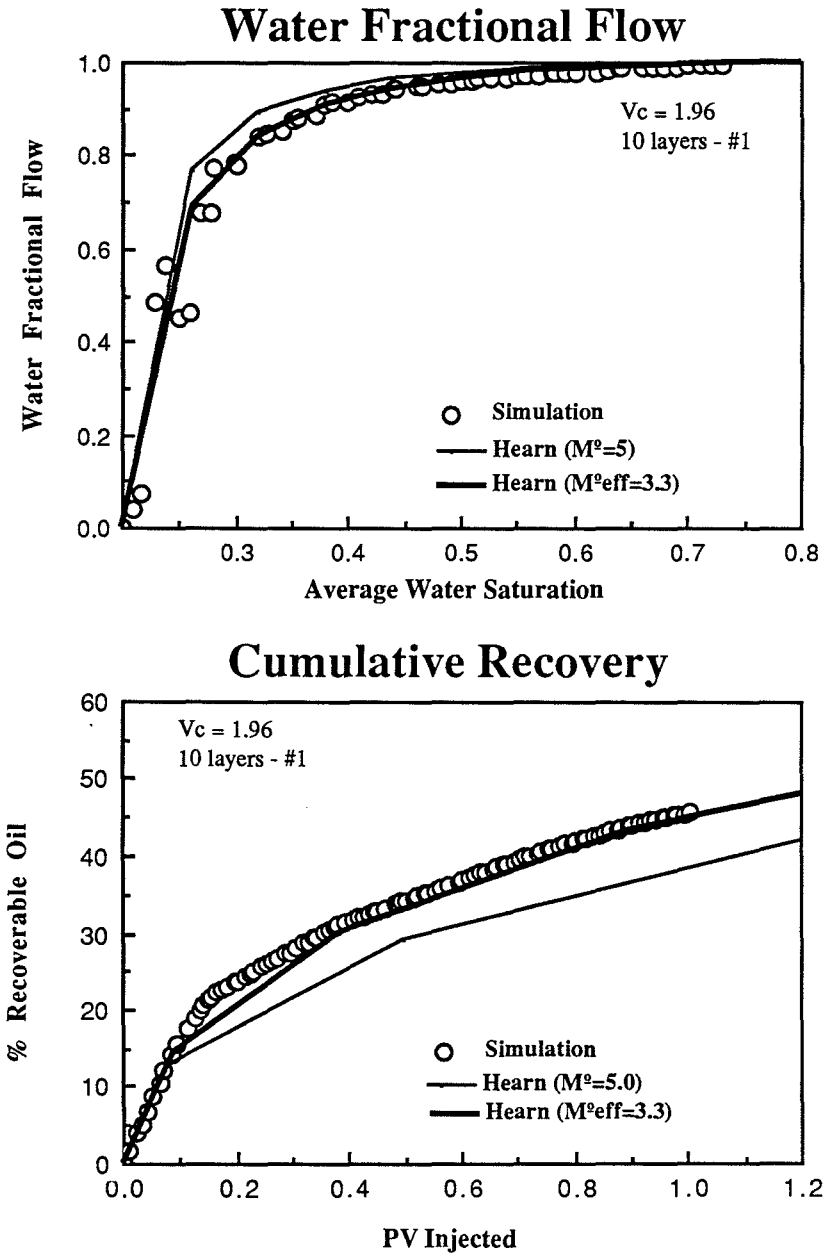

Fig. V.9: Water Fractional Flow and Cumulative Recovery (M^o=5.0; V_C=1.96)

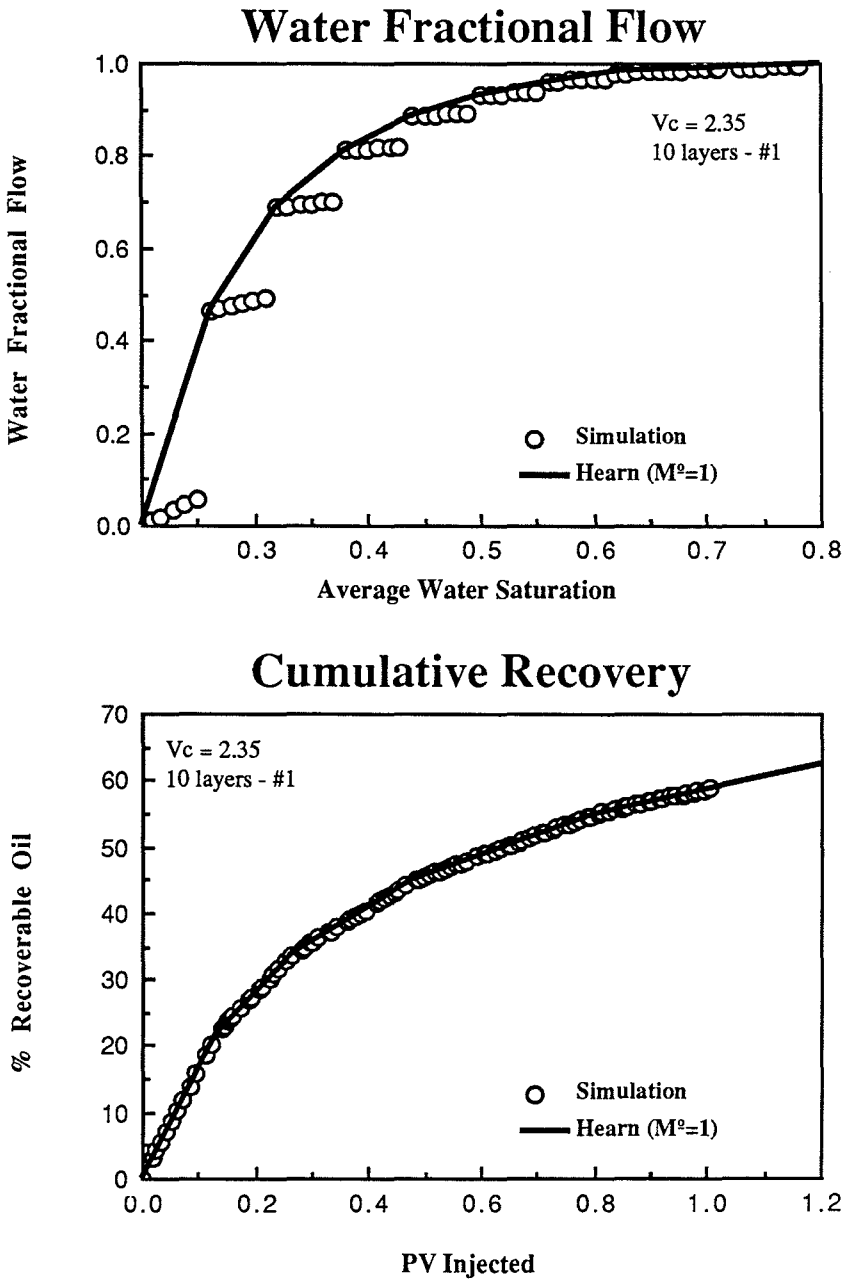

Fig. V.10: Water Fractional Flow and Cumulative Recovery (M^o=1.0; V_C=2.35)

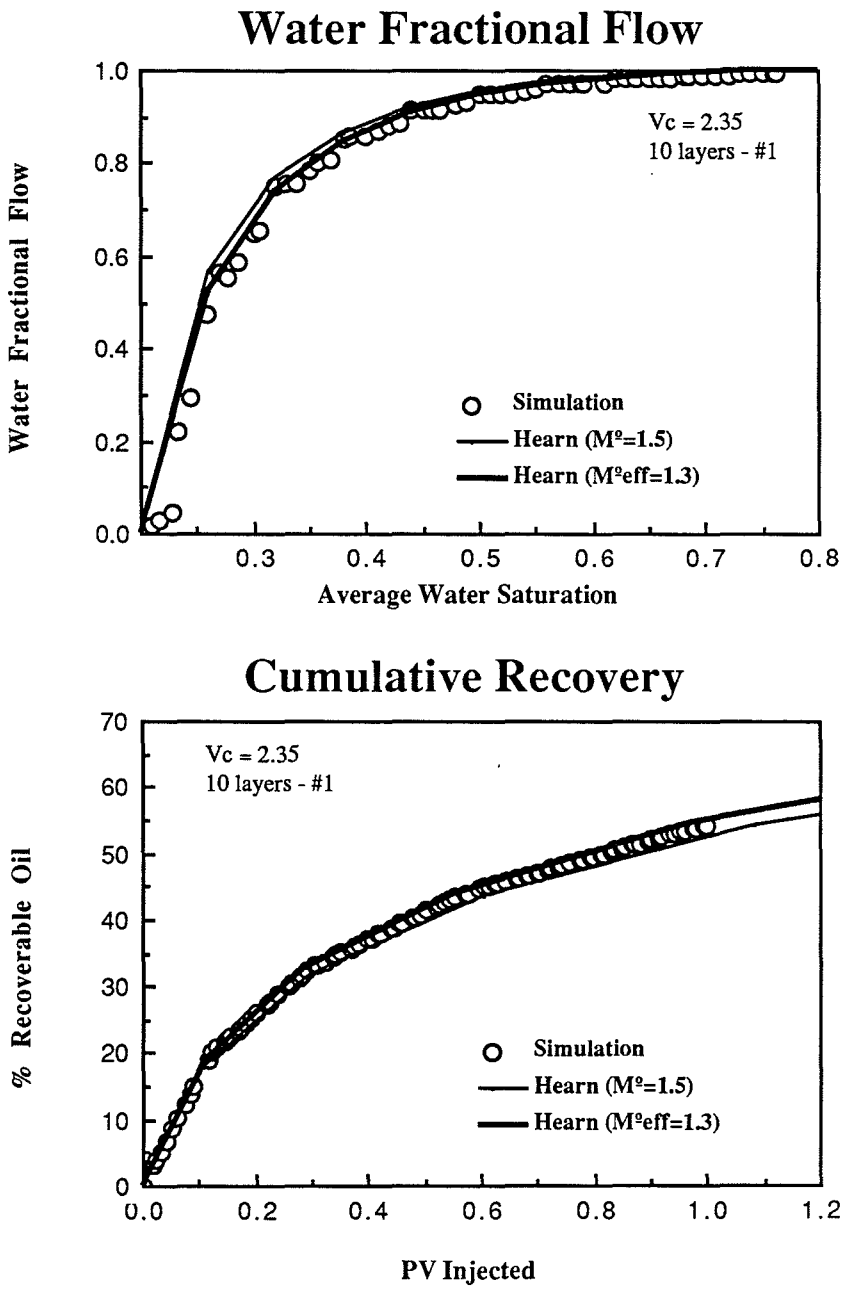

Fig. V.11: Water Fractional Flow and Cumulative Recovery (M^o=1.5; V_C=2.35)

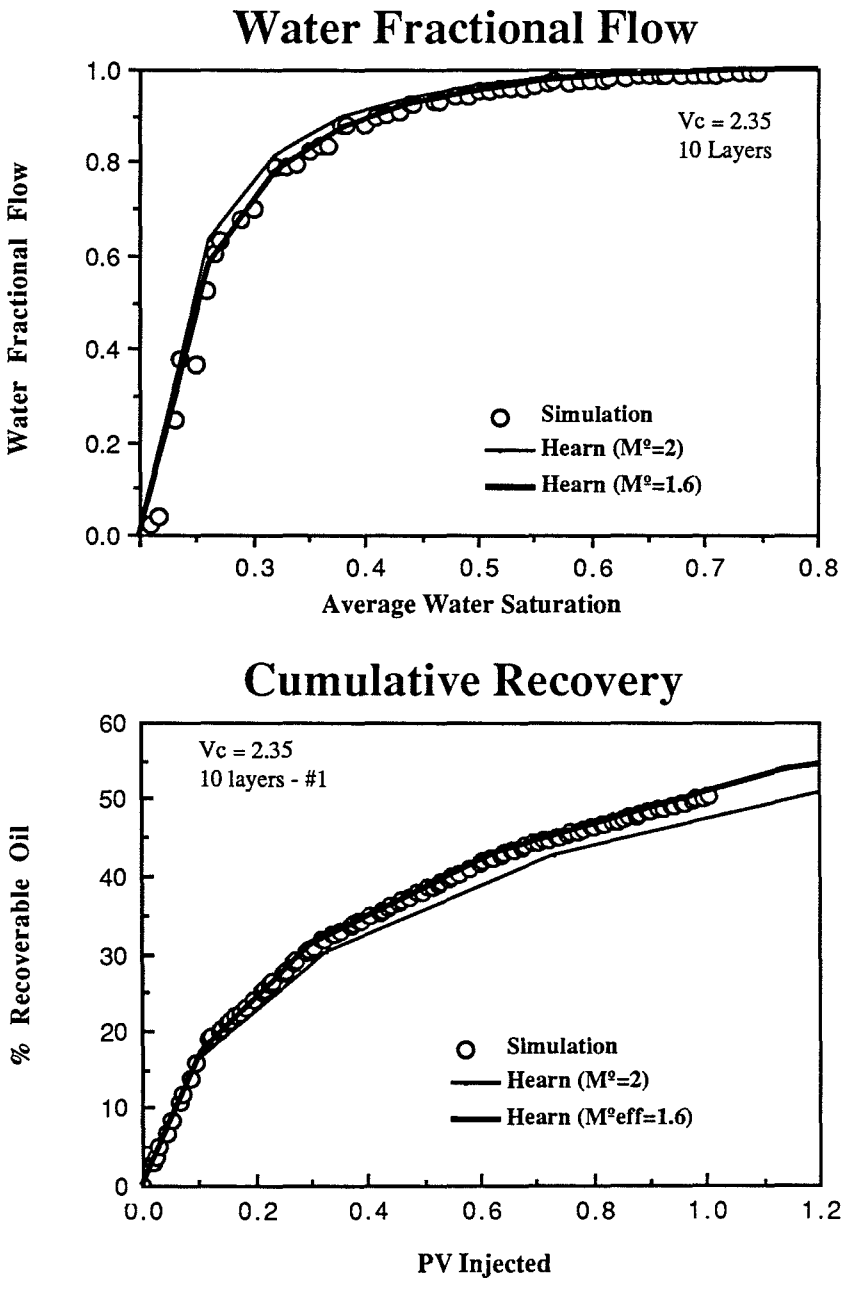

Fig. V.12: Water Fractional Flow and Cumulative Recovery (M^o=2.0; V_C=2.35)

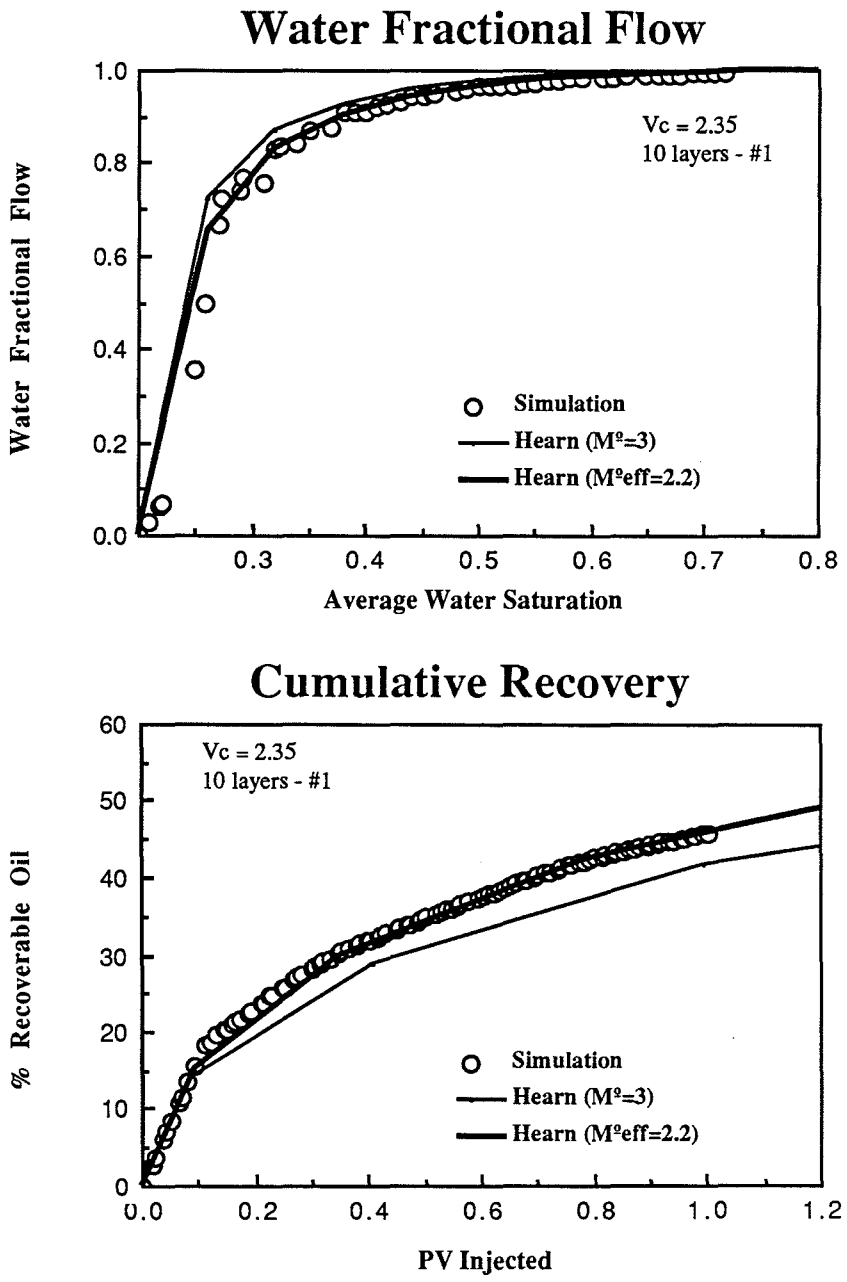

Fig. V.13: Water Fractional Flow and Cumulative Recovery (M^o=3.0; V_C=2.35)

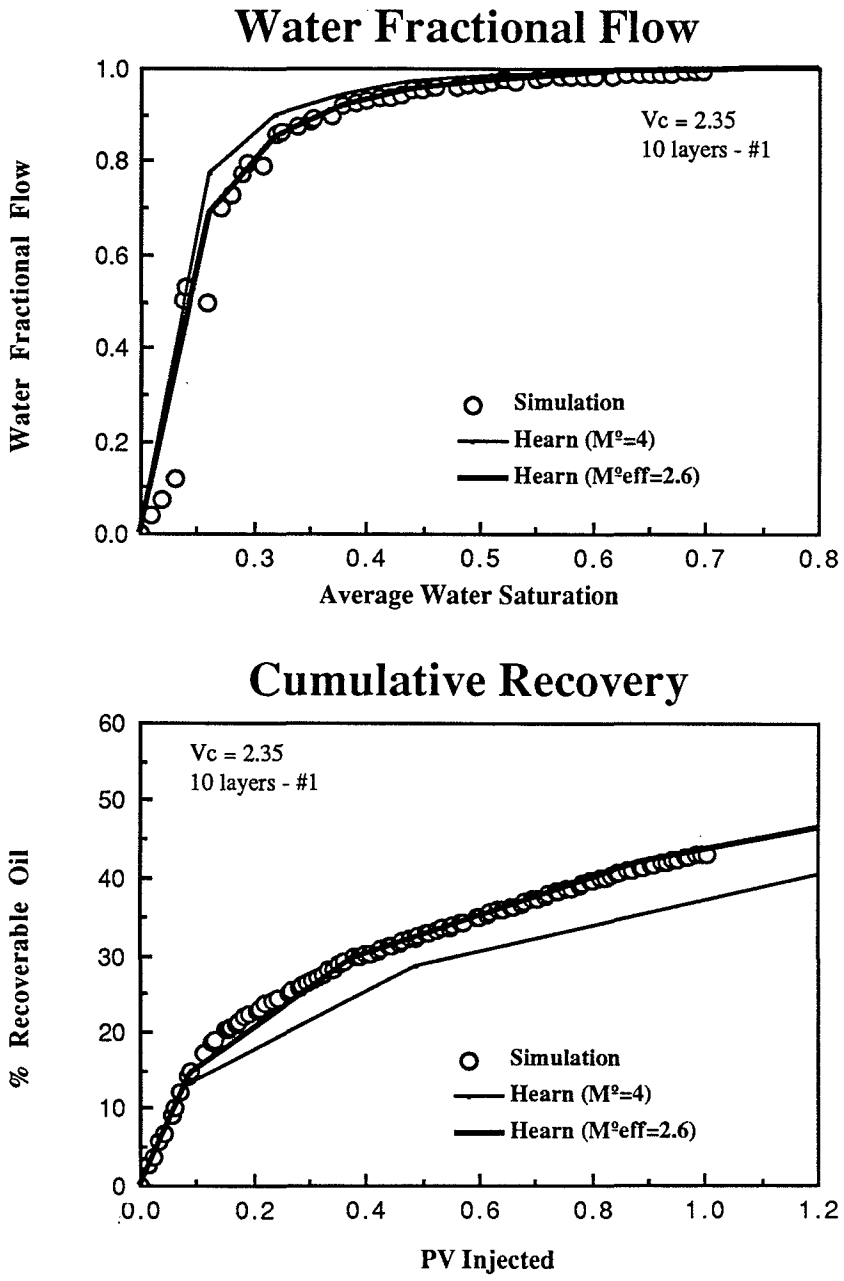

Fig. V.14: Water Fractional Flow and Cumulative Recovery (M^o=4.0; V_C=2.35)

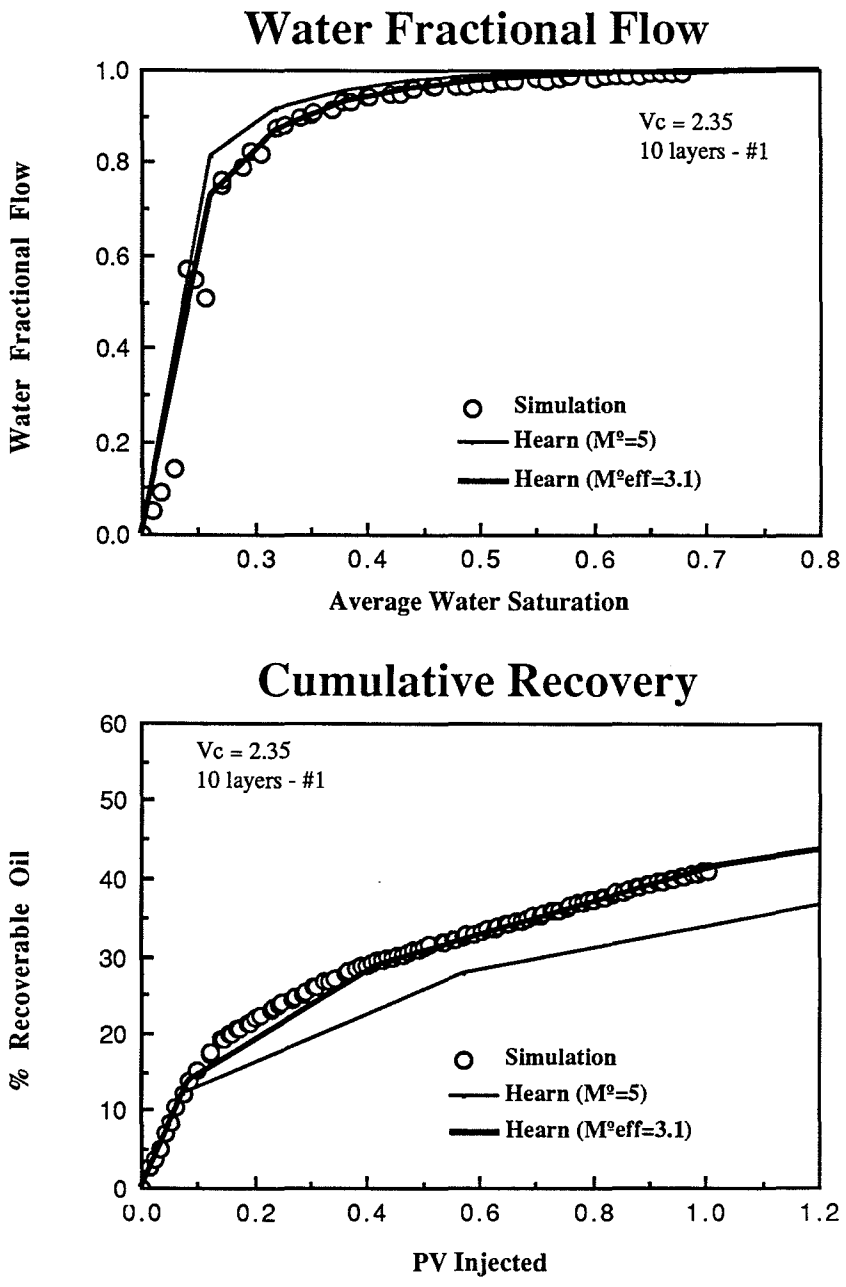

Fig. V.15: Water Fractional Flow and Cumulative Recovery (M^o=5.0; V_C=2.35)

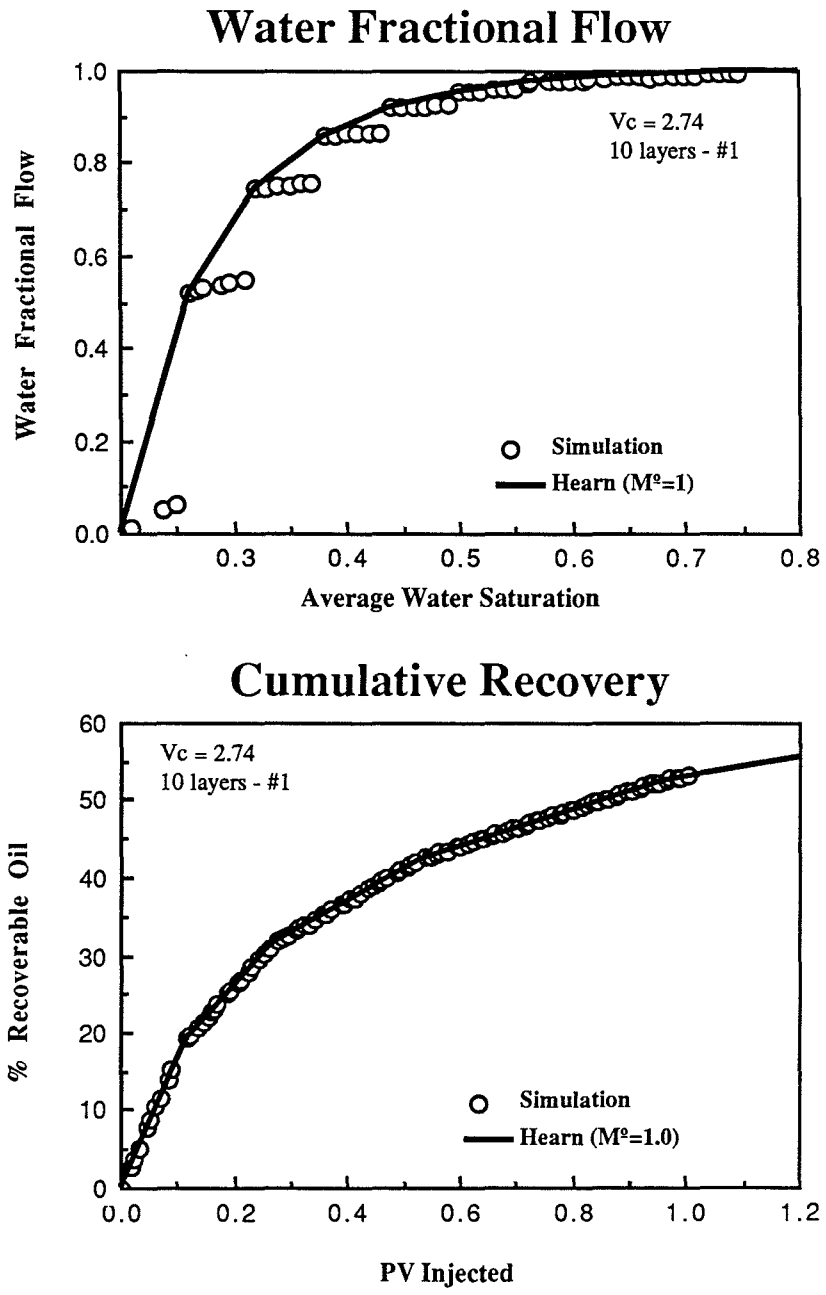

Fig. V.16: Water Fractional Flow and Cumulative Recovery (M^o=1.0; V_C=2.74)

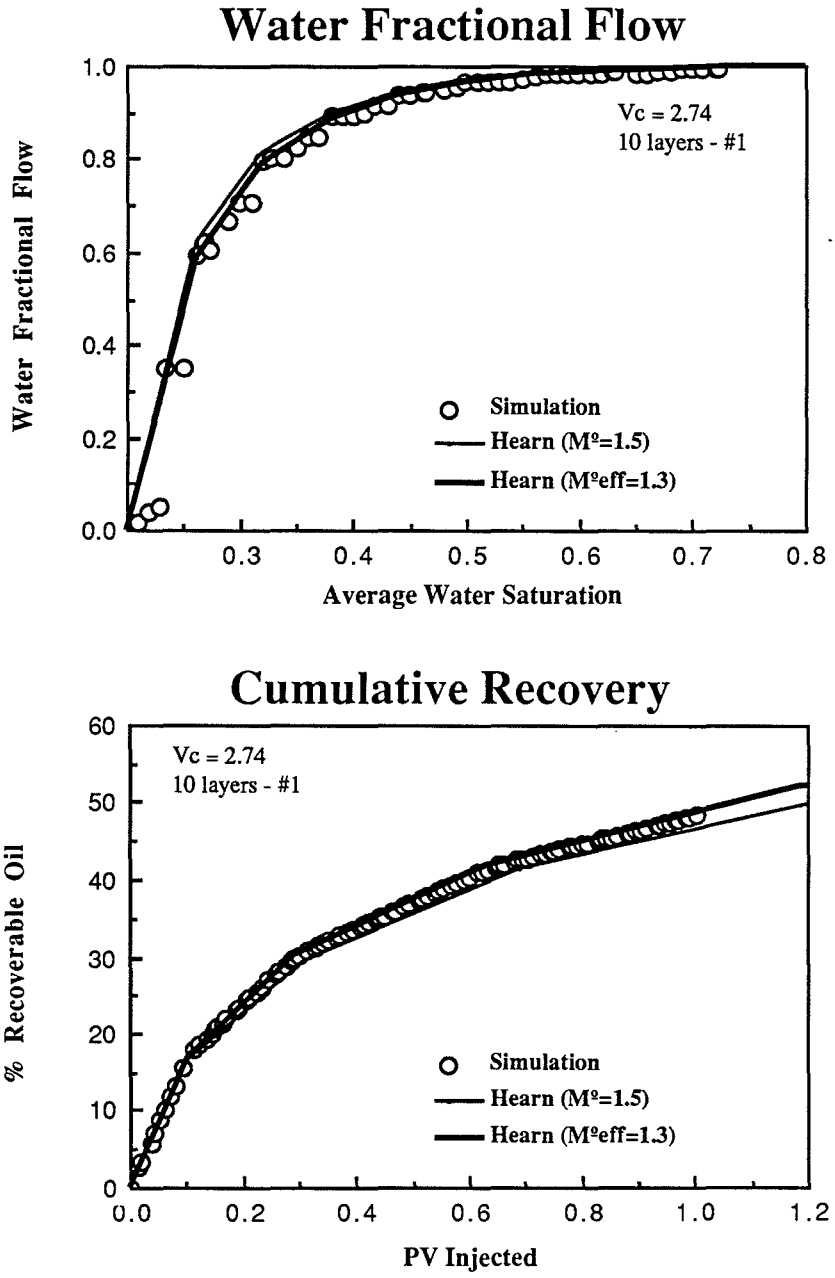

Fig. V.17: Water Fractional Flow and Cumulative Recovery (M^o=1.5; V_C=2.74)

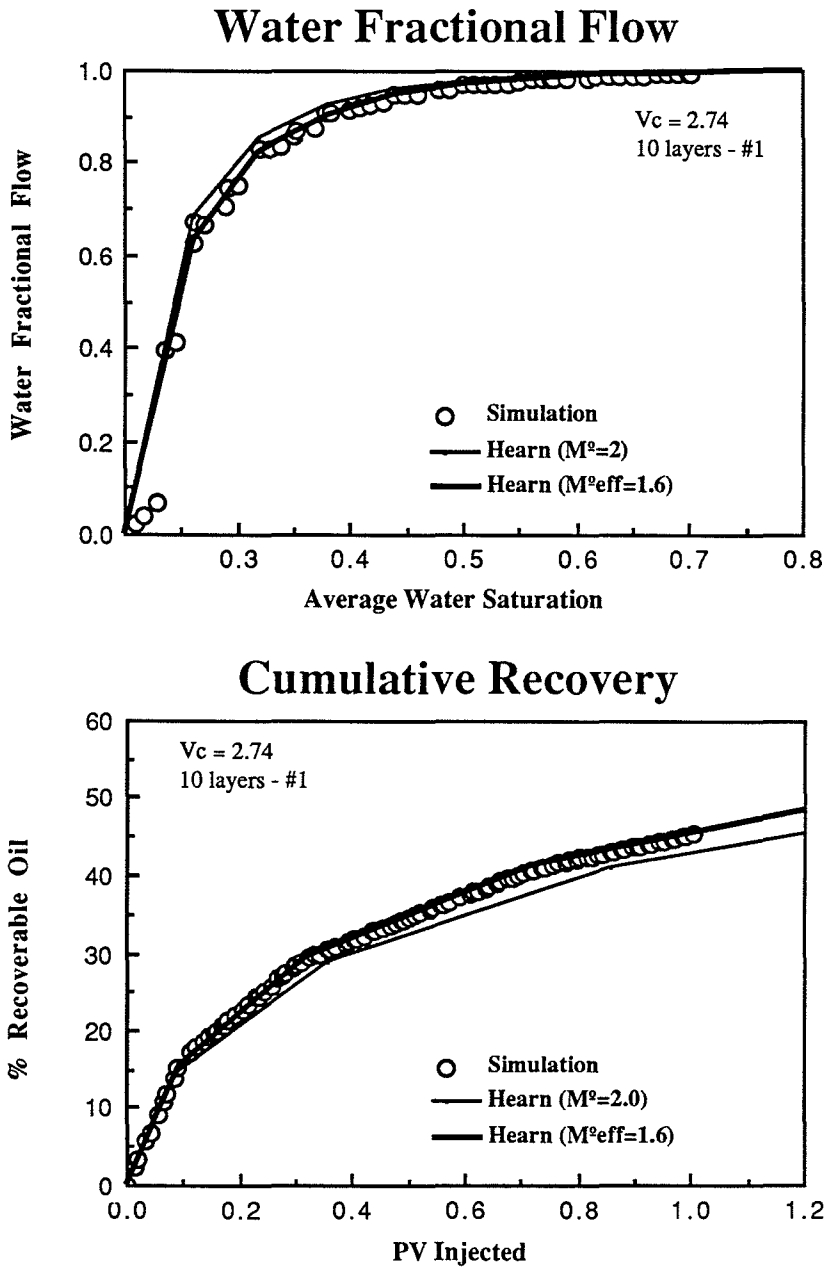

Fig. V.18: Water Fractional Flow and Cumulative Recovery
(M^o=2.0; V_C=2.74)

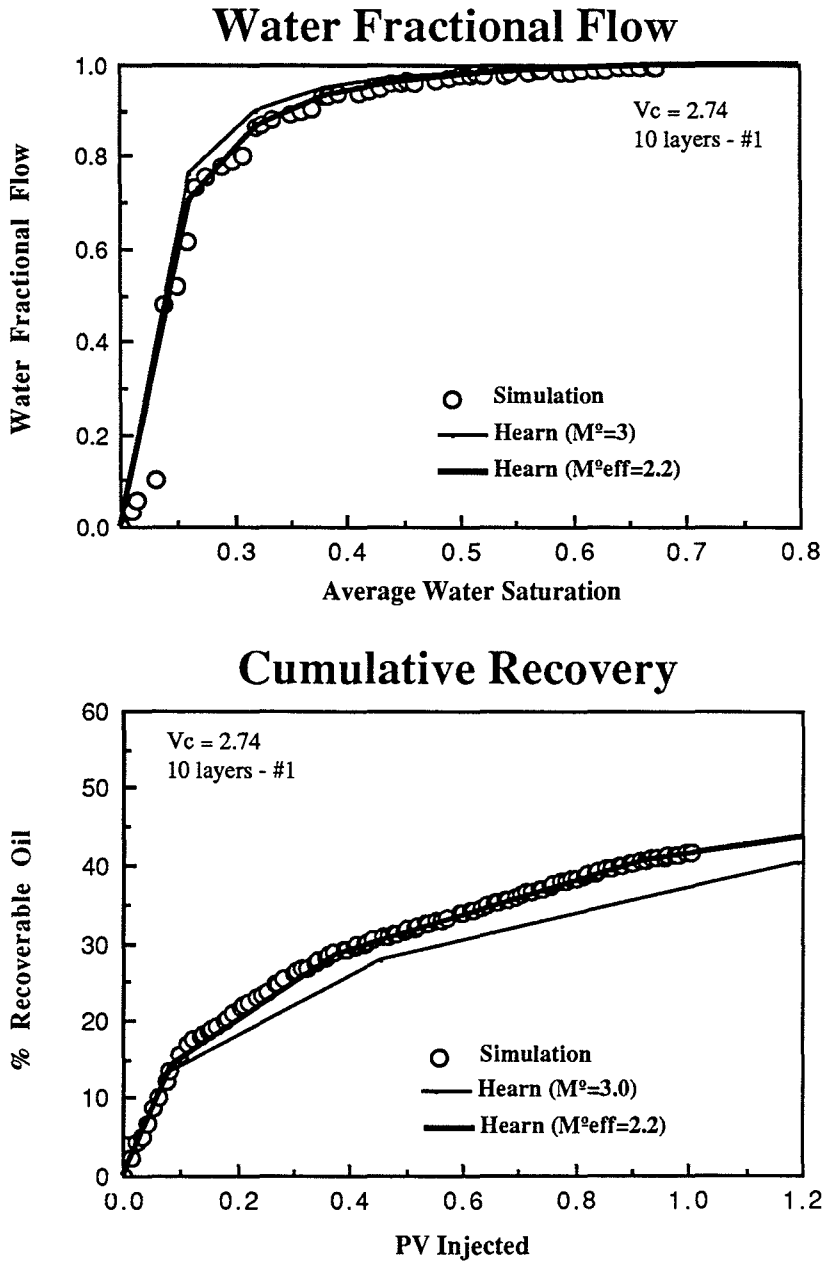

Fig. V.19: Water Fractional Flow and Cumulative Recovery (M^o=3.0; V_C=2.74)

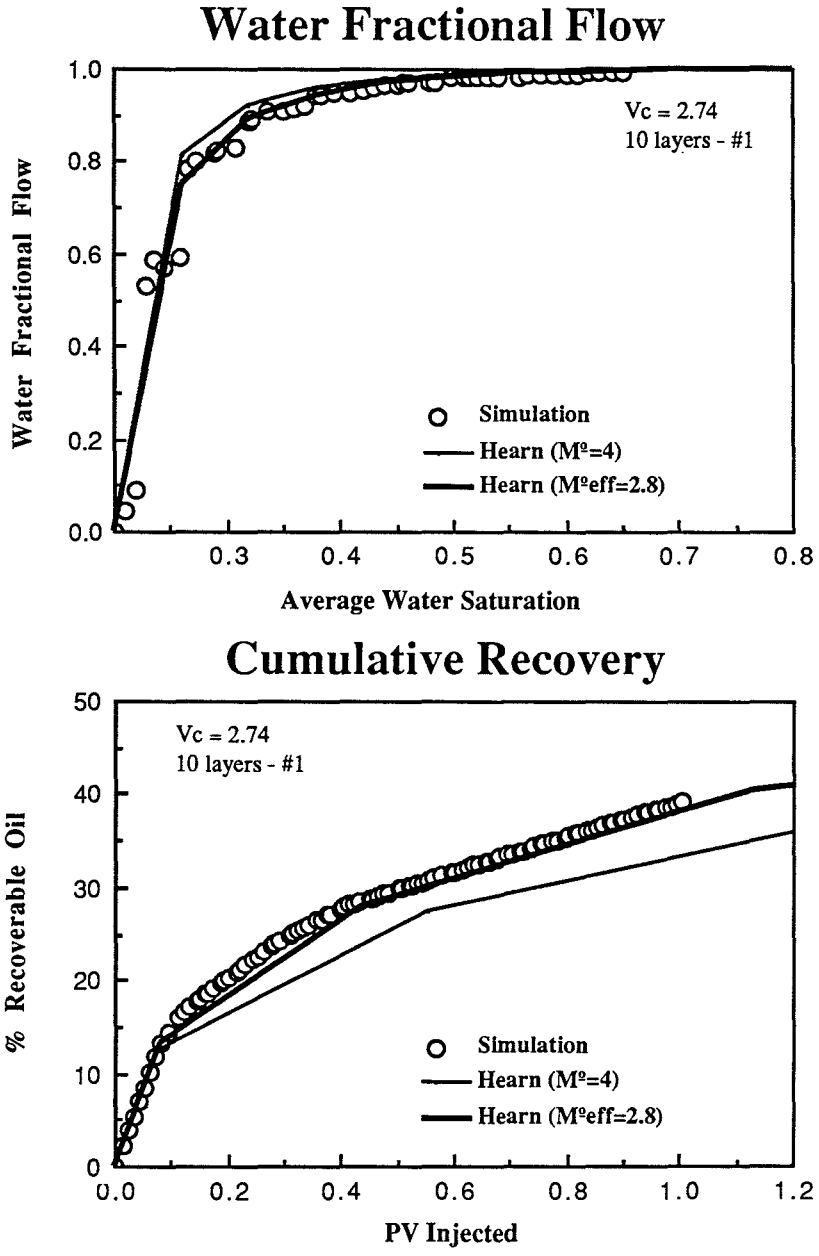

Fig. V.20: Water Fractional Flow and Cumulative Recovery (M^o=4.0; V_C=2.74)

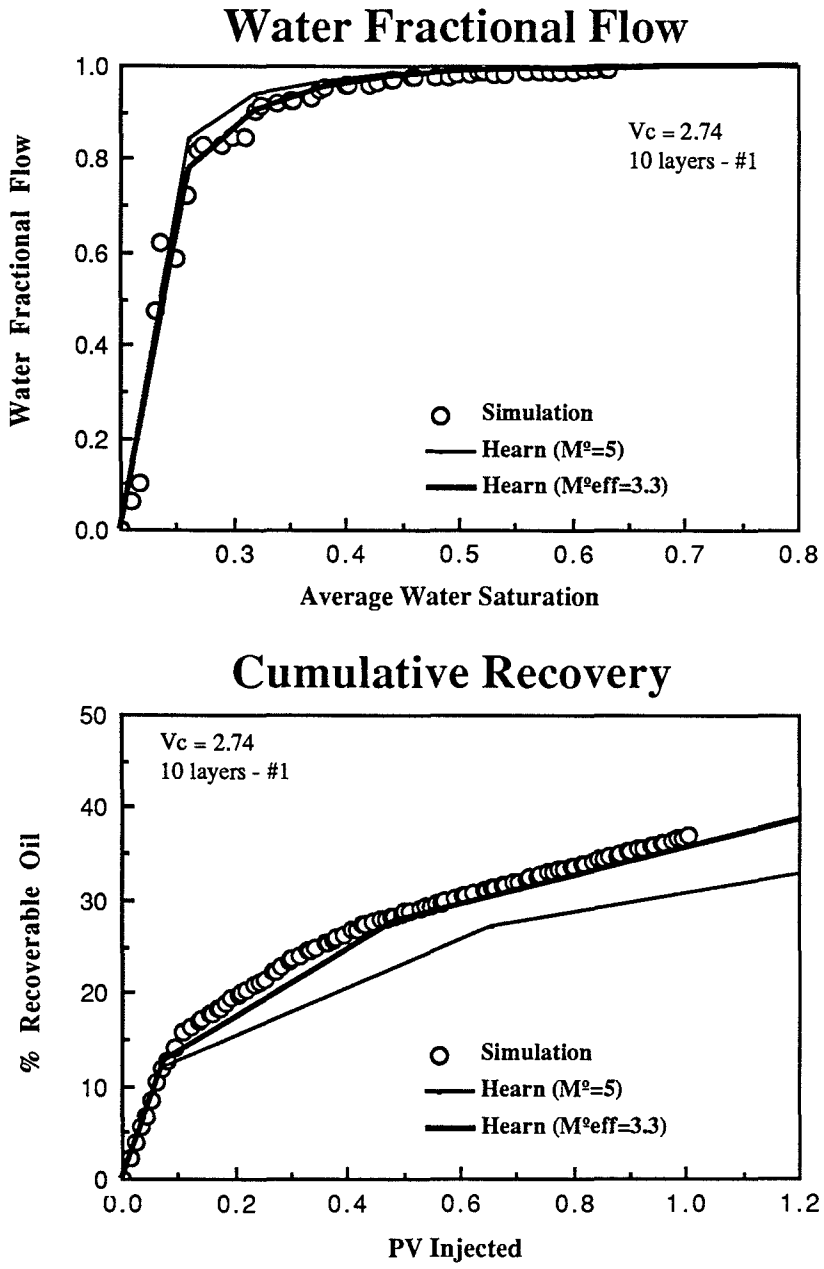

Fig. V.21: Water Fractional Flow and Cumulative Recovery (M^o=5.0; V_C=2.74)

While Eq. (V.3) represents a range in which the data falls, the preceding sensitivity discussion of the effective mobility ratio on the PV injected and the fractional flow curve suggest that the upper straight line of the region should be used to determine the effective mobility ratio. In this case the effective mobility ratio

		MOBILITY RATIO						
		0.5	1.0	1.5	2.0	3.0	4.0	5.0
CRAIG C.	1.96	0.5 0.5		1.3 1.3	1.6 1.6	2.2 2.2	2.8 2.6	3.3 3.0
	2.35		1.0 1.0	1.2 1.3	1.6 1.6	2.2 2.1	2.6 2.6	3.3 2.9
	2.74		1.0 1.0	1.3 1.3	1.6 1.6	2.2 2.1	2.8 2.5	3.3 2.9

x - Effective M from fractional flow curve
y - Effective M from cumulative recovery curve

Table V.2: Effective Mobility Ratios Regressed From Fig.'s V.4-V.21

would be given by

$$M^{o}_{eff} = 0.60\, M^{o} + 0.40 \qquad 1.0<M^{o}<5.0 \qquad \text{(V.3.a)}$$

Equation (V.3.a) matches the highest values in Fig.V.22.

One surprising feature of the results in Fig.V.22 is the apparent lack of sensitivity on the degree of heterogeneity of the medium, at least for the range of cases investigated here. Another characteristic is the increasing spread between the effective mobility ratio returned by the fractional flow curve and the one returned by the cumulative recovery curve with increasing true end-point mobility ratio and Craig coefficient. This is especially noticeable for the $M^{o} = 5$ cases as shown in Table V.2.

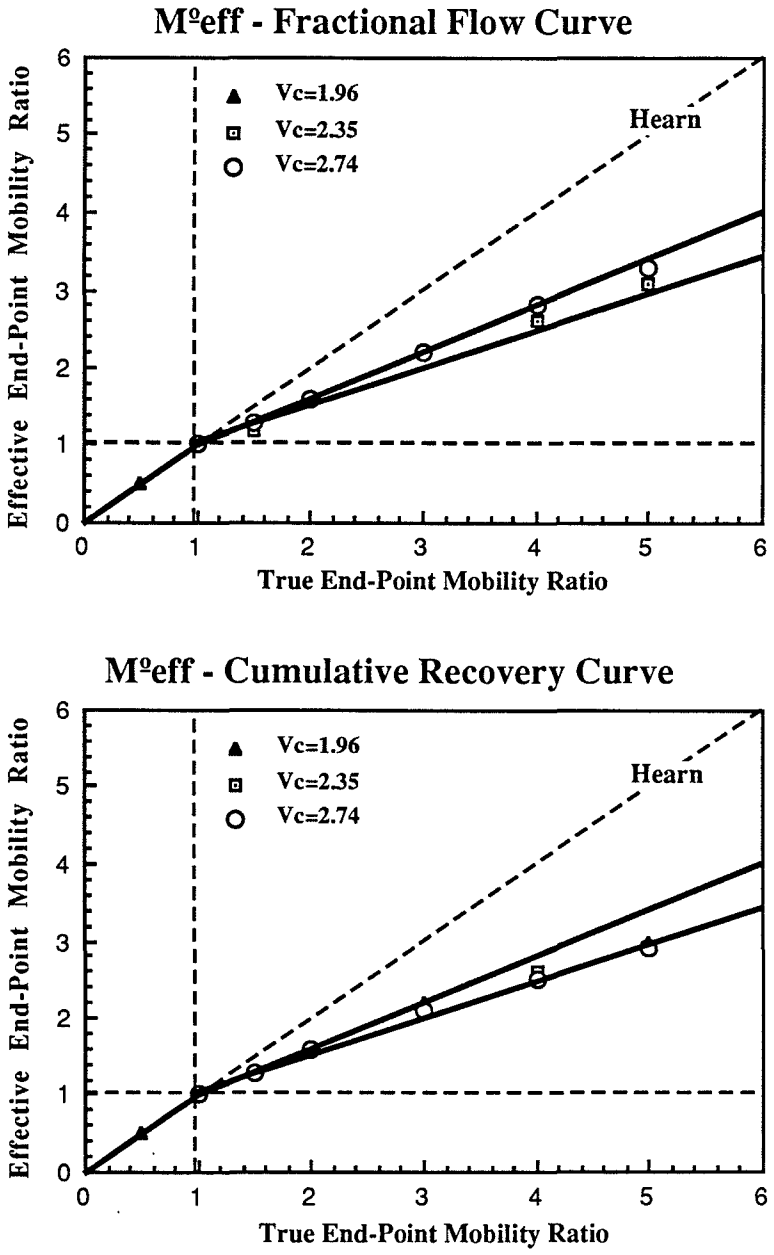

Fig. V.22: True End-Point Mobility Ratio vs. Effective End-Point Mobility Ratio

Some qualitative judgments can be made at this point. The effective mobility ratio will always be lower than the true end-point mobility ratio which is consistent with Koval's (1963) heterogeneity factor. It appears that viscous mixing attenuates the frontal advancement with respect to the Hearn model by lowering the mobility ratio across the interface between the displacing and the displaced fluid, which is also a conclusion drawn by Waggoner et al. (1988). Increased production with respect to the Hearn model results from displaced fluid being moved into the more permeable layers and channeled to the production well.

5.2 THE EFFECT OF LAYER ORDERING ON VISCOUS CROSSFLOW

It stands to reason that one of the parameters expected to have considerable effect on the extent of viscous mixing is the degree of reservoir heterogeneity since this dictates the positions of the fronts in the various layers with respect to each other. Yet surprisingly, the results in Sec. 5.1 show a lack of sensitivity of the effective mobility ratio on the Craig coefficient for the range of cases investigated.

All runs in Sec. 5.1 where done with a descending arrangement of the layer permeabilities. In order to verify the effect of the layer ordering scheme on the displacement process, it is first necessary to categorize various ordering arrangements and then investigate the effects of each ordering scheme on the displacement by numerical simulation.

5.2.1 ORDERING SCHEMES FOR A LAYERED SYSTEM

The assumptions of no capillary pressure and no gravity allow the use of symmetry and consequently reduce the number of possible ordering schemes. The four basic arrangements used in this part of the investigation are shown in Fig.V.23.

Scheme #1 is the descending ordering scheme used throughout Sec. 5.1. Scheme #2 is characterized by the highest permeability layers being in the middle

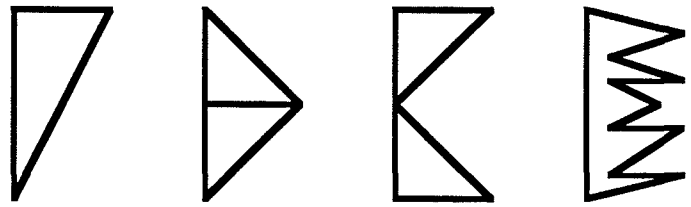

Fig. V.23: Ordering Schemes for Layered Systems

and the rest of the layer permeabilities decreasing outwards. Scheme #3 is the opposite of #2, with the lowest permeability layers in the middle and increasing permeabilities going outwards. Scheme #4 is a random ordering. Defining something as being random is somewhat difficult if there are only ten layers. Nonetheless, compared to schemes #1-#3, the idea is to have a ordering that is basically without structure.

5.2.2 Choosing a Distribution

The same permeability distribution as in Sec. 5.1 for a Craig coefficient of 2.74 was chosen for this part of the investigation. Shown in Table V.3 are the four resulting permeability arrangements used for the runs presented further on. V_C=2.74 is the largest Craig coefficient used in the previous section. The choice of which Craig coefficient to use is arbitrary but it can be argued that a larger heterogeneity contrast between layers may in fact amplify the effect of ordering, if there is one at all.

The layered systems in Table V.3 were simulated with a true end-point mobility ratio of three (M^o=3) and five (M^o=5) for a total of 8 runs.

The resulting effective mobility ratios are shown in Table V.4 and Fig.V.24 where they are compared to the straight line relationships of Sec.5.1. Figures V.25 and V.26 show the simulated cumulative recovery curves for each true end-point mobility ratio and clearly indicate a considerable variation in the degree of viscous crossflow and the resulting effect on the displacement efficiency.

#	1 	2 	3 	4 
1	913.3	2.595	963.3	115.4
2	414.3	11.89	210.2	6.034
3	210.2	37.98	115.4	414.3
4	115.4	115.4	21.66	65.83
5	65.83	414.3	11.89	21.66
6	37.98	913.3	2.595	210.2
7	21.66	210.2	6.034	11.89
8	11.89	65.83	37.97	913.3
9	6.034	21.66	65.83	37.98
10	2.595	6.034	414.3	2.595

Table V.3: Permeabilities in [md] For V_C = 2.74 and Ordering Schemes #1-#4

M	1 	2 	3 	4 
3.0	2.2 2.1	1.9 1.8	1.7 1.6	1.6 1.0
5.0	3.3 2.9	2.7 2.2	2.6 2.1	2.7 1.3

x - Effective mobility ratio from fractional flow curve.
y - Effective mobility ratio from cumulative recovery curve.

Table V.4: Effective Mobility Ratios For Ordering Schemes #1-#4 and V_C=2.74

Figure V.24 clearly indicates that the region for the effective mobility ratio obtained in Sec. 5.1 is not valid for all ordering types but rather is scheme-specific. Furthermore, as Fig.'s V.27 - V.34 show, the effective mobility ratio approach is not always able to modify Hearn's model so as to get a satisfactory match with the simulated results. Figures V.27 - V.34 show four curves plotted on each graph: the simulation result, the Hearn model with the true end-point mobility ratio, the Hearn model using the effective mobility ratio returned by the fractional flow curve, and the Hearn model using the effective mobility ratio returned by the cumulative recovery curve.

The differences in cumulative recovery because of layer ordering displayed by Fig. V.25 and Fig. V.26 are in line with ideas of viscous mixing. As mentioned at the end of Sec. 5.1, the displaced fluid (oil) is produced more efficiently compared to the no-mixing case since it is forced from the slow layers into the fast layers and channeled from there to the production well. In light of this, best recovery would be expected from a system in which fast layers are bounded on either side by slow layers. On the other hand, separating fast layers and slow layers

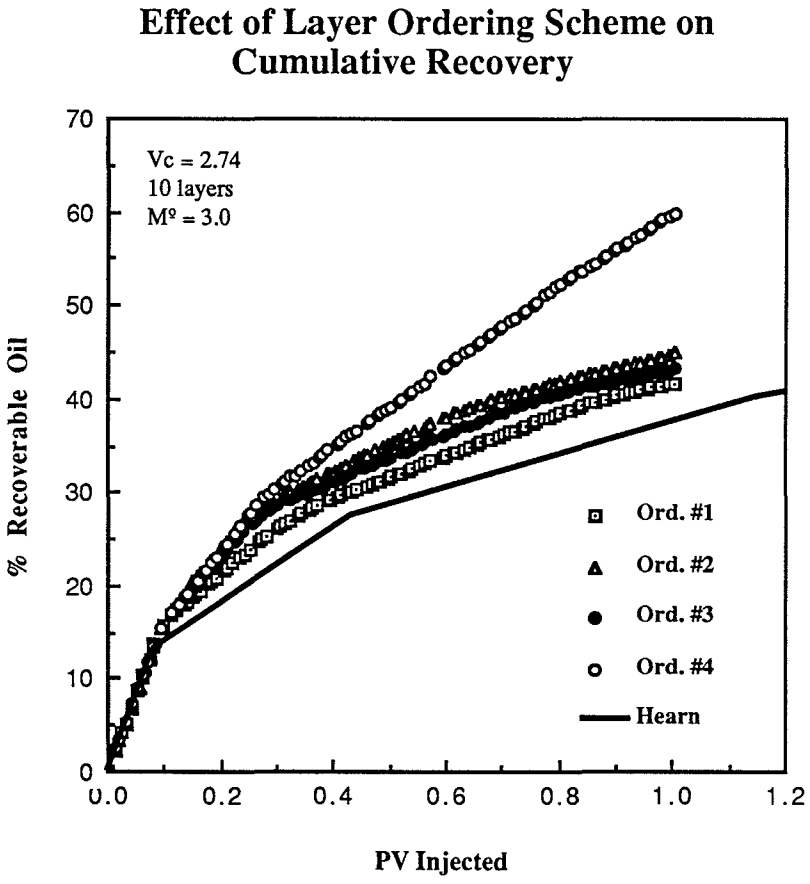

Fig. V.25: Cumulative Recovery For Schemes #1 - #4 (M^o=3.0)

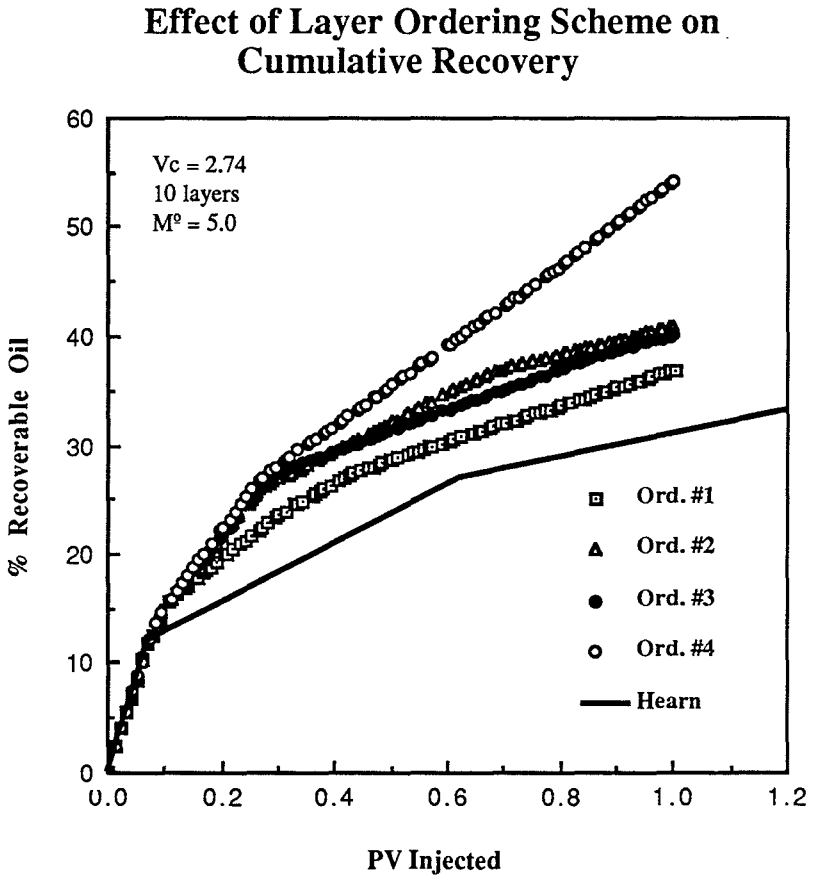

Fig. V.26: Cumulative Recovery For Schemes #1 - #4 (M^o=5.0)

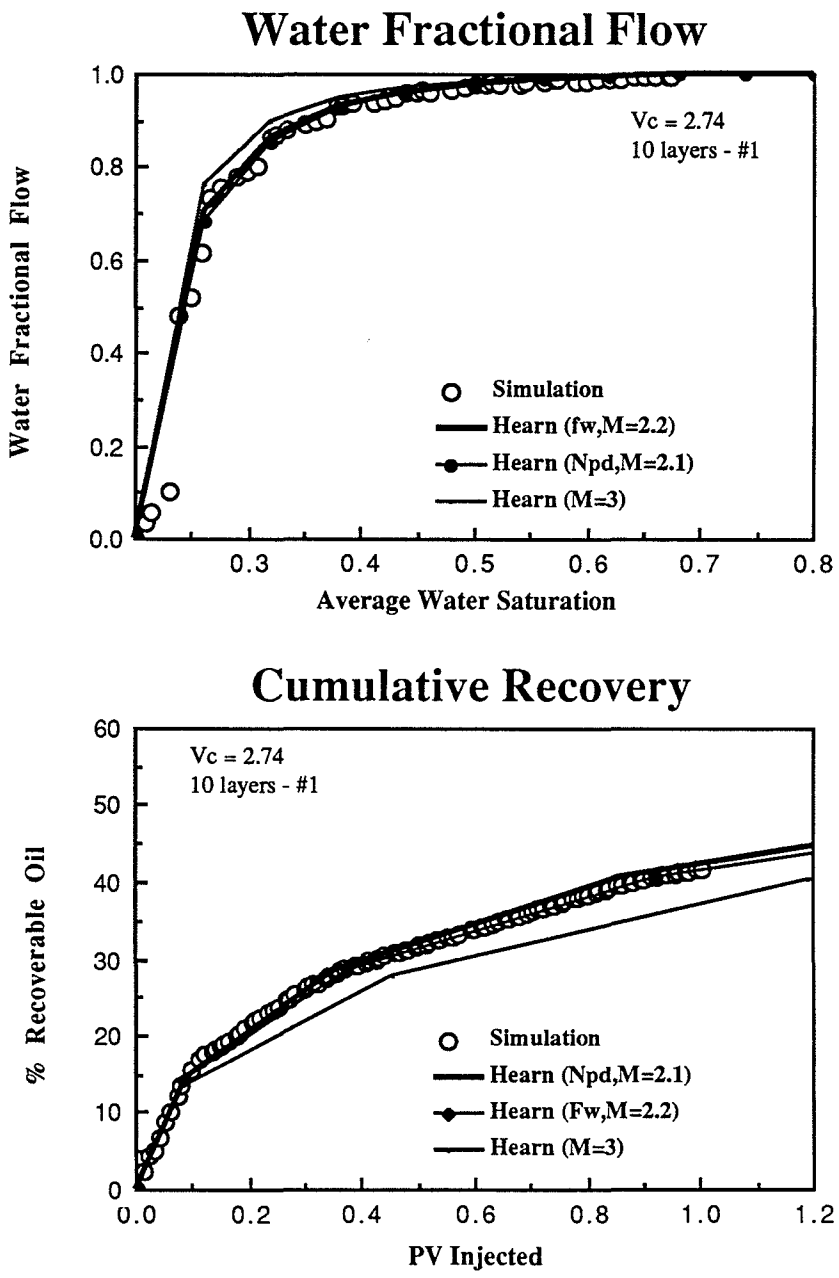

Fig. V.27: Water Fractional Flow and Cumulative Recovery (M^o=3.0; Ord. Scheme #1; V_C=2.74)

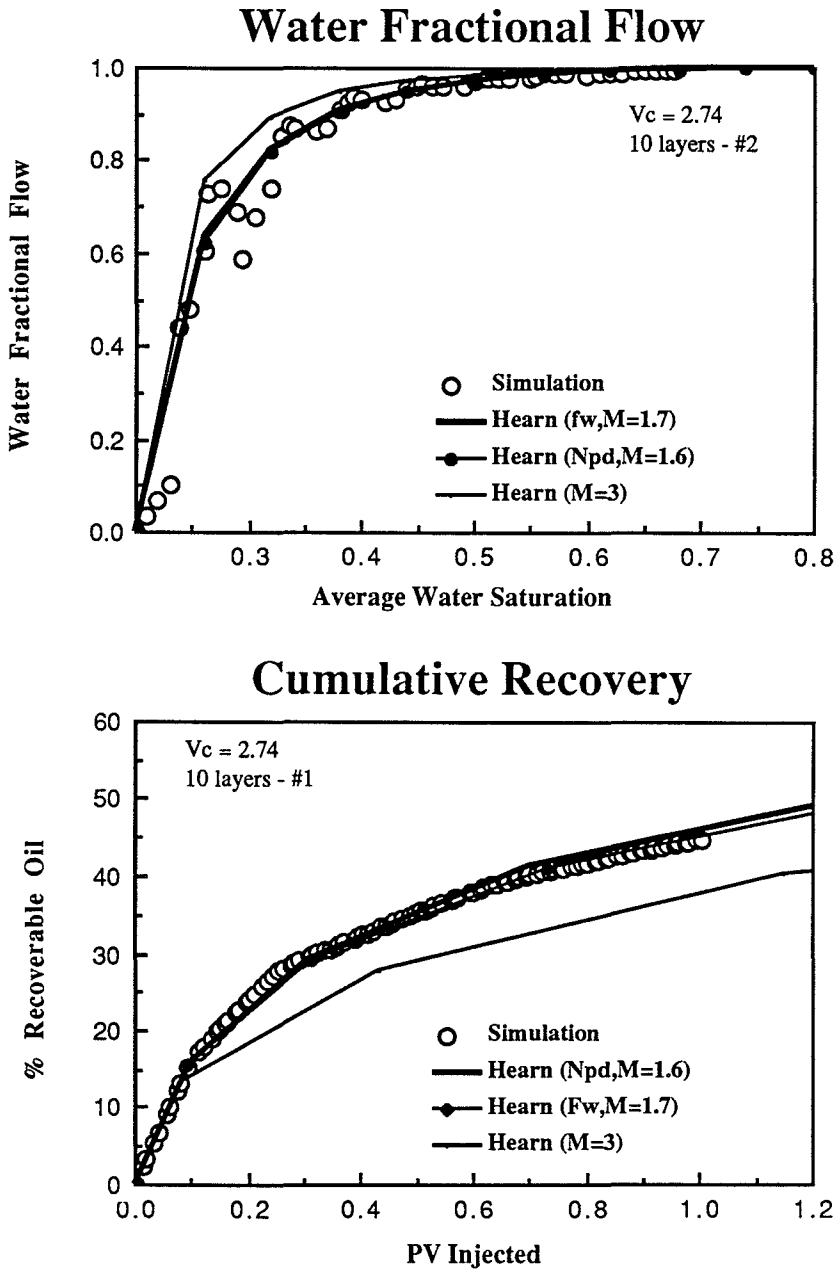

Fig. V.28: Water Fractional Flow and Cumulative Recovery (M^o=3.0; Ord. Scheme #2; V_C=2.74)

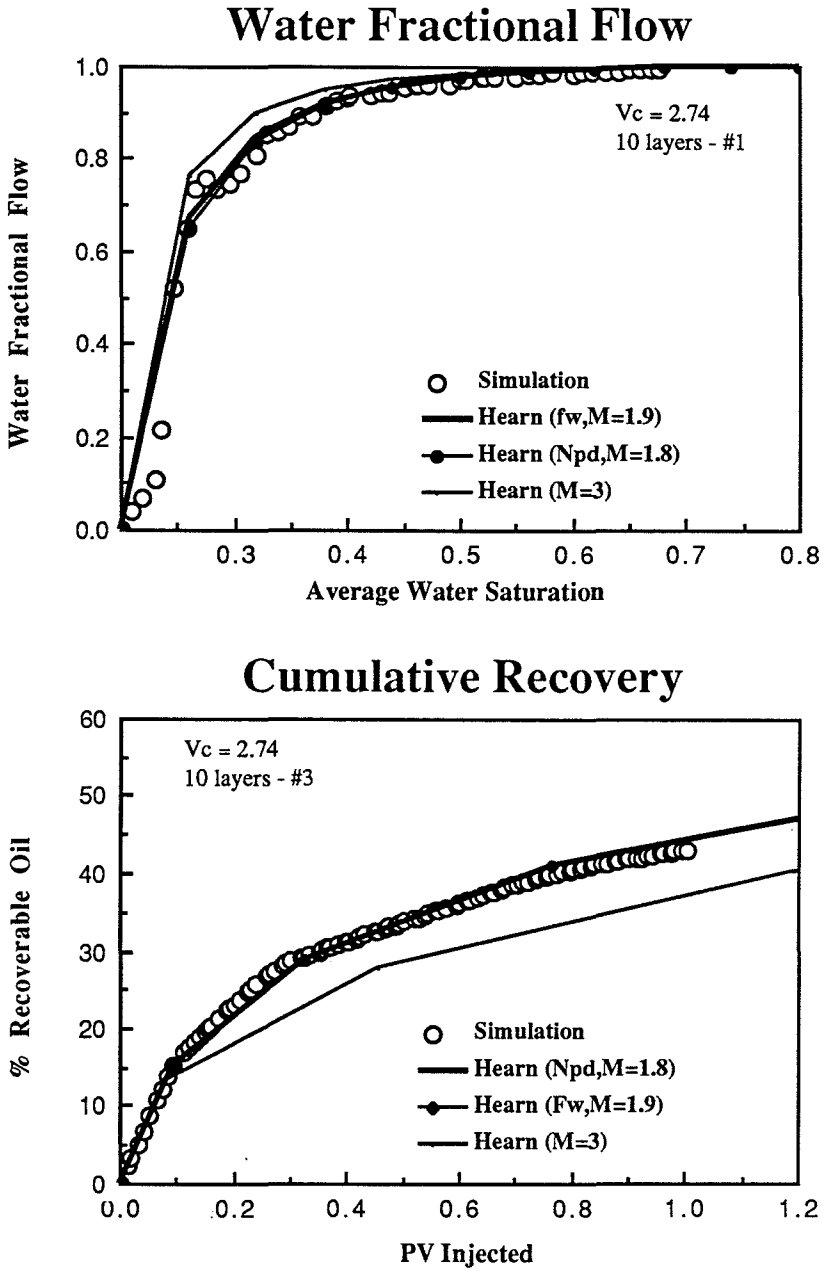

Fig. V.29 : Water Fractional Flow and Cumulative Recovery (M^o=3.0; Ord. Scheme #3; V_C=2.74)

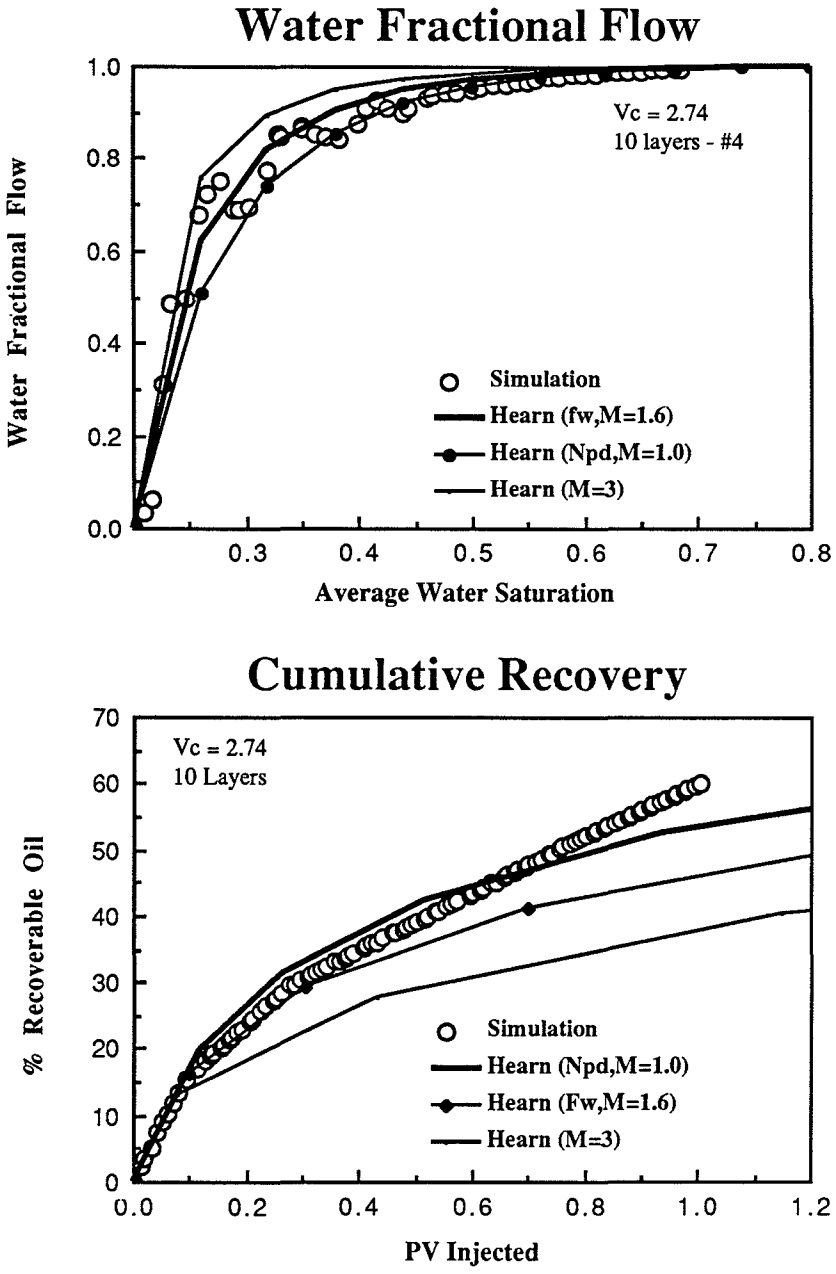

Fig. V.30 : Water Fractional Flow and Cumulative Recovery (M^o=3.0; Ord. Scheme #4; V_C=2.74)

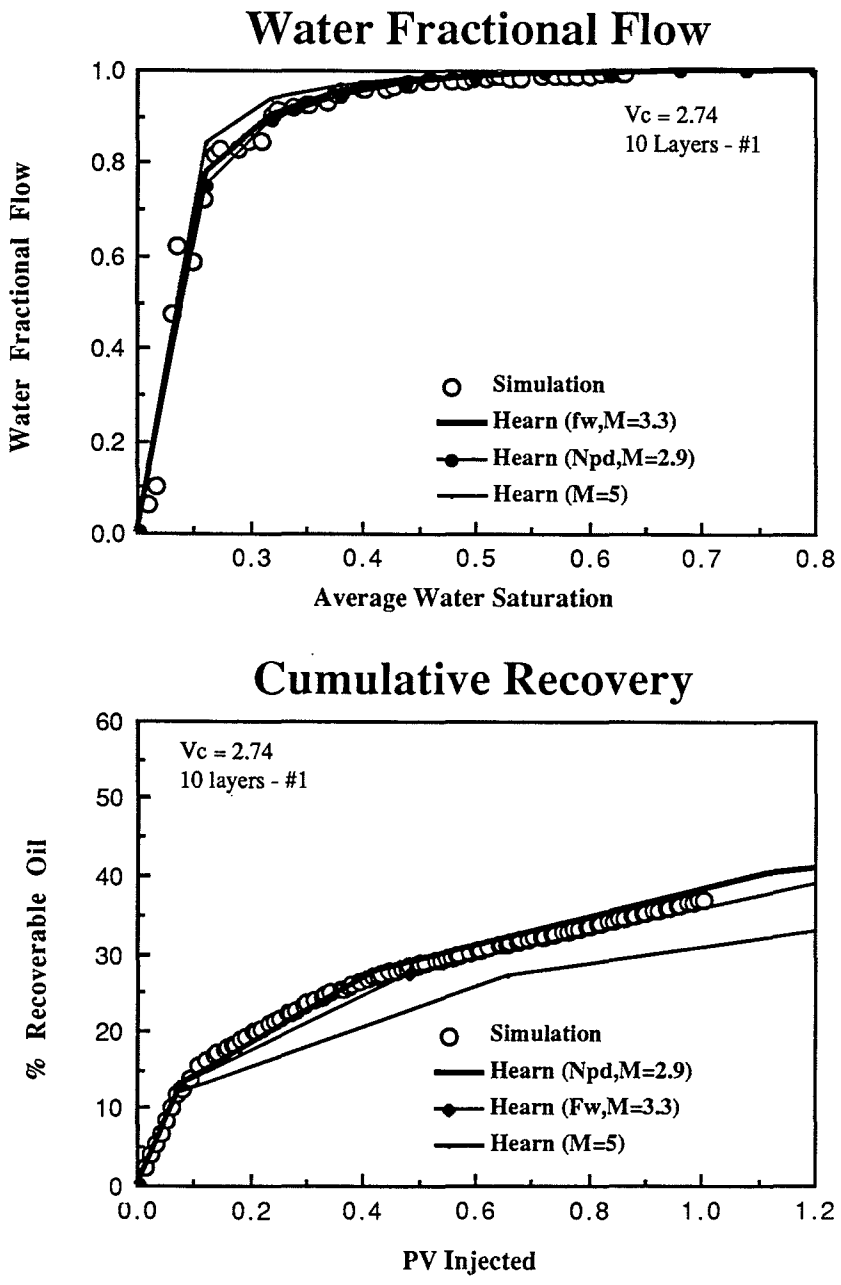

Fig. V.31 : Water Fractional Flow and Cumulative Recovery (M^o=5.0; Ord. Scheme #1; V_C=2.74)

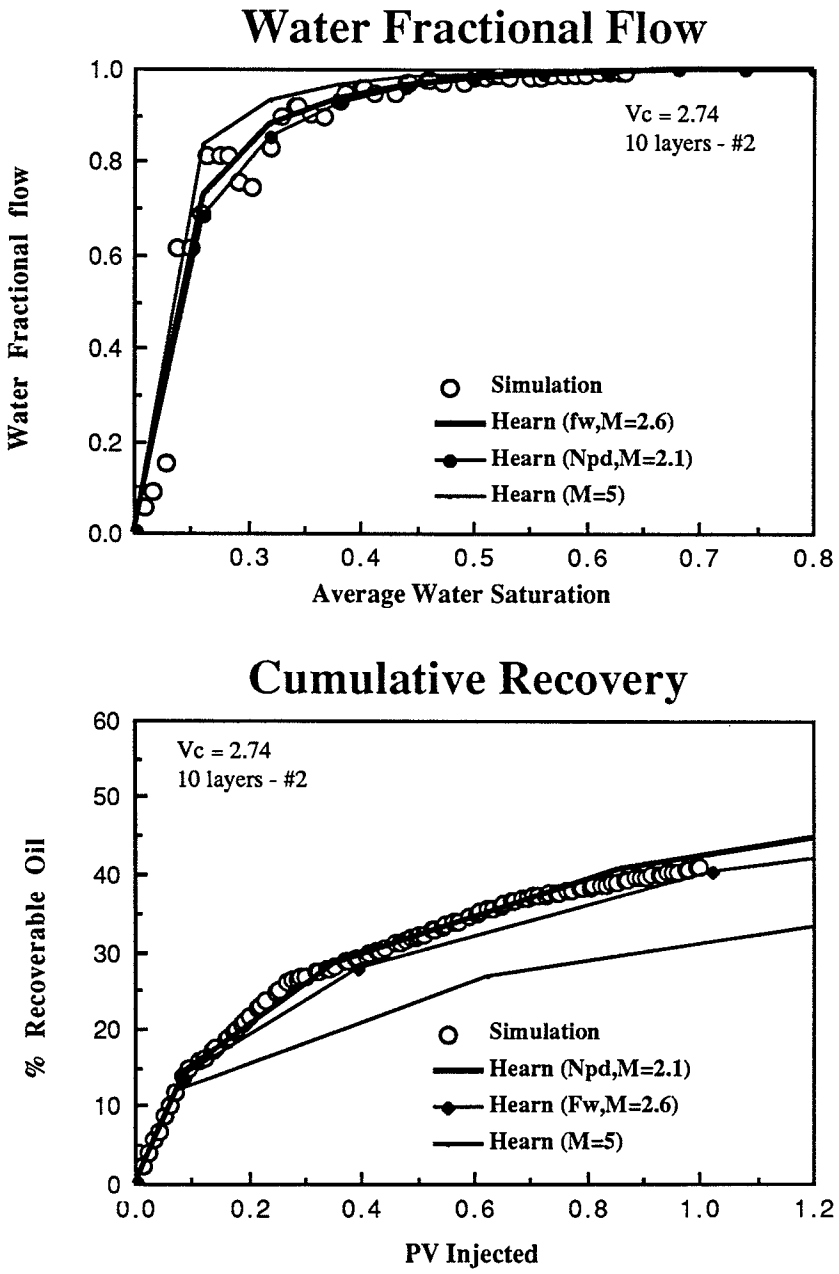

Fig. V.32 : Water Fractional Flow and Cumulative Recovery (M^o=5.0; Ord. Scheme #2; V_C=2.74)

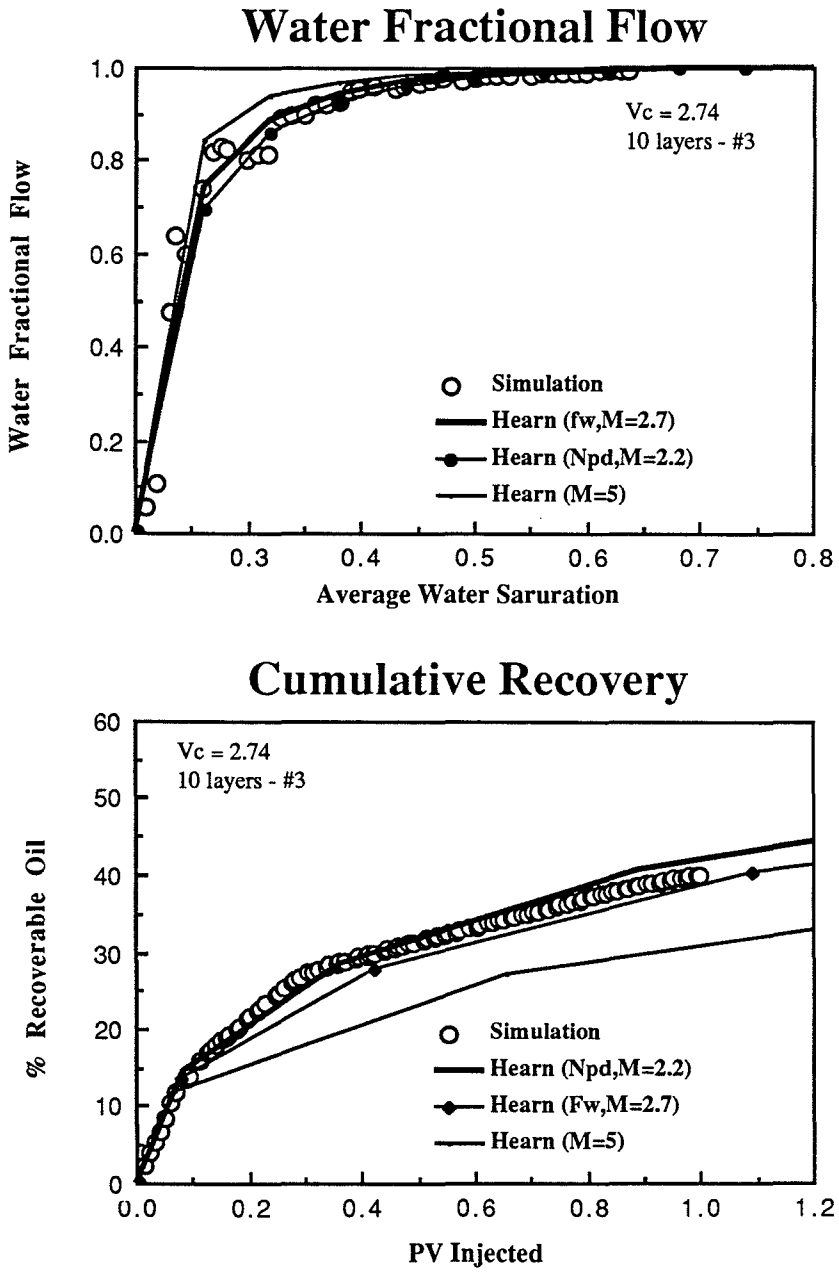

Fig. V.33: Water Fractional Flow and Cumulative Recovery (M^o=5.0; Ord. Scheme #3; V_C=2.74)

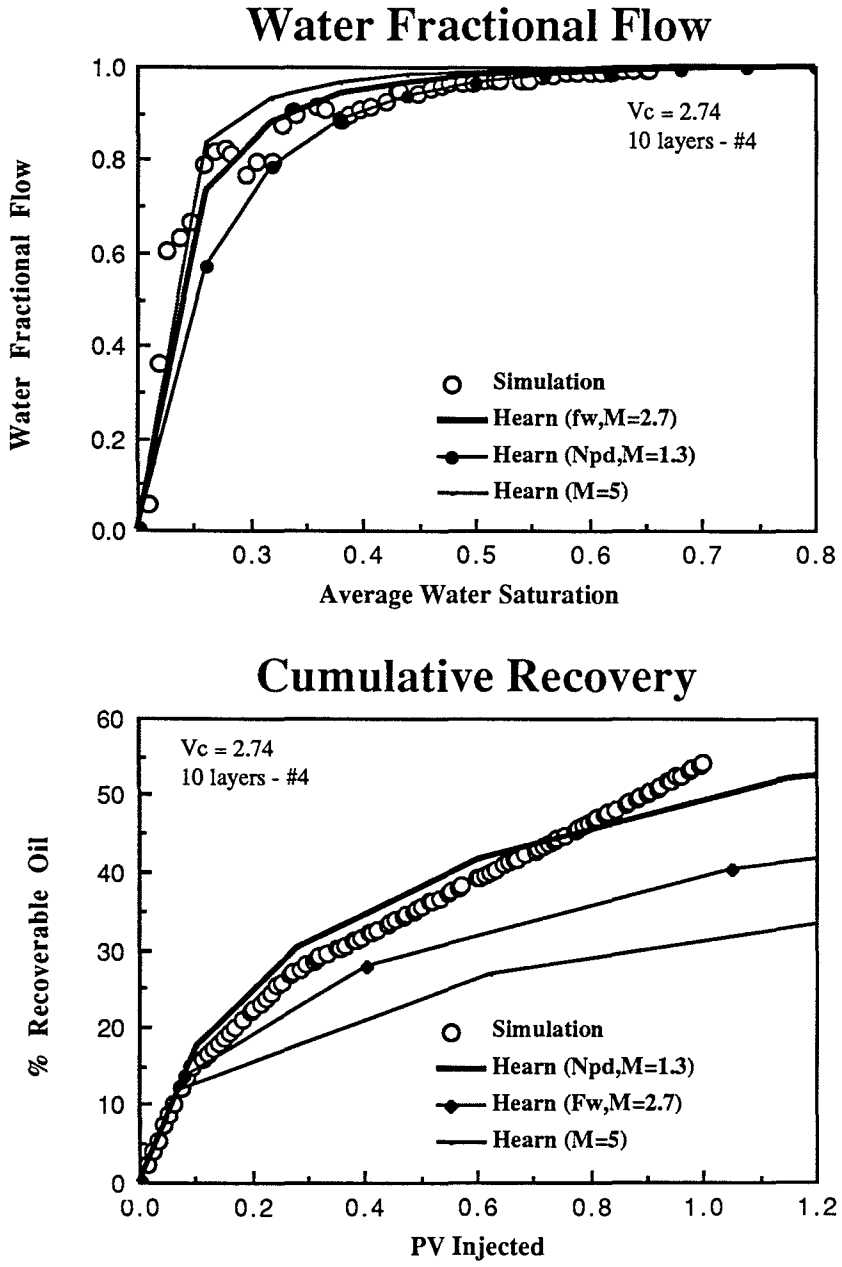

Fig. V.34 : Water Fractional Flow and Cumulative Recovery (M^o=5.0; Ord. Scheme #4; V_C = 2.74)

from each other so as to have two separate groups would mitigate the effects of viscous mixing. This general trend can be observed in Fig. V.25 and Fig. V.26.

The random layering scheme exhibits the best recovery since there exists a probability that a fast layer may be bounded by slow layers on either side. In other words, of the four schemes proposed, the random ordering comes closest to the ideal alternating scheme mentioned above. The descending (ascending) type layering on the other hand, is expected to have the worst recovery of the four since the fast layers and the slow layers are separated by a maximum distance and there is only one side of the fast layer open for oil to crossflow in and be channeled to the production well. Since schemes #2 and #3 are in between cases their production behavior is also expected to lie somewhere in between the descending (ascending) and random-layer production response. Between the two, the production response of scheme #2 seems to be slightly better than scheme #3. This is probably because in scheme #3 the fast layers are at the same time the boundaries of the system and therefore reduce the degree of viscous crossflow compared to scheme #2.

5.3 AN ALTERNATIVE APPROACH - EFFECTIVE LAYERING

The simulation runs presented in the previous section show that the effective mobility approach is not always successful in modifying the Hearn model to correct for the increased recovery due to viscous mixing. This is especially true if different ordering schemes for the layers are brought into the problem. Furthermore, it can be expected that with increasing Craig coefficient and/or increasing true end-point mobility ratio the same type of misfit, as with the different layering schemes, will be observed. This is expected since there is nothing physical about using an effective mobility ratio in the Hearn model and it really represents a simple one-parameter fit.

An alternative method for a better match of the data obtained in the simulations may be through the use of effective permeability-height products. That is, find an effective layering with permeabilities and heights such that the Hearn model will return the fractional flow and cumulative recovery curve obtained by the

simulator. Clearly, one advantage of this approach is that it becomes a multi-parameter fit. To be exact, there will be N-1 effective permeability-height values that can be solved for from the fractional flow curve. The N^{th} permeability-height product must be solved for with the aid of an additional constraining equation.

5.3.1 Solving For Effective Layers

The general idea is to modify Hearn's model to match the simulated results using effective permeability-height products instead of an effective end-point mobility ratio. Hearn's model then becomes

$$\tilde{f}_{w_n} = \left[1 + \frac{1}{M^o} \frac{\sum_{i=n+1}^{N} (k_i h_i)'}{\sum_{i=1}^{n} (k_i h_i)'} \right]^{-1} \qquad \text{(V.4)}$$

where

$(k_i h_i)'$ = Effective permeability-height product

M^o = True end-point mobility ratio

As discussed previously, one problem with using the simulated fractional flow curve directly in the analysis is that it suffers from considerable numerical dispersion and as the system increases in heterogeneity, can introduce large errors in the cumulative recovery because of deviations in the slope. Since it is the cumulative recovery that ultimately has to be fitted as best as possible, it is advisable to use this curve to calculate the effective permeabilities rather than the fractional flow curve.

Two variables returned by the cumulative recovery curve needed for calculating the effective permeability-height products are the average water saturation of the system and the slope of the fractional flow function at that average water saturation. From the Welge (1952) construction, the average water saturation for the entire system is given by

$$\overline{S}_w = \tilde{S}_{we} - \frac{1}{\left.\frac{d\tilde{f}_w}{d\tilde{S}_w}\right|_{\tilde{S}_{we}}} \left[\tilde{f}_{we} - 1\right] \qquad \text{(III.25)}$$

solving for $\tilde{f}_{we}$ gives

$$\tilde{f}_{we} = \left.\frac{d\tilde{f}_w}{d\tilde{S}_w}\right|_{\tilde{S}_w} (\tilde{S}_{we} - \overline{S}_w) + 1 \qquad \text{(III.25.a)}$$

In Eq.(III.25.a) the slope of the fractional flow curve and the average water saturation are given directly from the cumulative recovery curve. The effluent water saturation, on the other hand, must be determined indirectly from the slope and the average water saturation.

The slope is given by

$$\left.\frac{d\tilde{f}_w}{d\tilde{S}_w}\right|_{\tilde{S}_{we}} = \left.\frac{1}{\text{PV Injected}}\right|_{\tilde{S}_{we}} = \left.\frac{1}{t_D}\right|_{\tilde{S}_{we}} \qquad \text{(V.5)}$$

and the average water saturation is, according to Eq.(III.27)

$$\overline{S}_w = (1.0 - \tilde{S}_{or} - \tilde{S}_{wr})\, N_{PD}\Big|_{\tilde{S}_{we}} + \tilde{S}_{wi} \qquad \text{(III.27.a)}$$

where

N_{PD} = Dimensionless oil recovery

The effluent water saturation $\tilde{S}_{we}$ is no longer given by Eq.(III.24). Using the slope of the fractional flow function at a given average water saturation and solving for the effluent water fractional flow automatically fixes the effluent water saturation as well.

From Eq.(III.25.a),

$$\left\{ \left.\frac{d\tilde{f}_w}{d\tilde{S}_w}\right|_{\tilde{S}_w} (\tilde{S}_{we} - \overline{S}_w) + 1 \right\}_i = \left\{ \left.\frac{d\tilde{f}_w}{d\tilde{S}_w}\right|_{\tilde{S}_w} (\tilde{S}_{we} - \overline{S}_w) + 1 \right\}_{i+1}$$

and the corresponding effluent water saturations for each layer can be calculated by

$$\tilde{S}_{we_i} = \frac{(t_{Di+1}\overline{S}_{wi} - t_{Di}\overline{S}_{wi+1})}{(t_{Di+1} - t_{Di})} \qquad i=1,N-1 \qquad (V.6)$$

where

t_{Di} = Dimensionless breakthrough time of layer i

t_{Di+1} = Dimensionless breakthrough time of layer i+1

Equation (V.6) solves only for N-1 values. The N^{th} effluent water saturation is, of course, simply one minus the residual oil saturation. Knowing the effluent water saturations allows for the effective heights to be calculated through rearrangement of Eq.(III.24) into a system of linear equations.

$$\tilde{S}_{we} = \frac{\sum_{i=1}^{n} \{\phi\Delta Sh_{eff}(1-S_{or})\}_i + \sum_{i=n+1}^{N} \{\phi\Delta Sh_{eff}S_{wr}\}_i}{(\phi\overline{\Delta S})H} \qquad (III.24)$$

At this point everything in Eq.(III.25.a) is known and the effluent water fractional flow can be solved for. Once the effluent water fractional flow is known the effective permeability-height products can be calculated. Rearranging, Eq.(V.4) gives

$$\left\{\frac{1}{\tilde{f}_{w1}} - 1\right\} M^o = \frac{(k_2h_2)' + (k_3h_3)' + \ldots + (k_Nh_N)'}{(k_1h_1)'} \qquad (V.7.a)$$

$$\left\{\frac{1}{\tilde{f}_{w2}} - 1\right\} M^o = \frac{(k_3h_3)' + (k_4h_4)' + \ldots + (k_Nh_N)'}{(k_1h_1)' + (k_2h_2)'} \qquad (V.7.b)$$

$$\left\{\frac{1}{\tilde{f}_{w_{N-1}}} - 1\right\} M^o = \frac{(k_N h_N)'}{(k_1 h_1)' + (k_2 h_2)' + \ldots + (k_{N-1} h_{N-1})'} \qquad \text{(V.7.c)}$$

The last equation for the N^{th} layer can not be determined from Eq.(V.4) since $\tilde{f}_{w_N}$ is equal to one and the left side is equal to zero. (There are N+1 points on the fractional flow curve but the end points $(S_{wr},0)$ and $(1-S_{or},1)$ are fixed and independent of the permeability-height product; consequently there are only N+1-2 degrees of freedom). Therefore an additional equation is needed. It becomes arbitrary what constraining equation is used at this point. Probably the one that can be justified best from a physical point of view is the preservation of the mean of the permeability-height product which translates into Eq.(V.8)

$$\sum_{i=1}^{N} (k_i h_i)' = \sum_{i=1}^{N} k_i h_i \qquad \text{(V.8)}$$

Define

$$\alpha_n = \left\{\frac{1}{\tilde{f}_{w_n}} - 1\right\} M^o \qquad \text{(V.9)}$$

then the system of equations to be solved becomes

$$\alpha_1 (k_1 h_1)' - (k_2 h_2)' - (k_3 h_3)' - (k_4 h_4)' \ldots - (k_N h_N)' = 0 \qquad \text{(V.10.a)}$$

$$\alpha_2 (k_1 h_1)' + \alpha_2 (k_2 h_2)' - (k_3 h_3)' - \ldots - (k_N h_N)' = 0 \qquad \text{(V.10.b)}$$

$$\alpha_{N-1} (k_1 h_1)' + \ldots + \alpha_{N-1} (k_{N-1} h_{N-1})' - (k_N h_N)' = 0 \qquad \text{(V.10.c)}$$

$$(k_1 h_1)' + (k_2 h_2)' + (k_3 h_3)' + (k_4 h_4)' + \ldots + (k_N h_N)' = \sum_{i=1}^{N} k_i h_i \qquad \text{(V.10.d)}$$

Equation (V.10.a) through (V.10.d) is a system of linear equations that can be solved using standard linear algebra methods. Once the effective permeability-height products are determined, the effective permeabilities can be calculated by simply dividing through the the effective heights solved for using Eq.(V.24).

$$k'_i = \frac{(k_i h_i)'}{h'_i} \qquad i=1,N \qquad (V.11)$$

5.3.2 Effective Permeabilities for Various Cases

In order to visualize the change in the effective permeabilities of a system, it is worthwhile going through the exercise for a case in which the effective end-point mobility ratio method worked well. This allows for the effluent water fractional flow values, needed in Eq.(V.7), to be determined directly from the Hearn model using the effective mobility ratio rather than having to determine them graphically from the simulated data. Furthermore, it allows for the effluent water saturation to be calculated by Eq.(III.24) since the effective heights, in this specific case, will be equal to the original heights of the individual layers.

The cases used here are shown in Fig.V.5 through Fig.V.9 of sec.5.1. These were for a Craig coefficient of V_C = 1.96 and a #1 type layering scheme and

Layer #	Korig	M=1.5	M=2	M=3	M=4	M=5
1	413.7	378.7	359.7	339.6	329.0	316.0
2	226.4	225.9	224.7	222.6	221.1	219.0
3	139.5	146.4	149.9	153.3	154.9	156.7
4	90.88	98.62	102.9	107.5	109.9	112.9
5	60.85	67.50	71.37	75.69	78.04	81.05
6	41.08	46.25	49.35	52.89	54.85	57.41
7	27.51	31.29	33.59	36.26	37.76	39.73
8	17.93	20.53	22.13	24.00	25.07	26.47
9	11.04	12.70	13.72	14.93	15.62	16.54
10	6.043	6.966	7.543	8.223	8.612	9.129

Table V.5: Effective Permeabilities in [md] for V_C =1.94 and #1 Ordering Scheme

the effective mobility ratio approached worked well. The effective permeabilities solved for are tabulated in Table V.5 and compared to the original log-normal distribution in Fig.V.35. Figure V.35 shows the resulting permeability distributions listed in Table V.5. One immediate result that can be seen is that compared to the original distribution, viscous mixing effectively makes the layered system look less heterogeneous than it really is. Especially for the higher permeability layers, the deviation from the original distribution is considerable.

An example where the effective end-point mobility approach does not approximate the recovery curve well and consequently the effective permeability-height products must be determined graphically from the cumulative recovery curve is shown in Fig. V.36. Figure V.36 shows the result of a simulation run with a Craig coefficient of $V_C = 4.35$ and a #1 ordering scheme. The solid lines indicate various effective mobility ratios used in attempting to fit the data. It can be seen that the there will actually be no value for which the Hearn model can be made to fit the simulation data reasonably well.

To use the cumulative recovery curve the data is split up into three straight line portions given by

$$N_{PD} = 166.428\ t_D \qquad \text{(V.12.a)}$$

$$N_{PD} = 8.613 + 33.499\ t_D \qquad \text{(V.12.b)}$$

$$N_{PD} = 19.001 + 7.8625\ t_D \qquad \text{(V.12.c)}$$

If a third fictitious point is thought of as being at sweepout ($N_{PD} = 100\%$) then the three points to use from the simulated recovery curve become (0.0648,10.8), (0.405,22.2), and (10.3,100.). Using Eq.(V.6) the effluent water saturations can be determined to be

$$\tilde{S}_{w1} = 0.251771429;\ \tilde{S}_{w2} = 0.314085356;\ \tilde{S}_{w3} = 0.8$$

Then for

$$\{\phi\Delta S(1-S_{or})\}_i = 0.064 \qquad i=1,10$$

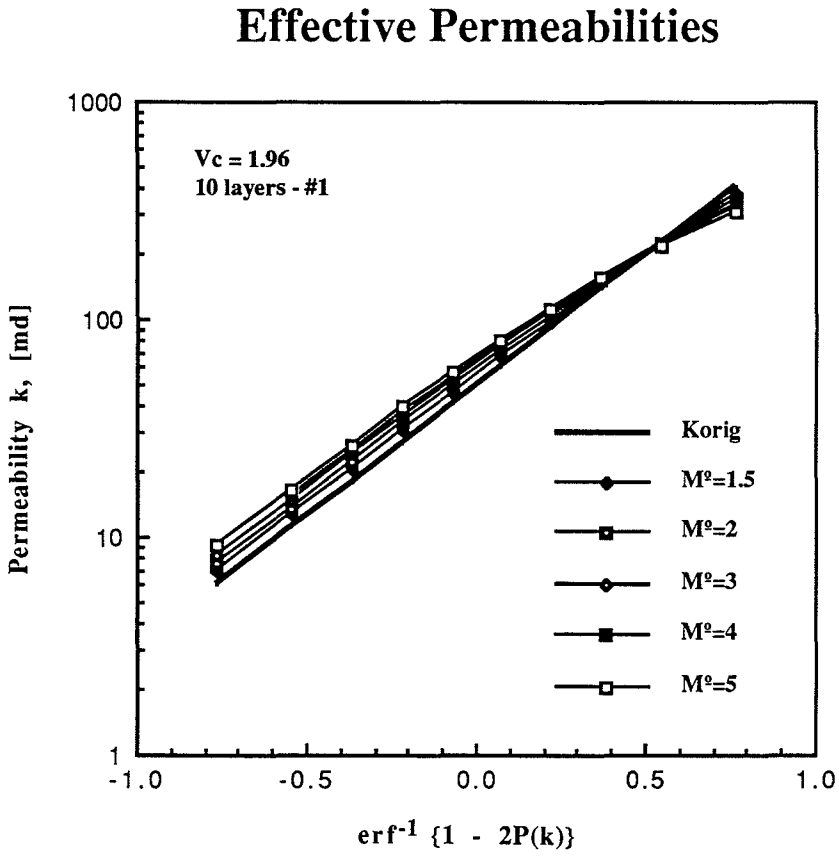

Fig. V.35: **Effective Permeabilities for V_C = 1.96 and #1 Ordering Scheme**

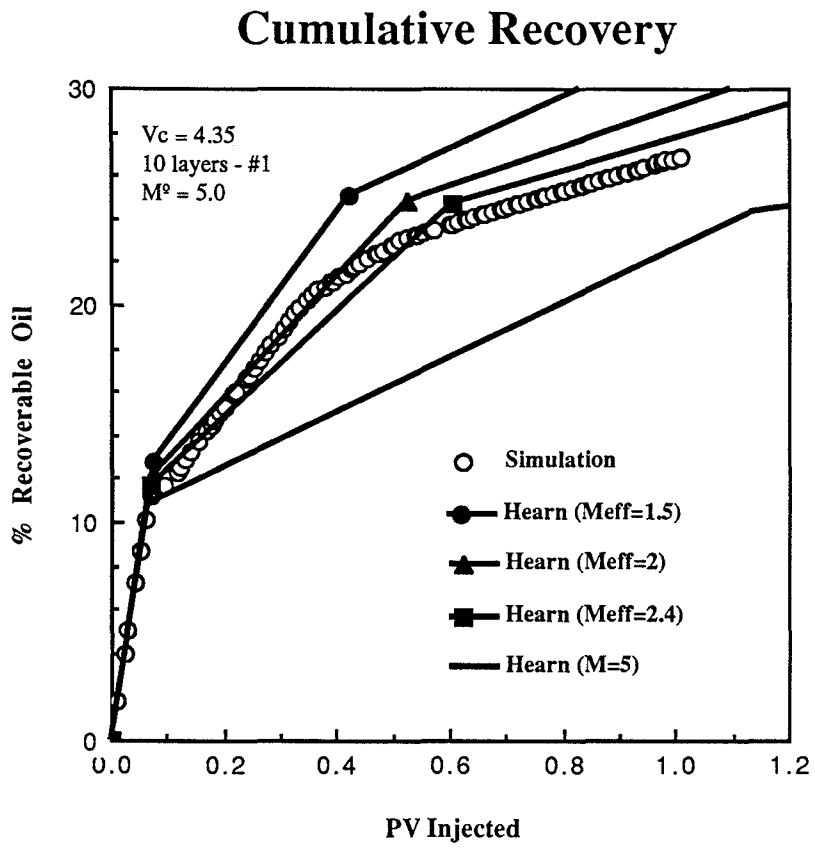

Fig. V.36: Cumulative Recovery for V_C=4.35, M^o=5, and #1 Ordering Scheme

$$\{\phi\Delta S(S_{wr})\}_i = 0.016 \qquad i=1,10$$

$$(\overline{\phi\Delta S})H = 0.08$$

the equations for the effective heights can be written in matrix form as

$$\begin{bmatrix} 0.8 & 0.2 & 0.2 \\ 0.8 & 0.8 & 0.2 \\ 0.8 & 0.8 & 0.8 \end{bmatrix} \begin{bmatrix} h'_1 \\ h'_2 \\ h'_3 \end{bmatrix} = \begin{bmatrix} 0.25177 \\ 0.31409 \\ 0.8 \end{bmatrix}$$

and returning

$$h'_1 = 0.086285715;\ h'_2 = 0.103856545;\ h'_3 = 0.80985774$$

The effluent water fractional flows are then given by Eq.(III.25.a)

$$\tilde{f}_{we} = \left.\frac{d\tilde{f}_w}{d\tilde{S}_w}\right|_{\tilde{S}_{we}} (\tilde{S}_{we} - \overline{\tilde{S}}_w) + 1 \qquad \text{(III.25.a)}$$

and thus

$$\tilde{f}_{w1} = 0.798941806;\ \tilde{f}_{w2} = 0.952803348;\ \tilde{f}_{w3} = 1.0$$

For alpha defined as

$$\alpha_n = \left\{\frac{1}{\tilde{f}_{we_n}} - 1\right\} M^o \qquad \text{(V.8.b)}$$

using the effluent fractional flow values will give

$$\alpha_1 = 1.258278090;\ \alpha_2 = 0.247672575$$

The original permeability distribution was

$$k = \{54952,\ 14383,\ 4894.5,\ 1888.5,\ 773.96,\ 323.02,\ 132.39,\ 51.078,\ 17.381,\ 4.549\}$$

and

$$h_i = 0.1 \qquad i=1,10$$

such that

$$\sum_{i=1}^{N} k_i h_i = 7742$$

The system of equations can then be represented in matrix form as

$$\begin{bmatrix} \alpha_1 & -.1 & -1 \\ \alpha_2 & \alpha_2 & -1 \\ 1 & 1 & 1 \end{bmatrix} \begin{bmatrix} (kh)'_1 \\ (kh)'_2 \\ (kh)'_3 \end{bmatrix} = \begin{bmatrix} 0 \\ 0 \\ 7742 \end{bmatrix} \qquad \text{(V.9)}$$

Solving Eq.(V.9) for the effective permeability-height products gives

$$(kh)'_1 = 3428.2757;\ (kh)'_2 = 2776.8778;\ (kh)'_3 = 1536.8464$$

Dividing by the effective heights returns the values for the effective permeabilities.

The resulting effective layering of the $V_C = 4.35$ case with $M^o = 5.0$ such that the Hearn model correctly approximates the cumulative recovery curve is

$k_1 = 39732$ md; $\quad h_1 = 0.086$
$k_2 = 26738$ md; $\quad h_2 = 0.104$
$k_3 = 1897.7$ md; $\quad h_3 = 0.810$

The Hearn solution using the above permeabilities and heights with M^o=5.0 is compared to the simulated data in Fig.V.37. Also, the permeabilities are

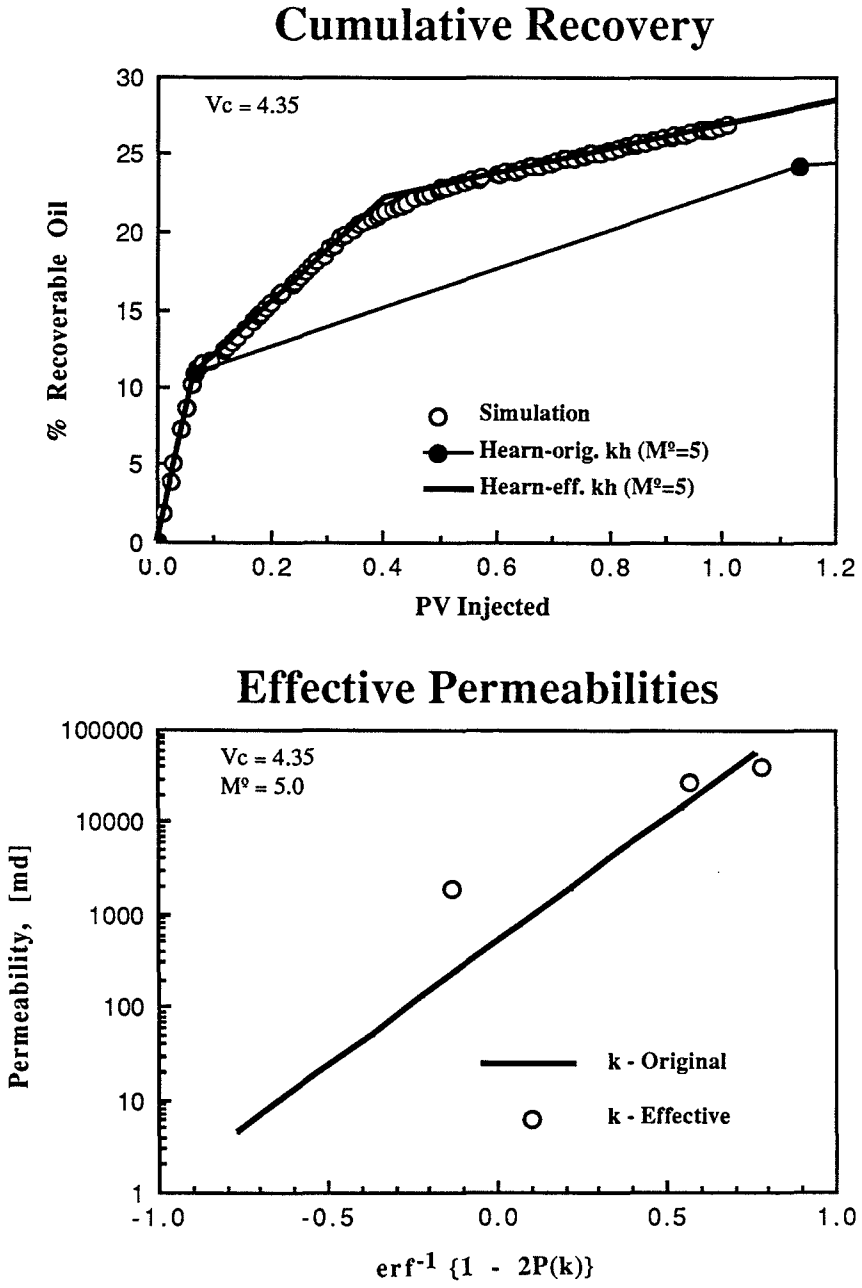

Fig. V.37: Effective (kh) Method; Cumulative Recovery Curve for V_C=4.35, M^o=5, and #1 Ordering Scheme

compared to the original distribution. While the above method is unquestionably more tedious, it does offer the possibility to match the simulated recovery when the effective mobility ratio approach fails.

As in the previous calculation, again the system effectively acts as if it were less heterogeneous than the original layering. In this case the first layer kh is lower and the second layers kh higher than the original values. The influence of the other layers is somewhat difficult to judge since there is no simulation data to back any claim. Nevertheless, from Fig. V.35 it appears that crossflow in the lower permeability layers is less important since the actual permeability distribution, i.e. Craig coefficient, hardly changes.

The tendency for the system to behave as it were less heterogeneous was demonstrated in Sec. 3.2.1 for favorable mobility displacements under vertical equilibrium. Specifically, Equation (III.13.c) showed that an end-point mobility ratio can be picked such that the permeability contrast vanishes entirely.

For the unfavorable mobility ratio case there appears to be a similar behavior. As the end-point mobility ratio increases the effective permeability contrast between layers seen by the displacement becomes smaller. In theory, the limiting case for complete suppression of heterogeneity would occur for an infinite end-point mobility ratio if one were able to retain a sharp front displacement. This, of course, is unrealistic but nevertheless indicates a trend.

5.4 PSEUDO RELATIVE PERMEABILITIES

Hearn's (1971) original intent was to derive pseudo relative permeability curves for displacements occurring in vertical equilibrium and where the dominant forces where viscous forces. Since the results presented in the previous sections retain the basic features of the Hearn model, pseudo relative permeability curves can be calculated using the same procedure as proposed by Hearn but using effective properties as explained in sec.5.3 instead of the original permeability-height products. The equations proposed by Hearn, modified for effective properties become

$$\tilde{S}_{w_n} = \frac{\sum_{i=1}^{n} \{\phi\Delta S(1-S_{or})h_{eff}\}_i + \sum_{i=n+1}^{N} \{\phi\Delta S S_w h_{eff}\}_i}{(\phi\overline{\Delta S})H} \qquad (V.13)$$

$$\tilde{k}_{w_n} = k_{wr} \frac{\sum_{i=1}^{n} (k_i h_i)_{eff}}{\sum_{i=n+1}^{N} (k_i h_i)_{eff}} \qquad (V.14)$$

$$\tilde{k}_{o_n} = k_{or} \frac{\sum_{i=n+1}^{N} (k_i h_i)_{eff}}{\sum_{i=1}^{n} (k_i h_i)_{eff}} \qquad (V.15)$$

where

$\tilde{k}_{w_n}$,$\tilde{k}_{o_n}$ = Pseudo relative water and oil permeabilities

$\tilde{S}_w$ = Thickness averaged water saturation

k_{wr} , k_{or} = End-point relative permeabilities of original curves

Using the effective properties in Table V.5, the pseudo relative permeabilities are compared to the original Hearn curves in Fig.'s V.38-V.39. While the Hearn pseudo relative permeabilities do not change with increasing end-point mobility ratio, the ones calculated with the effective properties do.

The shift in the direction of the pseudo relative permeabilities curves with increasing true end-point mobility ratio compared to the original Hearn curve again indicate an overall effective decrease in medium heterogeneity due to viscous mixing and crossflow.

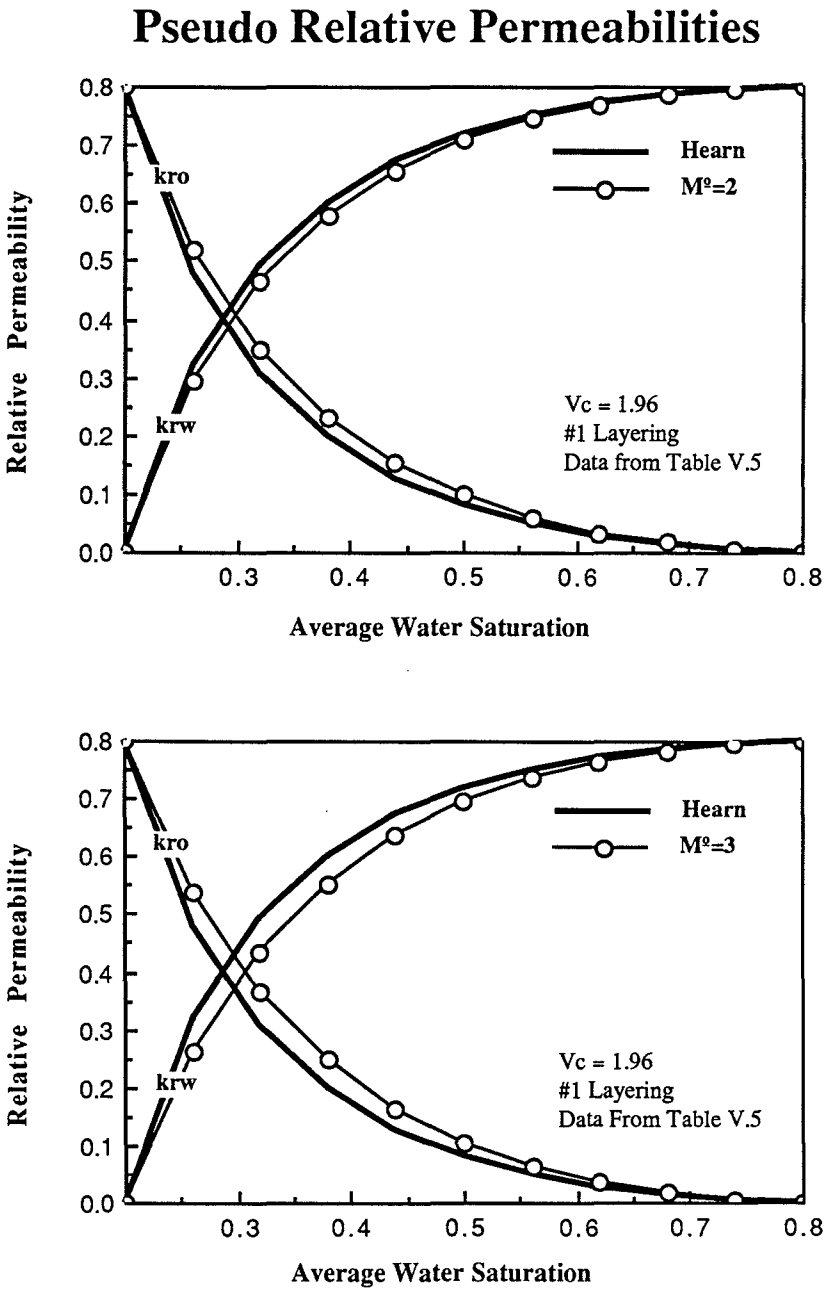

Fig. V.38: **Pseudo Relative Permeabilities Using Effective Permeability-Height Products**

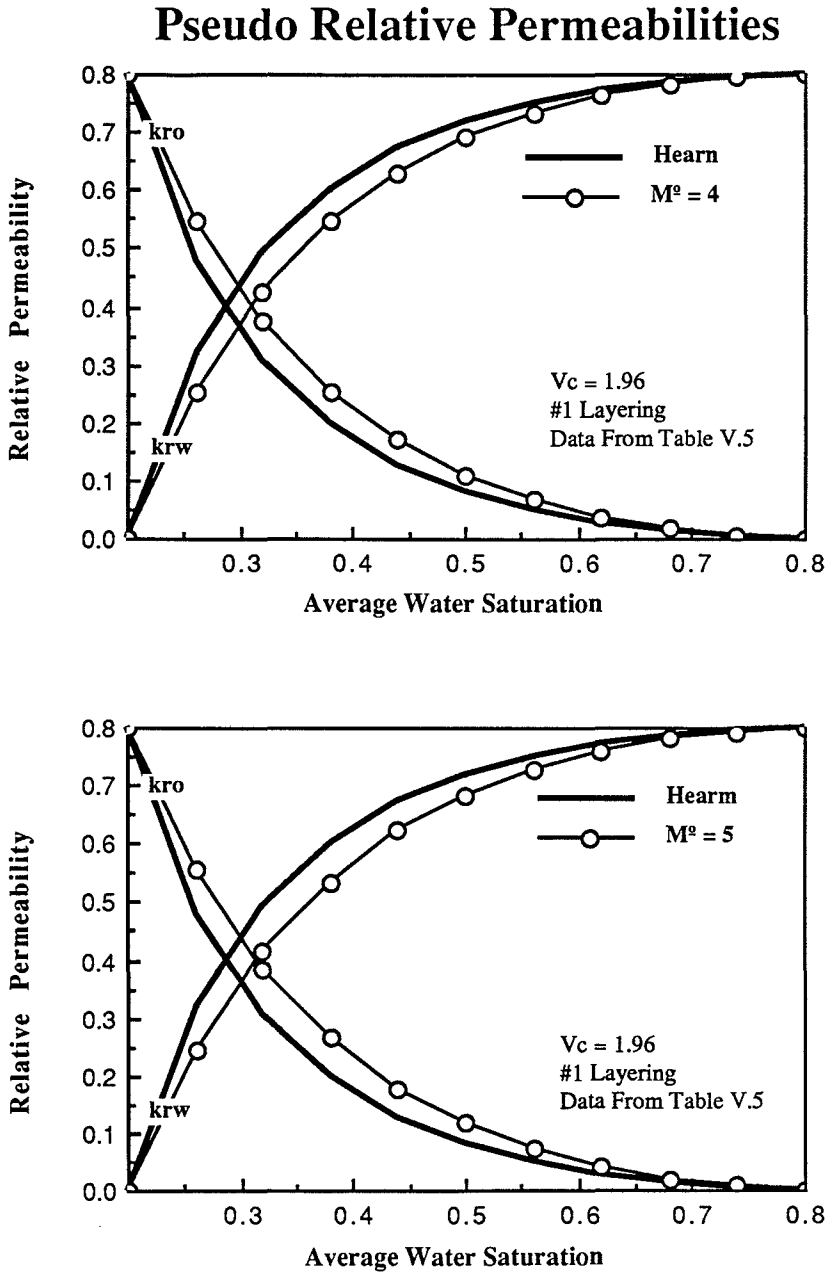

Fig. V.39: **Pseudo Relative Permeabilities Using Effective Permeability-Height Products**

CHAPTER VI

CONCLUSIONS AND RECOMMENDATIONS

6.1 CONCLUSIONS

1. For the case in which only viscous forces are considered and the displacement is assumed piston-like in each layer, the onset of vertical equilibrium can be related to a single dimensionless parameter called the effective length-thickness ratio. For all practical purposes, the limits for the

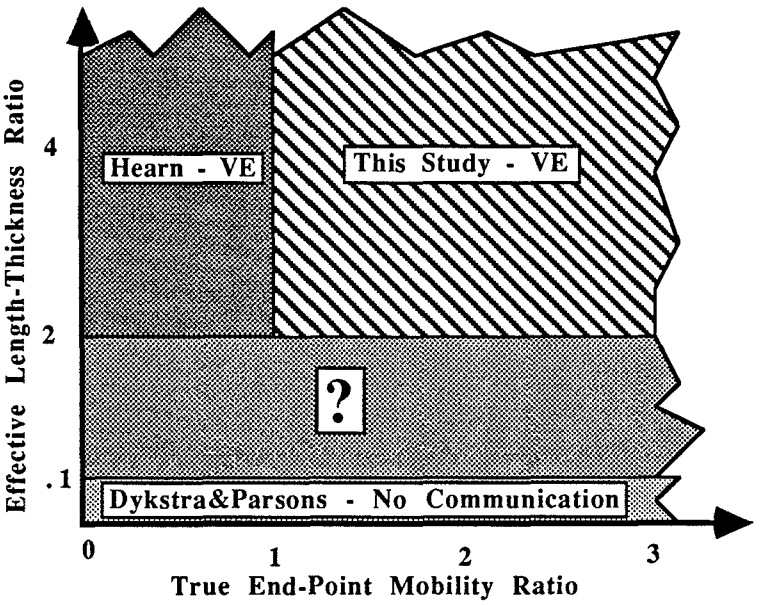

Fig. VI.1: Solution Space For Layered Systems

vertical equilibrium case and the no communication case are

$R_L \geq 2$ Vertical Equilibrium

$R_L \leq 0.1$ No Communication

2. The Hearn model is only correct for end-point mobility ratios less or equal to one ($M^o \leq 1$). For end-point mobility ratios greater than one ($M^o > 1$) and an effective length-thickness ratio greater than two ($R_L > 2$), the direction of crossflow is such that the flow in the bulk direction of flow does not remain segregated, as the Hearn model assumes. The net effect, caused by the reversal of the direction of crossflow, is the movement of displacing fluid (water) into less permeable layers and of displaced fluid (oil) into more permeable layers causing viscous mixing. Because the displaced fluid (oil) is channeled to the more permeable layers and as a result is produced earlier, the vertical sweep efficiency will increase compared to the Hearn model.

3. Increased recovery caused by viscous mixing was investigated with respect to three parameters: the true end-point mobility, the Craig coefficient, and the layer ordering scheme. Of the three, the layer ordering was found to have the largest impact on the degree of viscous mixing. Four categories of ordering were proposed, with the "random" ordering exhibiting the largest additional recovery.

   From a qualitative point of view, it is suggested that the descending (ascending) ordering will exhibit the lowest amount of increased recovery while a system with alternating high and low permeability layers will result in a maximum increase of recovery because of viscous crossflow.

4. For the descending (ascending) layer ordering scheme, a pseudofunction approach using an effective mobility ratio was used to correct Hearn's model for viscous mixing. For a Craig coefficient less than three ($V_C < 3$) and a true end-point mobility ratio less or equal to five ($M^o \leq 5$) a

simple linear relationship is proposed. Figure VI.2 illustrates the correct solution space.

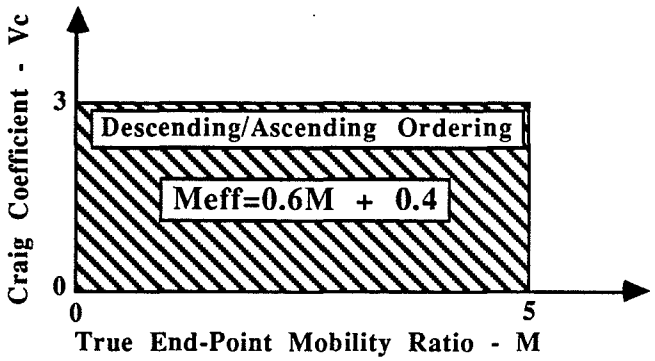

Fig.VI.2: Solution Space For Effective End-Point Mobility Ratio

5. The effective end-point mobility ratio is always less than the true end-point mobility ratio. An interpretation of this is that, effectively, viscous mixing attenuates the frontal advancement by lowering the mobility ratio across the interface between the displacing and the displaced fluid.

6. An alternative pseudofunction approach to Hearn's model is proposed through the use of effective permeability-height products. Contrary to the one parameter effective end-point mobility ratio approach this is a N-1 parameter fit, where N is the number of layers, and allows for the calculation of pseudo relative permeability curves. An additional equation is need to solve for the last permeability value (N^{th} layer). The preservation of the mean permeability-height product is used here.

7. From the effective permeability-height product it is shown that, to the Hearn model, viscous mixing makes the medium look less heterogeneous than it really is. The trend can be seen from the absolute permeability height

product distribution as well as from the pseudo relative permeability curves. As a theoretical limit, it is proposed that if a sharp front displacement could be maintained as the true end-point mobility ratio approaches infinity, viscous mixing would effectively make the medium look homogeneous.

6.2 RECOMMENDATIONS

1. Of the three parameters investigated with respect to viscous mixing, layer ordering was found to have the strongest influence on the displacement efficiency. For the descending (ascending) type ordering, the effective mobility ratio approach worked well within certain limits of the true end-point mobility ratio and Craig coefficient. It remains to be shown that for the other type ordering schemes this approach may work as well.

2. For the cases in which the simulation results could not be modelled by an effective mobility ratio approach an alternative method was presented using effective permeability-height products in the Hearn model. The potential of this method in trying to quantify the effects of viscous mixing by the deviation it causes in the original permeability distribution should be investigated.

3. The sensitivity of the pseudo relative permeability curves with respect to the parameters used in this investigation should be studied. For this, the effective permeability-height product approach is particularly convenient.

4. Once the sweep efficiency for displacement under vertical equilibrium conditions is quantified for the various parameter configurations a natural extension would be to investigate the region in between the vertical equilibrium and the no-communication (Dykstra-Parsons) model. In terms of the effective length-thickness ratio this region is given by $0.1 \leq R_L \leq 2$.

5. In a more general perspective, a similar pseudofunction approach, as presented here for viscous forces only, is necessary for displacements including other driving mechanism such as capillary, gravity, and dispersive forces as well as fractional flow effects. In particular it is of interest to quantify the onset of vertical equilibrium under these conditions by the use of dimensionless groups in the same fashion as the length-thickness ratio was used here.

BIBLIOGRAPHY

API, 1961, History of Petroleum Engineering, Dallas, TX.

Buckley, S.E. and Leverett, M.C., 1942, Mechanism of Fluid Displacement in Sands, *Trans.*, AIME 146, pp.107-116.

Caudle, B.H., 1968, Fundamentals of Reservoir Engineering - Part II, SPE, Dallas.

Craig, F.F., 1971, The Reservoir Engineering Aspects of Water Flooding, AIME, Dallas.

Craig, F.F., Sanderlin, J.L., Moore, D.W., and Geffen, T.M., 1957, A Laboratory Study of Gravity Segregation in Frontal Drives, *Trans.*, AIME 210, pp.275-281.

Coats, K.H., Dempsey, J.R., and Henderson, J.H., 1971, The Use of Vertical Equilibrium in Two-Dimensional Simulation of Three-Dimensional Reservoir Performance, SPEJ, March, pp.62-71.

Dykstra, H. and Parsons, R.L., 1950, The Prediction of Oil Recovery by Waterflood, *Secondary Recovery of Oil in the United States*, 2nd ed., API, pp.160-174.

Fettke, C.R., 1938, Bradford Oil Field, Pennsylvania and New York, *Pennsylvania Geological Survey*, 4th series, M-21.

Goddin, C.S. Jr., Craig, F.F., Wilkes, J.O., and Tek, M.R., A Numerical Study of Waterflood Performance in a Stratified System With Crossflow, *Soc. of Petroleum Engineering Journal*, June, pp.765-771.

Hearn, C.L., 1971, Simulation of Stratified Waterflooding by Pseudo-Relative Permeability Curves, *Journal of Petroleum Technology*, July, pp.805-813.

Hiatt, W.N., 1958, Injected-Fluid Coverage of Multi-Well Reservoirs with Permeability Stratification, *Drill. and Prod. Prac.*, API, p.165.

Hutchinson, C.A. Jr., 1959, Reservoir Inhomogeneity Assessment and Control, *Pet. Eng.*, Sept., V.31, pp.B19-26.

Jensen, J.L. and Lake, L.W., 1986, The Influence of Sample Size and Permeability Distribution Upon Heterogeneity Measures, SPE paper 15434, presented at 61th Annual Technical Conference in New Orleans, LA.

Johansen, T., Tveito, A., and Winther, R., 1988, A Riemann Solver for Two-Phase Muticomponent Process, Research Report, Univ. of Oslo, Dept. of Informatics.

Koval, E.J., 1963, A Method for Predicting the Performance of Unstable Miscible Displacement in Heterogeneous Media, *SPEJ*, June, pp.145-154.

Lambert, M.A., 1981, A Statistical Study of Reservoir Heterogeneity, MS Thesis, U. of Texas at Austin.

McDonald, R.C., 1969, A Finite Difference Method for Simulation of Coning, TPRC Report No. UT-69-4, University of Texas at Austin, Dec.

Pope, G.A., Lake, L.W., and Helfferich, F.G., 1978, Cation Exchange in Chemical Flooding: Part I-Basic Theory Without Dispersion, *SPEJ*, Dec., pp.418-434.

Root, P.J. and Skiba, F.F., 1965, Crossflow Effects During an Idealized Displacement Process in a Stratified Reservoir, *SPEJ*, Sept., pp.229-238.

Rapoport, L.A., 1955, Scaling Laws for Use in Design and Operation of Water-Oil Flow Models, *Trans.*, AIME, V.204, pp.143-150.

Stiles, W. E., 1949, Use of Permeability Distribution in Waterflooding Calculation, *Trans.* AIME, V.186, pp.9-13.

Waggoner, J.R., 1985, A Study of the Effects of Heterogeneity on Immiscible Displacements and Their Representation in Numerical Simulators, MS Thesis, U. of Texas at Austin.

Waggoner, J.R., Zapata, V.J., and Lake, L.W., 1988, Viscous Mixing in Flows Through Permeable Media, submitted for pubblication to *Transport in Porous Media.*

Warren, J.E. and Cosgrove, J.J., 1964, Prediction of Waterflood Behaviour in a Stratified System, *Soc. of Petroleum Engineering Journal*, June, pp.149-157.

Welge, H.J., 1952, A Simplified Method for Computing Oil Recovery by Gas or Water Drive, *Trans.*, AIME 195, pp.91-98.

Zapata, V.J. and Lake, L.W., 1981, A Theoretical Analysis of Viscous Crossflow, SPE paper 10111, presented at 56th Annual Technical Conference in San Antonio, TX.

Zapata, V.J., 1979, The Effects of Viscous Crossflow on Sharp Front Displacements in Two-Layered Porous Media, MS Thesis, U. of Texas at Austin.

VITA

Marco Roberto Thiele was born in Bolzano, Italy, on the 16th of June, 1963, the son of Maria Gloria Thiele, born Guglielmi, and Roberto Thiele. Much of his youth was spent in foreign countries. From 1963 to 1966 in Munich, W. Germany, 1967 in Trapzon, Turkey, 1967 to 1968 in Teheran, Iran, 1968 to 1969 in Hsinchu, Taiwan. After a two year period in Rome, Italy, where he began elementary school, he spent from 1971 to 1974 in Monrovia, Liberia, 1974 to 1975 in Freetown, Sierra Leone, and 1975 to 1976 in Bong Mine, Liberia. In 1976 he returned to Rome, Italy, where he entered the 8th grade at the German School Rome. He graduate with the German Abitur in the summer of 1982. In the Fall of 1982 he was admitted to the pre-engineering program at Texas Christian University. In the Fall on 1983 he entered the University if Texas at Austin from which he graduated with a Bachelor of Science in Petroleum Engineering in December of 1986. In the Spring of 1987 he was admitted to the graduate program in Petroleum Engineering at the University of Texas at Austin and graduated with a Master of Science in December of 1988.

His work experience include two summer internships, in 1985 and 1986 respectively, at the Shell Exploration&Production laboratories in Rijswijk, The Netherlands, one summer internship at the Atlantic Richfield Company Exploration&Production laboratories in Plano, Texas, and the Fall of 1987 at the Institute for Energy Technology in Kjeller, Norway.

Permanent Address: Hof Himmelreich
39040 Siusi (BZ)
ITALY

This thesis was typed by Marco Thiele.